Energy Research and Development Division

FINAL PROJECT REPORT

# Photovoltaic and Behind-the-Meter Battery Storage: Advanced Smart Inverter Controls and Field Demonstration

California Energy Commission

Gavin Newsom, Governor

May 2019 | CEC-500-2019-XXX

**PREPARED BY**:

**Primary Author(s)**:
Christoph Gehbauer (cgehbauer@lbl.gov)
Joscha Müller
Tucker Swenson
Evangelos Vrettos

Lawrence Berkeley National Laboratory
One Cyclotron Road
Berkeley, CA 94720
Phone: 510-486-4000 | Fax: 510-486-4000
https://www.lbl.gov/

**Contract Number**: EPC-14-035

**PREPARED FOR**:
California Energy Commission

Hassan Mohammed
**Project Manager**

Aleecia Gutierrez
**Office Manager**
**ENERGY GENERATION RESEARCH OFFICE**

Laurie ten Hope
**Deputy Director**
**ENERGY RESEARCH AND DEVELOPMENT DIVISION**

Drew Bohan
**Executive Director**

# ACKNOWLEDGEMENTS

This work was supported by the California Energy Commission through its Electric Program Investment Charge Program on behalf of the citizens of California and under the United States Department of Energy, under Contract No. DE-AC02-05CH11231.

The authors would like to thank the following contributors at Lawrence Berkeley National Laboratory:

Rahul Chopra

Ravi Prasher

Ramesh Ramamoorthy

Cindy Regnier

Alastair Robinson

Alina Sari

Alecia Ward

The authors would also like to thank SolarEdge, and in particular Noah Tuthill, for the support with setting up the StorEdge inverters and Tesla PowerWall, and providing full control access to their inverters.

Technical Advisory Committee Members included:

Bill Abolt, AECOM

Richard Bravo, Southern California Edison

Angela Gould, California Energy Commission

Thomas Lee, Strategen

Alexandra Sascha von Meier, University of California Berkeley, California Institute for Energy and Environment

Sankar Narayan, Microgrid Labs

Harby Sehmar, Pacific Gas and Electric Company

Franz Stadtmueller, Pacific Gas and Electric Company

Kristine Walker, Prospect Silicon Valley

# PREFACE

The California Energy Commission's Energy Research and Development Division supports energy research and development programs to spur innovation in energy efficiency, renewable energy and advanced clean generation, energy-related environmental protection, energy transmission and distribution and transportation.

In 2012, the Electric Program Investment Charge (EPIC) was established by the California Public Utilities Commission to fund public investments in research to create and advance new energy solution, foster regional innovation and bring ideas from the lab to the marketplace. The California Energy Commission and the state's three largest investor-owned utilities – Pacific Gas and Electric Company, San Diego Gas & Electric Company and Southern California Edison Company – were selected to administer the EPIC funds and advance novel technologies, tools, and strategies that provide benefits to their electric ratepayers.

The Energy Commission is committed to ensuring public participation in its research and development programs that promote greater reliability, lower costs, and increase safety for the California electric ratepayer and include:

- Providing societal benefits.
- Reducing greenhouse gas emission in the electricity sector at the lowest possible cost.
- Supporting California's loading order to meet energy needs first with energy efficiency and demand response, next with renewable energy (distributed generation and utility scale), and finally with clean, conventional electricity supply.
- Supporting low-emission vehicles and transportation.
- Providing economic development.
- Using ratepayer funds efficiently.

*Photovoltaic and Behind-the-Meter Battery Storage: Advanced Smart Inverter Controls and Field Demonstration* is the final report for the Demonstration of Integrated Photovoltaic Systems and Smart Inverter Functionality Utilizing Advanced Distribution Sensors project (Grant Number EPC-14-035) conducted by Lawrence Berkeley National Laboratory. The information from this project contributes to the Energy Research and Development Division's EPIC Program.

For more information about the Energy Research and Development Division, please visit the Energy Commission's website at www.energy.ca.gov/research/ or contact the Energy Commission at 916-327-1551.

# ABSTRACT

Electric utilities have little visibility of the electrical distribution system, and consequently, limited diagnostic capabilities. The distribution grid was designed for a unidirectional power flow, where energy is supplied by few large centralized power plants; however, this is set to change to meet California's aggressive decarbonization goals. The large-scale deployment of distributed renewable generation, such as photovoltaics (PV), can have many negative effects on an unprepared grid. As illustrated in the California "duck curve," PV generation modifies load profiles during the day, which causes steep ramping in the evening. This effect indicates the need to revise the electrical grid's design and operation. This project sought to (a) create a centralized resource in California to test and validate distribution technology controls with industry standard PV, storage, and high-fidelity sensors, (b) support strategic and operational decisions for new grid architectures by providing simulation models, (c) promote new ways to control clusters of PV smart inverters, in accordance with California Rule 21, and (d) innovate, develop, and field test a predictive controller to maximize economic profit for the customer while supporting the grid. The controller was built using the state-of-the-art model predictive control methodology to optimally control behind-the-meter PV and battery storage. In consideration of the duck curve, the controller optimally controls the battery dispatch by charging during excess generation periods and discharging during the critical afternoon demand hours. The controller was evaluated in annual simulations and revealed the potential cost-effectiveness of behind-the-meter battery storage. The simulations showed that the annual electricity bill could be reduced by as much as 35 percent, with a payback period of the investment in battery storage in about 6 years – significantly shorter than the manufacturer's 10-year warranty. All developed simulation models, the grid event library, and the MPC controller are open-source and available online.

Keywords: *Smart Inverter, Behind-the-Meter Battery Storage, Advanced Distribution Grid Sensor, Model Predictive control, Machine Learning*

Please use the following citation for this report:

Gehbauer, Christoph, Joscha Müller, Tucker Swenson and Evangelos Vrettos. 2019. *Photovoltaic and Behind-the-Meter Battery Storage: Advanced Smart Inverter Controls and Field Demonstration*. California Energy Commission. Publication Number: CEC-500-2019-XXX.

# TABLE OF CONTENTS

# LIST OF FIGURES

Page

# LIST OF TABLES

Page

# EXECUTIVE SUMMARY

## Introduction

Today's electric distribution system is designed for a limited number of large central power plants serving mostly residential and commercial buildings and industrial facilities. However, California's aggressive goals to reduce the state's greenhouse gas emissions to 1990 levels by 2020, 40 percent below 1990 levels by 2030, and 80 percent below 1990 levels by 2050 is leading to increasing amounts of renewable generation in the system, particularly from photovoltaics (PV) and battery storage. This transition changes the architecture by introducing many small-sized generation plants which are distributed along the power grid and alter the power flows from one-way to two-way. In turn, this creates new challenges to the existing power distribution system and requires more advanced scenario-based planning combined with real-time data management, new control frameworks, and cyber-risk mitigation, to maintain safety and reliability.

Voltage variability is one of the system challenges posed by increased levels of distributed generation. The critical aspect here is the voltage level at the customer, which is defined by United States standards to be within plus-or-minus 5 percent of 120 volts (114 volts to 126 volts). When voltages are outside this range, motors, electronics, lights, or other equipment could be permanently damaged and pose a safety risk for the user. With only few large power plants, up to now the voltage change from the point of supply to the customer has been relatively straightforward to estimate using the physics of electrical systems and connecting cables. However, as the grid network changes to include many small-scale distributed generators, projecting voltage changes becomes more difficult because voltages at different points along the power grid can rise or fall, depending on whether distributed generation is present or not. Aggravating the situation, existing power distribution systems have little visibility (that is, data on the location and size of distributed resources and how they are being operated on a real-time basis), and consequently have limited diagnostic capabilities. So when distributed generation causes voltage variability issues, utilities and system operators cannot anticipate or quantify them.

In addition to voltage variability challenges, distributed generation results in a "masked load", where renewable generation offsets the load, resulting in a distorted net load (the difference between customer load and expected electricity production from variable generation resources). Modified net load profiles due to the deployment of PV are becoming common within the California power grid. The California "duck curve," shown in Figure ES-1, is an early indicator of the need to revise the way the electrical grid is designed and operated to address short, steep ramps when the system operator must increase or decrease generation to meet varying electricity demand, and to deal with the risk of oversupply when more electricity is supplied than is needed to satisfy real-time demand.

A typical load profile (the use of electricity over time) of the California power grid in 2012 is shown in gray, with two peaks. In the morning hours, the residential and commercial loads ramp up, and in the evening hours the commercial loads decrease but are compensated by the

ramp up of residential loads. The integration of PV generation causes an offset of the typical load profile by generating electricity in the daylight hours from 9 AM to 6 PM, shown as annual projections by the colored lines.

**Figure ES-1: California Duck Curve**

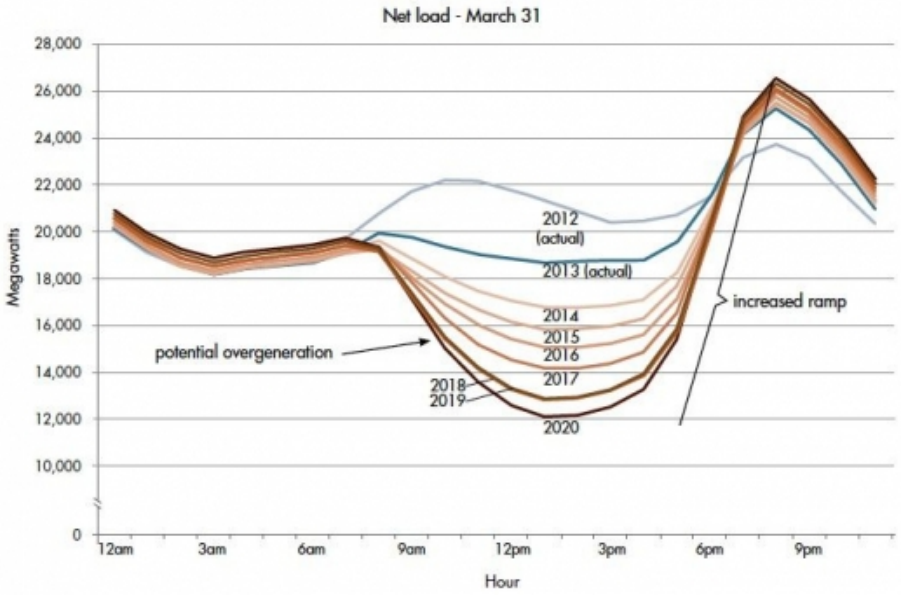


Source: California Independent System Operator 2016.

The challenge here is the steep ramping in the evening hours, when PV starts to decrease while residential loads are getting online. This ramping is very expensive, as it requires (typically fossil-fired) power plants to be on standby and available just for this few-hours period. This demand is currently met by spinning generators such as gas-fired power plants. The spinning generators are typically coupled to rotating gas or steam turbines and can provide inertia to the grid to ensure reliable service during abnormal conditions. Distributed generation, on the other hand, uses devices based on power electronics that act instantly and cannot provide this kind of inertia. With California's decarbonization goals, alternatives will have to be available to support future low-emission grids. This trend will put additional pressure on how to build the grid network and optimally manage the resources.

## Project Purpose

This project's purpose was to investigate solutions to enable high levels of renewables in the electricity system to support California in reaching its greenhouse gas emission reduction goals. The approach was multifold. First, the research team designed and built a central testing facility for evaluation of distributed generation technology in California. This facility allowed the research team to study the impact of renewable distributed generation on the power grid. The facility also allowed researchers to evaluate novel control systems in a controlled environment. Second, for rapid scenario evaluation, the researchers developed and validated simulation models based on the testing facility. The models were made publicly available to support strategic and operational decisions of the different stakeholders (grid operators,

investors, and owners). Third, the team conducted a simulation study on optimally controlled distributed generation to reduce the overall cost of electricity and maximize usage of distributed resources. Fourth, researchers developed a controller for combined PV and storage systems to mitigate the California duck curve, provide benefit to the grid operator, and maximize revenue for the customer in the current regulatory framework.

## Project Process

The project included four consecutive steps that addressed the test facility, simulation models, optimal control of smart inverter, and optimal control to mitigate the duck curve.

### Test Facility (Flexgrid)

The project team designed and built Flexgrid, a full-scale testbed for renewable distributed generation. The facility includes a 1,000 square foot PV installation, with 15 kilowatts (kW) of peak power, and three household-scale batteries, totaling 19 kilowatt-hours (kWh) of storage. The high-fidelity sensing devices installed – micro-synchrophasor measurement units – provide readings of 120 samples per second to accurately evaluate and analyze the electrical power grid during critical conditions. The equipment manufacturers include Tesla Energy, SolarEdge, and Power Standards Lab, all located in California. The first use of the facility was to study the impact of renewables on the power grid. The sensing equipment was used to record any variation in supply voltage during periods with and without PV generation. The measured voltage violations were stored in a digital library of grid events, and used to prototype an algorithm to predict the severity of these very short-lived (typically in the order of 0.1 second) events. The library is published online to provide access to academia, researchers, and industry.

### Simulation Models

The data recorded at the testing facility was also used to inform the creation and validation of simulation models. These models include component and system models of PV, batteries, inverters (electronic devices used to convert direct current to alternating current), and the power grid. Simulation models are very important for grid planning and controls evaluation. With a simulation model of the entire grid, researchers can study different levels of PV deployment and quantify their impact. However, a full grid simulation involves many components that are typically not designed to be simulated together. One example would be a power grid simulation, which focuses on the electrical power flow, and a battery storage simulation, which focuses on the battery chemistry. The simulation models developed in this project are not domain-specific and allow the simulation of full grids. They are open-source to allow researchers and stakeholders to make informed decisions.

### Optimal Control of Smart Inverters

A smart inverter is the improved version of an inverter that can actively regulate power generation in accordance with locally observed quantities, which could be voltages. The functionalities are based on California Rule 21 (a mandate that describes the interconnection and of generation facilities to be connected to a utility's distribution system) to allow more flexibility and adaptability of distributed generation. In an example application of the

developed simulation models, the objective was to determine the best control setpoints for various smart inverters connected within the electrical grid. While these configurable parameters are currently predetermined by the utility company and are static for all locations, this project investigated the use of dynamic setpoints that depend on the location and season. Optimizing these parameters can also lead to reductions in the levelized cost of electricity, especially for grid networks with high PV penetrations.

### Optimal Control to Mitigate Duck Curve

While the optimal control of smart inverters focused on control settings of the inverter, the team also took a deeper dive into the capabilities of distributed generation. Here, the combination of distributed PV and battery storage was analyzed and the operation optimized. The controller was implemented as a model predictive control, where an internal mathematical model is evaluated and solved to a global optimum at each controller time step. The inputs were forecasts of weather data, PV generation, and load for the upcoming 24 hours. The objective was to maximize the revenue for the generating asset owner while providing additional services to the grid. The grid services explored in this project included time-varying pricing schemes and the response to critical periods.

From the projections illustrated in the California duck curve, it is anticipated that more and more ramping in the evening hours will be required. Model predictive controllers can optimally control the battery by charging it during periods with excess generation and discharging it during the critical afternoon or evening hours. This active participation in the grid management will help to maximize the number of renewables that can be connected to the grid. The controller was evaluated in annual simulations and in a field test conducted at the Flexgrid test facility.

## Project Results

The results of this project are multifold and well-aligned with the overall objective of enabling large renewable generation on the electrical power grid. The results are ranked by their immediate benefit to California, if deployed widely:

- During the field test for the model predictive controller for PV and battery storage, the controller responded to changing environmental conditions and provided near optimal control of the storage system for a time-varying electricity price. The annual simulation indicated cost savings of up to 35 percent, with a payback time of about 6 years. This is significantly shorter than the manufacturer's warranty of 10 years. The installation of a battery storage system can financially benefit both residential and commercial ratepayers, as well as grid operation and reliability overall. Further benefits assessment could be conducted at the Flexgrid facility, where synthetic grid events or different customer configurations could be generated and applied to the controller in a full-scale field test.
- The assignment of variable smart inverter control setpoints revealed the potential to decrease the capacity of the inverter while providing the same generation output. This would decrease the levelized cost of electricity (the measure of lifetime costs divided by

energy production over the lifetime of the resource) for distributed generation. In scenarios with high PV penetration, it would be even more advantageous to use variable control setpoints by preventing the curtailment of PV power generation during peak hours, a common industrial practice today. Ratepayers would see improved reliability compared to a case where high PV penetration exists but is not coordinated and managed as proposed in this project. Further investigations of associated grid distribution losses and inverter investment costs could be conducted to thoroughly evaluate the control approach and benefit for different customer types in California.

- The Flexgrid facility, built with funds from this project award, is a central base for testing new renewable technologies and their integration issues in California. It allows the evaluation of novel control systems in a controlled, emulated environment and enables real-time comparisons between end-user demand, renewables, inverters, and storage. Flexgrid was used throughout this four-year project, serving the data collection, simulation model development for component and system models related to PV, smart inverter and battery storage, development of a grid event detection algorithm, and evaluation of a novel model predictive controller. This state-of-the-art research facility is available for future research projects in California.
- The measurements from Flexgrid were used to develop and validate a package of simulation models that include PV, battery, smart inverter, and the power grid component and system models. While the models were mainly developed for this project, they are generic and can be combined and parameterized to reflect other systems. The package is published online and can support stakeholders, regulators and researchers involved in investment and planning decisions.
- The micro-synchrophasors installed at Flexgrid recorded roughly two years' worth of data, with 120 samples per second which totals about 4 terabytes of data. An event detection algorithm was developed and applied, which resulted in the detection of 27 voltage events over the course of this study. The events were stored in a digital library and used to perform two methods of short-term forecasting. Both methods revealed that the initial slope of a voltage event is a good parameter to predict the event's severity and duration. This information can be vital for inverter settings, in accordance with California Rule 21, with the overall objective to improve the reliability of the electrical grid.

Both control approaches, namely, (1) the controller for PV and battery storage and (2) the variable smart inverter control setpoints, can increase the allowable amount of PV on the grid in different ways: (a) offsets retail energy purchases; (b) increases the ability to earn PV-based revenue due to an increase in the type of energy services PV and battery storage can provide (that is, grid support or mitigation of the duck curve); and (c) helps California to achieve its aggressive climate goals to decarbonize the grid.

All simulation models, the grid event library, and the model predictive control framework developed by this project are open-source and available online.

## Technology/Knowledge Transfer/Market Adoption (Advancing the Research to Market)

This project was conducted with a variety of industry project partners and advisors. These included Tesla Energy, SolarEdge, Power Standards Lab, Pacific Gas and Electric, Southern California Edison, Microgrid Labs, Strategen, Prospect Silicon Valley, as well as the University of California Berkeley as an academic partner, all located in California. Two technical advisory committee meetings were held to incorporate insights and feedback from industry, and specify use cases for the developed tools. Results from this project were presented in two conferences. The developed tools and models were published on four public repositories on GitHub.

The electricity tariff for commercial customers, with its time-varying energy cost and demand charge, provides a good opportunity to employ the developed controller, especially if battery storage is already installed. However, the electricity grid and rate structure are undergoing incremental restructuring to better represent the actual energy production cost, particularly with increasing levels of renewable generation. With energy storage as a central resource to balance this fluctuating generation, the role of residential customers will get more significant. At this point, the developed controller for battery storage could provide financial benefits to both commercial and residential customers.

With all developments and findings being publicly available, and the collaboration with industry leaders, it is up to them to pick up the technology for commercialization. Important to note is that this project conducted the ground work to investigate different control approaches and identified a path to a potentially cost-effective operation. While the published controller is one example of viable technical implementation, companies may adopt the underlying control logic within their framework, for example, to be implemented inside the inverter of a combined PV and storage system. That said, the technology is particularly interesting for PV inverter manufacturers and system integrators of combined PV and battery storage systems.

## Benefits to California

The project resulted in a variety of outcomes for California, its residents, investors, stakeholders, and developers. This includes the design and installation of a central testing facility for renewable generation to test new developments from industry in a controlled and safe environment, before the deployment at California ratepayers. All funds to build this facility and conduct the research were spent in California to promote local businesses. And the goals and challenges of the California electricity grid were discussed at two conferences and two technical advisory committee meetings. However, most compelling is the development and field testing of a model predictive control framework that showed potential cost-effectiveness of battery storage, by reducing annual electricity bills by up to 35 percent. The payback time is about 6 years, which is significantly shorter than the manufacturer's offered warranty of 10 years. When deployed, this technology can increase the allowable amount of renewable generation on the grid, for example by avoiding the need to upgrade grid infrastructure such as distribution lines, while providing financial benefits to both residential and commercial ratepayers realized as lower electricity charges due to responding to dynamic grid tariffs.

# CHAPTER 1: Introduction

Historically, power distribution systems have not been the focus of research and development investments and have little visibility and consequently limited diagnostic capabilities. Distribution systems were designed for a radial and unidirectional power flow, supplied by centralized power plants. This scenario, however, is set to change. California has aggressive goals to grow distributed energy resources (DER), in particular solar photovoltaic (PV), to reduce the state's greenhouse gas emissions to 1990 levels by 2020, 40 percent below 1990 levels by 2030, and 80 percent below 1990 levels by 2050.[1] A future grid with large installations of this often inertia-less[2] distributed generation from PV or batteries will require different, and more complex, control mechanisms. Coordinated control of utility distribution equipment with DER will become a necessity. The detrimental impacts of high levels of PV on the current distribution grid involve: (a) voltage violations and phase imbalances, (b) potential flicker and other power quality issues, (c) reverse power flow and protection coordination issues, (d) increased wear and tear on utility equipment, (e) real and reactive power imbalances, and (f) ramping issues as recently discovered in California's "duck curve" models. These impacts are potential barriers to the widespread dissemination of DER; however, advanced sensors and controls, combined with existing technologies, could mitigate or overcome those barriers. This project seeks to understand and mitigate these issues depicted in events ranging from sub-seconds up to minutes or even hours.

Grid events are sudden conditions that occur randomly and without notification. The current electrical grid architecture, which consists of a relatively small number of large power generators, makes grid events relatively straightforward to identify, control or isolate. However, future grids with high levels of DER pose a significant challenge to safe and reliable grid operation. One example of a grid event is a voltage-sag, where the system voltage momentarily drops below 90 percent of the nominal voltage value for a short period of time. A single voltage sag could trip thousands of DER, which in turn would abruptly increase the load on the grid. In the worst case scenario, this could result in wide-area blackouts. Further aggravating the situation, voltage sags typically occur on a very fast timescale and only last for fractions of a second. While current monitoring of distribution grids is mainly focused on the aggregated feeder head,[3] at timescales larger than seconds grid events may occur on nodes remote to the feeder head and on much faster timescales, which often make them invisible to system operators. Advanced distribution phase measurement units (PMUs) can provide highly precise

[1] Assembly Bill 32, Núñez, Chapter 488, Statues of 2006; Senate Bill 32 (Pavley, Chapter 249, Statutes of 2016); and Governor Edmund G. Brown, Jr. Executive Order B-30-15.

[2] Traditional power plants use spinning generators which inherently have inertia that helps reduce frequency fluctuations. On the other hand, inverters, as used for DER, are based on power electronics and cannot provide such a type of inertia.

[3] This is the point of interconnection of the distribution feeder with the transmission or sub-transmission grid.

measurements on timescales well beyond traditional systems. The microsynchrophasor measurement unit (µPMU), as an example of distribution PMU, is able to take measurements at a rate of 30,000 Hertz (Hz), and output the measurements in 120 Hz, or 120 samples per second. This rate is sufficient to capture most voltage sags.

To capture, characterize, and mitigate grid events, this project was conducted to install a total of three distribution PMUs at Lawrence Berkeley National Laboratory (LBNL) campus. Further, a 15 kilowatt (kW) PV system from SolarCity/Tesla Energy, three 6.4 kilowatt-hour (kWh) Tesla PowerWall energy storage systems, and three single-phase 7.6 kilovolt-ampere (kVA) SolarEdge StorEdge inverters were installed to form a testbed (Flexgrid) and study the impact of DER on the grid, with a sub-campus of LBNL acting as a fully functioning living lab. This testbed also allows the study of effects caused by different penetration levels of PV.

The California duck curve shown in Figure 1 is an early indicator of the necessity to revise the way the electrical grid has to be designed and operated. Modified load profiles at the feeder head, due to the deployment of PV, are becoming common within the California power grid.

**Figure 1: California Duck Curve**

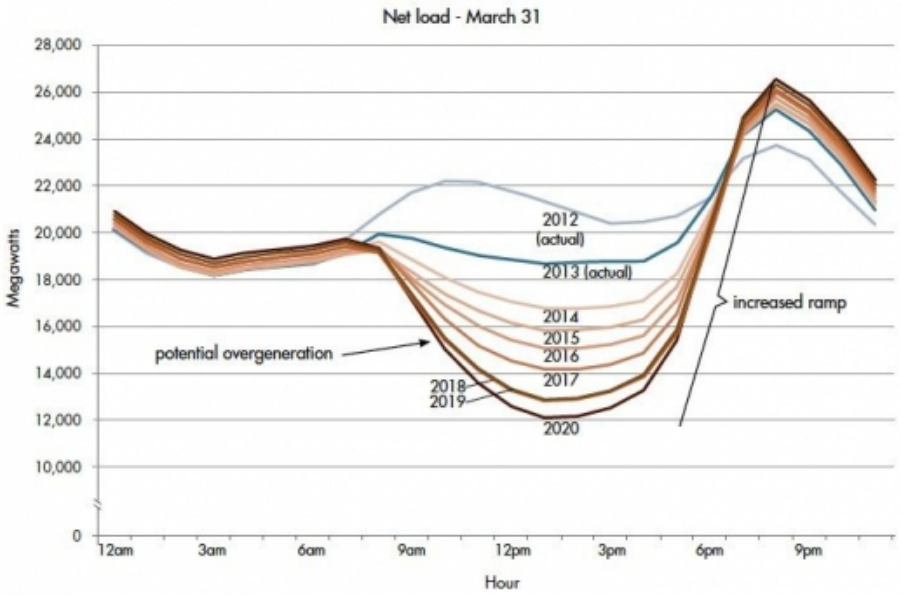


Source: California Independent System Operator 2016

Here, the load profile, shown in gray, is offset by the PV generation during the daylight hours from 9 AM to 6 PM. The most apparent problem arises in the evening hours, when PV starts to ramp down, but residential loads are rising. A large amount of ramping is required to keep the grid balanced. This ramping is very expensive, as it requires entire power plants to be available just for this few-hour period. While this ramping currently can be covered by spinning generators such as gas power plants, in a future of low-emission grids dominated by distributed energy resources (DERs) alternatives must be available. One potential solution investigated is the use of customer-owned (behind-the-meter) battery storage, where excess

energy can be stored during the daytime and used in the evening hours, coinciding with the ramp up demands shown in the California duck curve.

This project's broad goals were to:

- Develop a centralized testbed in California for advancing the understanding of DER technologies.
- Accelerate distributed PV deployment by using new sensor technology and simulation tools to prototype novel control systems.
- Identify functional requirements and control algorithms for existing and future grid integration issues of controllable PV and/or behind-the-meter battery storage.
- Develop a controller for optimal control of behind-the-meter energy resources.
- Conduct simulations to represent high PV penetrations on the distribution grid and assess potential benefits for advanced controls in California.

This project's specific objectives were to:

- Work with Solar City, Tesla Energy, and SolarEdge to develop and demonstrate control of an advanced PV inverter storage system and load using data collected from Power Standard Lab's µPMUs installed on the LBNL distribution grid and PV/storage system.
- Conduct applied research using the integrated PV system with relevant conditions or anomalies on LBNL distribution feeders that require a mitigation strategy, including voltage sags/swells and reverse power flow.
- Simulate the installation to scale, using state-of-the-art cosimulation tools, and validate the models with the distribution PMU data.
- Use this testbed to design and enable predictive multi-objective control functionality for both mitigation and control of voltage and power variability issues in high-penetration scenarios, while optimizing customer's local economic objectives.
- Quantify the benefit of advanced sensor networks and multi-objective control strategy for both PV inverters and storage, to both California and the local commercial system.

The project advanced scientific and technical knowledge and innovation in this area and California by:

- Having a central testbed in California to study effects of DER integration.
- Validating grid performance, including steady-state and time-series voltage profile before and after installation of a distributed PV system, as well as with and without advanced control objectives.
- Developing a functional control strategy for advanced PV inverters, in conjunction with behind-the-meter battery storage, which can be replicated at the high penetration feeder level.
- Using high-fidelity sensor data for visualization, event identification, and control objectives.

This report covers the full spectrum, from data collection to controller development and testing, to improve DER utilization, in particular smart PV inverters, in accordance with the latest California Rule 21 interconnection standard (CEC 2014), and the optimal control of behind-the-meter battery storage. It begins by describing Flexgrid (the test facility) and outlines the data collection and grid event analysis. It then illustrates the development of the required simulation models and design of a controller to maximize economic and grid supportive operation, and evaluates the controller in simulation and real-world situations. It concludes with a summary of benefits for California.

# CHAPTER 2:
# Experimental Test Facility

The LBNL campus is a widespread research community, located in Berkeley, California. It consists of more than 100 office buildings and experimental research facilities. Examples are the Advanced Light Source,[4] which is a synchrotron facility that provides users access to high-energy beams for scientific research and technology development in a wide range of disciplines, and the Facility for Low Energy Experiments for Buildings[5] (Flexlab), which enables users to develop and test energy-efficient building systems individually or as integrated system, under real-world conditions. The Flexlab facility is also part of the campus that hosts the power grid-related research at LBNL.

## Installation of Photovoltaic and Storage Systems

Using the Energy Commission's award to the project, Flexlab was expanded and interconnected with a collection of PV and energy storage systems. This expansion enhanced Flexlab as a platform for grid interactive field testing. Further investments from United States Department of Energy (USDOE) funded projects in grid emulation components resulted in a central hardware-in-the-loop[6] testing facility for California, branded Flexgrid. The flexible design of photovoltaics, storage system, and the high fidelity instrumentation plays a central role at Flexgrid, to conduct novel research and development of grid technologies. Figure 2 shows an overview of the facility.

**Figure 2: Overview of Flexgrid Facility**

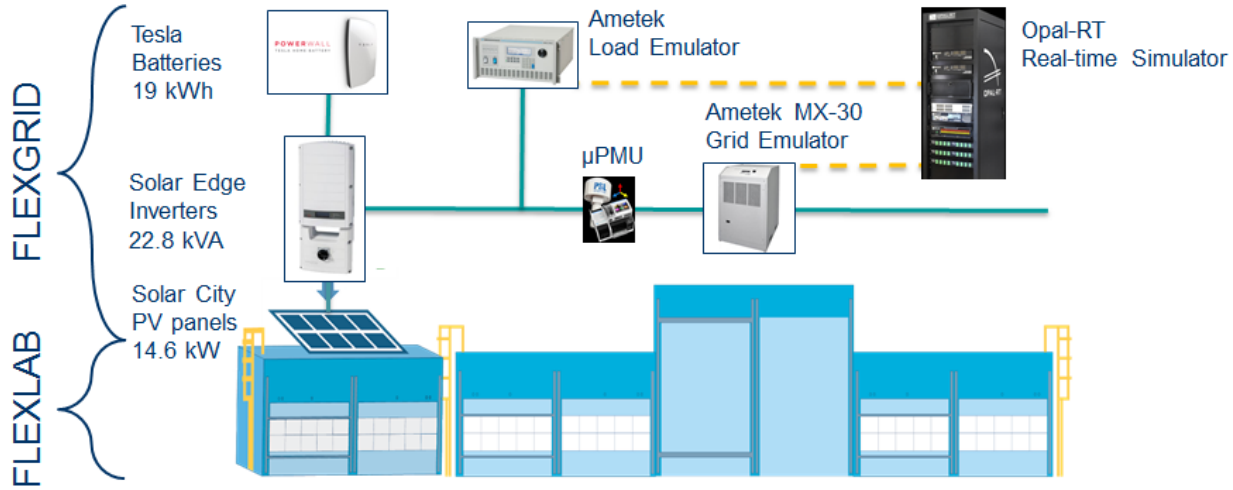


[4] https://als.lbl.gov/

[5] https://flexlab.lbl.gov/

[6] A testing procedure where a controller is connected to a virtual grid with real-time feedback.

Source: Lawrence Berkeley National Laboratory

Flexgrid allows for a systematic evaluation of a broad range of scenarios to be tested under emulated or real-world conditions. The Flexgrid setup includes an Opal-RT real-time simulator[7] as the center of operation, with an Ametek 30 kVA variable voltage source[8] as a grid emulator, and one Ametek 3 kVA load emulator.[9] The PV array consists of four strings with a total output of 14.6 kW, which feeds a three delta-connected and single-phase SolarEdge StorEdge[10] inverter, with a maximum output of 7.6 kVA each. Three 6.4 kWh Tesla PowerWall[11] batteries are connected to the inputs of each inverter. The power flow is measured by high-fidelity distribution phasor measurement units (PMUs).

## Installation of Advanced Measurement Devices

The microsynchrophasor measurement unit[12] (µPMU) is a low-cost distribution PMU developed by Power Standards Lab in partnership with LBNL and the University of California, Berkeley, with support of an Advanced Research Projects Agency-Energy (ARPA-E) grant in 2014. The accurate measurement of phase angles and magnitudes was for a long time a privilege of the transmission grid only. The compact µPMU makes available this unique capability to the distribution grid, at a significantly reduced cost (von Meier et al. 2017). It reports data at a 120 Hz acquisition rate, which is twice per cycle or 120 samples per second, as a phasor representation[13] of voltage and current for each phase. The measurements are based on the fundamental grid frequency of 60 Hz in the United States. For synchronicity, µPMUs are connected to a global positioning system receiver to synchronize the timestamp for the phase angles accurately, to an order of 50 nanoseconds. The data is available as a continuous live stream, in accordance with the Institute of Electrical and Electronics Engineers (IEEE) C37.118 communication protocol for PMUs, or periodically sent as a comma-separated values file to a central server. To enable research on power quality issues associated with DER, an array of µPMUs was deployed at Flexgrid to study impacts of PV, battery storage, and transactive buildings on the power grid. Figure 3 shows an overview of the installation and system boundaries.

The three PMUs are arranged in a layered setup, stretching over different system boundaries of Flexgrid only (orange), Flexgrid and Flexlab (blue), and the addition of a medium-sized office building (green).

---

[7] Opal-RT Technologies. https://www.opal-rt.com/

[8] AMETEK. California Instruments MX Series. https://www.powerandtest.com/power/ac-power-sources/mx-series

[9] AMETEK. California Instruments 3091LD Series. https://www.powerandtest.com/power/electronic-loads/ac-electronic-load-3091ld

[10] SolarEdge. StorEdge™ Products for On-grid Applications & Backup Power. https://www.solaredge.com/us/products/storedge

[11] Tesla. Powerwall. https://www.tesla.com/powerwall

[12] PSL. microPMU. https://www.powerstandards.com/product/micropmu/highlights/

[13] Magnitude and phase angle.

**Figure 3: Overview of Synchrophasor Measurement Unit Sensor Installation**

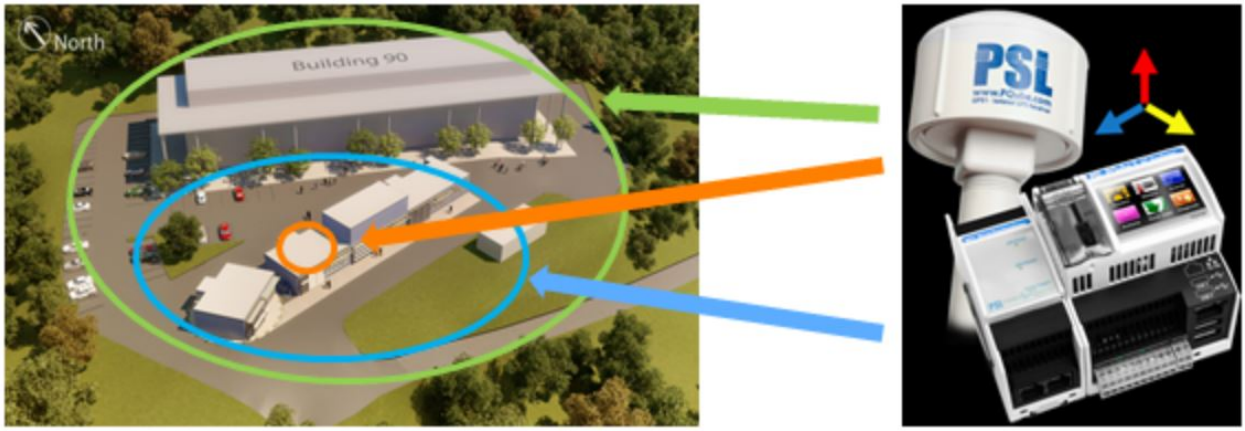


Source: Lawrence Berkeley National Laboratory

# CHAPTER 3:
# Data Collection and Analysis

This chapter describes the data collection architecture and framework from the distribution PMUs installed at LBNL, the grid event detection and analysis using a custom algorithm developed at LBNL, and results from Flexgrid. The whole chapter is based on a conference paper accepted to the IEEE Power & Energy Society General Meeting in 2019 (Swenson et al. 2019).

## High-Fidelity Data Collection

One challenge that PMUs pose is the large amount of data they produce, about 1 gigabyte (GB) per day for each PMU, which has to be stored and analyzed. To ease these processing concerns, the University of California, Berkeley, developed a Berkeley Tree Database (BTrDB) (Andersen et al. 2016), which is a high-speed time-series database specifically designed to handle high data flows. The major innovation is the tree-based architecture, where basic statistics such as minimum, mean, and maximum are calculated at the time of insertion of any new data and block size. For example, the statistics of the raw 120 Hz data are calculated for second, minute, hour, day, and month block sizes. Therefore, querying the highest block size of monthly aggregation, for a time frame of one year, only 12 data points with three statistics each (totaling to 36 values) are received, in comparison to the approximately 4 billion raw data points. This approach allows for rapid event detection and data analytics based on the precomputed statistics. Figure 4 illustrates the structure of the BTrDB.

**Figure 4: Structure of the Berkeley Tree Database**

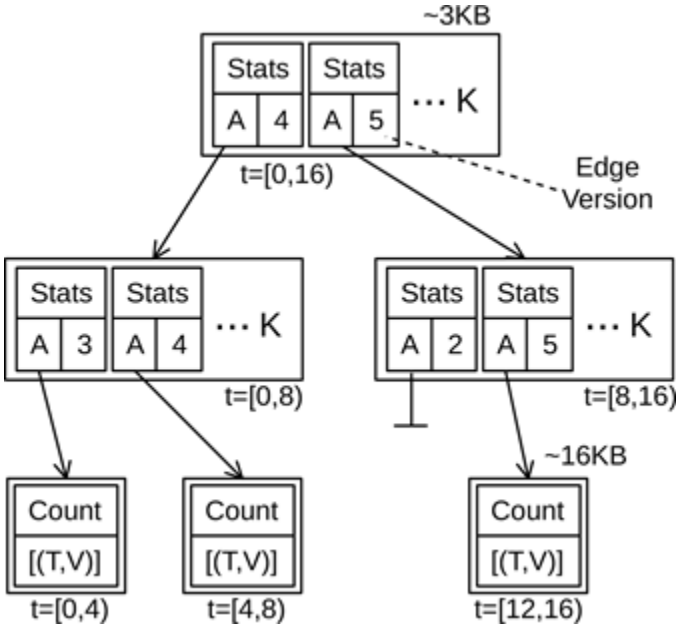


Source: Lawrence Berkeley National Laboratory

The lowest level in the BTrDB, shown at the bottom of Figure 4, is the raw data stored as pairs of time, *T,* and value, *V.* Note that time can be accurately stored in a nanosecond timescale. BTrDB then calculates basic statistics, for the higher level block sizes. This structure accelerates the search for grid events by an order of magnitude in comparison to other real-time databases, by allowing search algorithms to zoom into the data starting from the highest block size, ultimately down to the raw data of the grid event in question. The aggregations can be seen by the time indices. The middle layer in this example aggregates eight time steps, from 0 to 7 and 8 to 16. The highest aggregation aggregates the two middle layers, which results in an aggregation of the full 16 time steps.

# Grid Event Definition

To detect and categorize grid events, the numeric thresholds that characterize them must first be identified. To detect voltage sags and swells, where the voltage momentarily falls or rises, this analysis refers to the voltage ranges and durations put forth by IEEE, which stringently defines voltage swells and sags as a ±10 percent deviation from nominal site voltage, for durations from 0.5 cycles, which are about 8 milliseconds (ms), up to one minute (Alves and Ribiero 1999). Furthermore, as this analysis is concerned with distribution feeders, it is also relevant to refer to the American National Standards Institute's (ANSI) tolerable end-use voltage range, which prohibits deviations more than ±5 percent of the nominal service voltage for periods of time longer than momentary excursions (ANSI 2016; PG&E 1999). Extended voltage deviations outside of these bounds will then constitute an over- or under-voltage event.

To detect significant frequency events, the threshold the frequency bound that will prompt inverters to trip and become inactive. This defines the upper bound of acceptable frequencies as 60.5 Hz, while the lower bound is defined as 59.3 Hz (CEC 2014). However, these thresholds constitute extreme and uncommon frequency deviations in the bulk power system (Dargatz 2010). Thresholds for grid events of abnormal current and power flow, phase angle imbalances, grid impedance, power factor, and rates of change of voltage and current magnitudes are not easily objectively defined, so these grid events were omitted in this analysis. Instead, this study focused primarily on detection and characterization of voltage sags and swells that are well defined and occur relatively frequently. However, it is plausible to detect events by metrics other than voltage, should one have a quantifiable threshold with which to define the occurrence of an event as measured by that quantity.

# Event Detection Algorithm

This project used the programming language Python[14] to interface with BTrDB and the recorded PMU data. An event search algorithm was developed to detect events and return the corresponding data. The inputs to the program module are the universal unique identifiers of the PMU data channels and the search window start and end times. The program separately

[14] Python 3.7.2 documentation. https://docs.python.org/.

looked at each channel within each location, splitting the data from its start time to its end time into a user-defined number of subsections, and it leveraged the BTrDB's functionality to look only at the extreme values of each section. The timestamp corresponding to any window in which an extreme value crossing the event threshold was logged for further processing. After all subsection time windows were investigated at this coarse level, the program discarded all windows in which the extreme values did not show an event occurring. Then, windows that contained extreme values were themselves successively cut with a user-defined number of points of division. This created further subregions whose extreme values were retrieved from the BTrDB to further narrow the time interval over which the event transpired; this also served the purpose of detecting whether or not multiple events occurred within one larger time interval. This exponential process of window refinement occurred until the time window was narrowed to approximately one second, or until the BTrDB's mean value for that time window exceeded the threshold that defined the event. In this way, the program did not "over-zoom" into longer, more sustained sags or swells exceeding one second in duration. Figure 5 shows the refinement process that the exponential search function undergoes when presented with the entire dataset.

**Figure 5: Exponential Event Search Functionality**

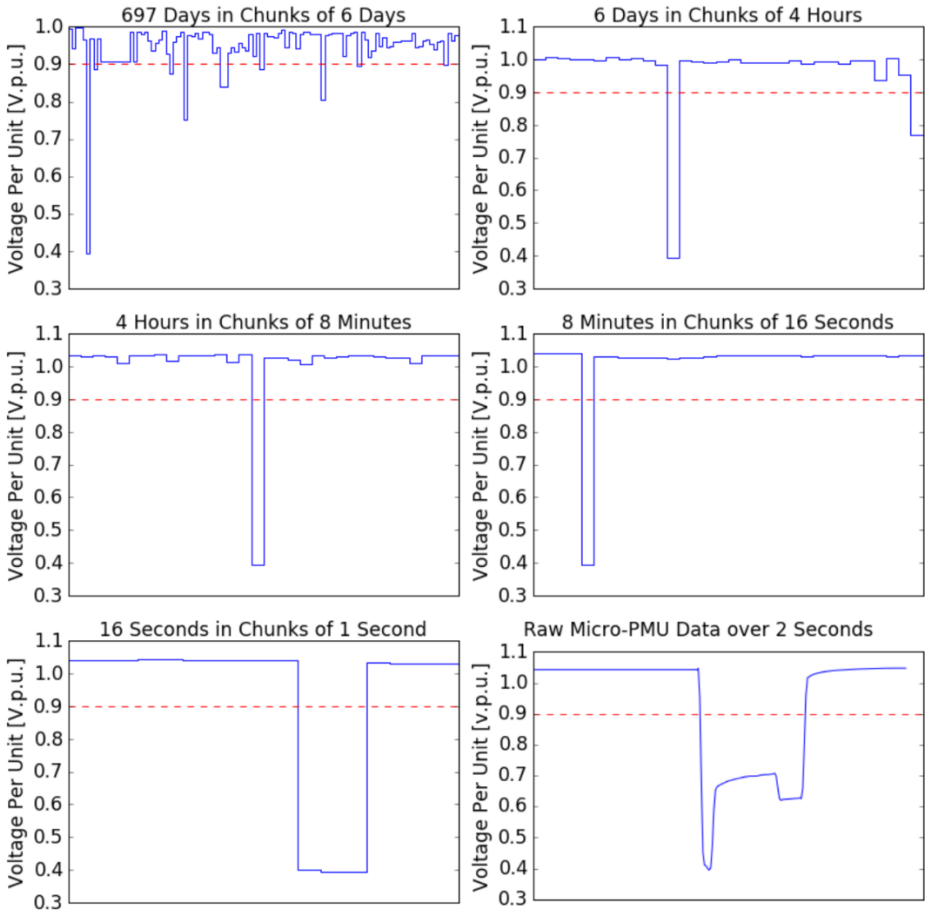


Source: Swenson et al. 2019

The program initially split the roughly two years of data into six-day-long subsections, and then represented each window with its minimum value obtained from the BTrDB. The script then noted that, for example, a data window in January contains a minimum value below the defined voltage sag threshold, here indicated by the red dotted line at 0.9 per unit. It refined this window by progressively splitting it until the script ultimately determined that an event occurred somewhere within the time window of 23:29:17 (hh:mm:ss) to 23:29:19. Once the time window was narrowed to this scale, the raw data of the event could be quickly queried, as illustrated on the last plot in Figure 5.

There are notable trade-offs that one must consider while determining how many points of division should be drawn by the exponential search function at each step. With a high number of points of division, it is possible to adequately zoom into an event with fewer calls to the BTrDB's database, and thus experience less overhead in communication time. However, this approach runs the risk of heavy-handedly zooming in too far and accidentally capturing only portions of events. Furthermore, if a large number of events exist in the time window that is presented to the script, computation time is wasted, as the program processes the values of the many time windows that do not contain events. Meanwhile, if a small number of points of division are drawn at each step, that is, splitting the windows in half each time, very little computation is wasted in dealing with time windows whose extreme values do not indicate an event. However, the extreme coarseness of this approach causes some events to be missed entirely, and means that the BTrDB might need to be called upwards of 20 to 30 times per PMU to isolate events at the level of one second, increasing communication overhead. For these reasons, an optimal section size of 2^11 (2048) for the first call to the BTrDB was determined on the data available to this project. This was followed by subsequent splits into 32 subsections as events were refined. The initial, fine-granularity split allows for events to immediately be identified to a narrow time window, with only one call to the BTrDB.

# Analysis

Once each detected event was trimmed in time to only the relevant abnormal data, the raw 120 Hz data of current and voltage magnitudes and phase angles, across all three phases, was stored. The subsequent sets of distilled PMU measurements were used to calculate and store data of active, reactive, and apparent power, as well as frequency and power factor. Detected events also were parameterized to enable further analysis and categorization. The parameterization function began by splitting the raw event data into five sections, as illustrated with a sample voltage sag in Figure 6.

The first section captures the half-second, front-padded data that preceded the voltage event. The second section encapsulates data from the point of the event start, that is, the point at which grid conditions began to deviate from normal operating conditions, to the point at which the threshold constituting a voltage, frequency, or current sag/swell was crossed. To take voltage sags as an example, the second section would capture data from the event start, to the data point at which voltage magnitude drops below 90 percent. The third section captures all data points for which the threshold was actively exceeded. Following the previous voltage sag example, this would correspond to all data points below the 90 percent threshold.

**Figure 6: Visualization of Event Parameterization**

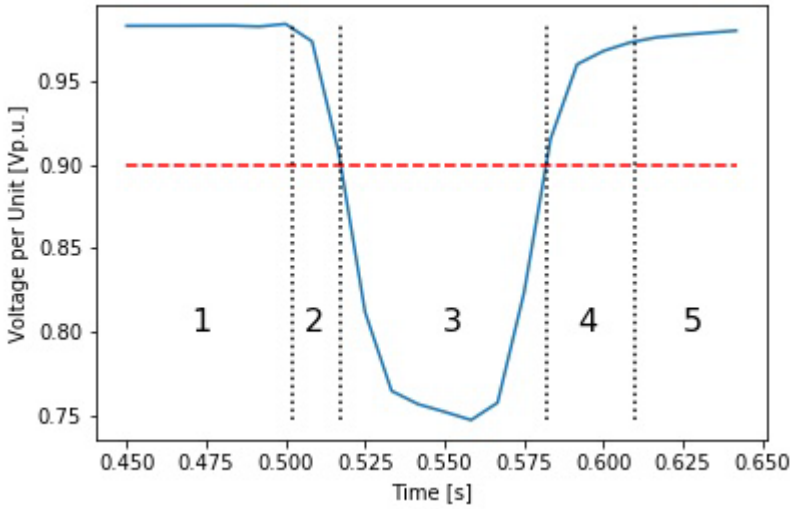


Source: Swenson et al. 2019

The fourth section of data corresponds to all data points over which the event threshold was no longer exceeded and in which the data points were returning to normal operating conditions. The fifth and final section contains the half-second of padded data immediately following the voltage event. With these separations in place, the parameterization function combed through the data points within each section separately and determined the following parameters:

- Flags to indicate the type of event, for example, voltage sag or swell, and whether PV generation was present.
- The start time and duration of the section.
- The maximum, minimum, and mean slopes achieved for voltages and currents.
- The maximum, minimum, and mean voltage and current magnitude values.

If, however, the parameterization function cannot identify any data points which drop below the event threshold, it instead defaults to placing all abnormal data (that is, the raw data that is bound by the slopes which constitute an event start and end) into one all-encompassing region whose parameters are measured. In this case, the first and last regions that covered nominal operations immediately preceding and following the event were still parameterized separately. This created three regions of parameters instead of the typical five for a full event.

## Grid Events

The LBNL developed event search function was applied to the dataset recorded at LBNL. For the time interval of December 2016 to October 2018, 27 voltage sag events were detected. These occurred within Building 90, Flexlab, and Flexgrid where site voltages dipped below 90 percent of their nominal values. These events typify the short-term grid events that PMU sensors are ideal in detecting, as they last for fractions of a second only and require detection and response schemes that are just as rapid to counteract effectively.

Because the threshold for grid events is user-defined and the program collects duration as an event parameter of interest, events may be filtered based upon their duration. Using this method, a search for prolonged under-voltage events, exceeding one second in duration, was conducted. While no extended voltage sags meeting IEEE's criteria occurred, three such extended under-voltage events were detected using ANSI's definition of acceptable distribution voltages. All three events in question occurred on October 24, 2017, during a week in which the building loads in Building 90 and Flexlab were twice that of their typical daytime loads. A likely explanation for these conditions is an unusually heavy air conditioning load during a particularly hot week, as evidenced by historical weather data. This created an environment on the distribution grid in which the most minor voltage dips were liable to pull operating voltages below ANSI tolerable limits for a prolonged period of time while voltage recovered. This provides insight into the types of ambient grid conditions that create an environment in which prolonged voltage deviations are most prone to occur, and future grid simulations will seek to determine whether or not proactive action on the part of smart inverters, once these risky ambient grid conditions are detected, might prevent the occurrence of such prolonged voltage deviations.

While not strictly grid events, long-term trends illustrate how grid conditions are apt to change over the course of days, weeks, or seasons. From the heatmap in Figure 7, for instance, a trend of summer months having higher baseloads can be observed, presumably as air conditioning makes up a more significant percentage of the area's power consumption.

**Figure 7: Long-Term Current Magnitude Trend at Building 90**

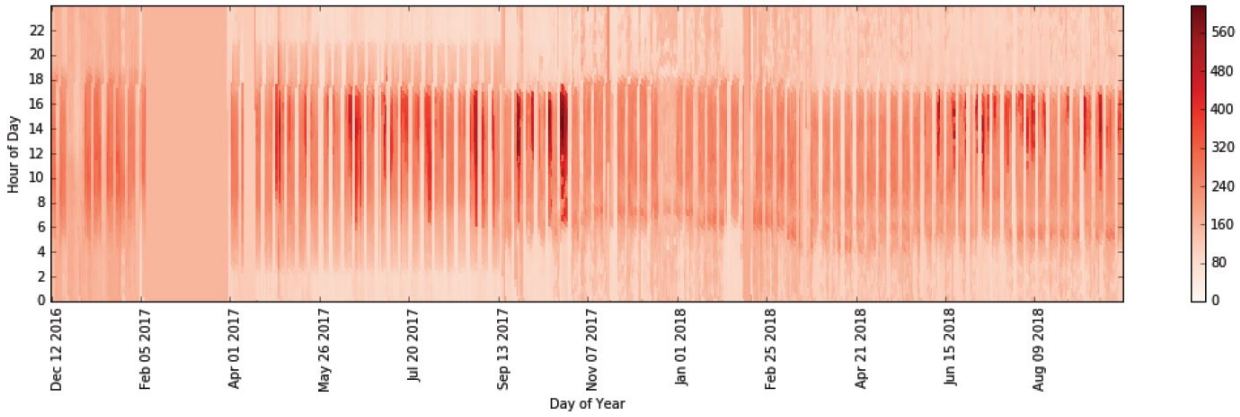


Source: Lawrence Berkeley National Laboratory

This heat map shows the current demand over the period of about two years. The day is shown on the x-axis and the time of day is shown on the y-axis. The value of the current is shown by the color indicator. A white color corresponds to 0 Amperes (A), whereas dark red corresponds to the maximum of about 580 A. The daily trends of occupation can be seen by the elevated currents during the daylight hours from about 6 AM to 6 PM. The peak period appears to be in October 2017, where currents reached up to 550 A. Another way of illustrating the trends is a heat map for weekly averages, as illustrated in Figure 8.

**Figure 8: Hourly and Weekly Voltage Imbalance at Building 90**

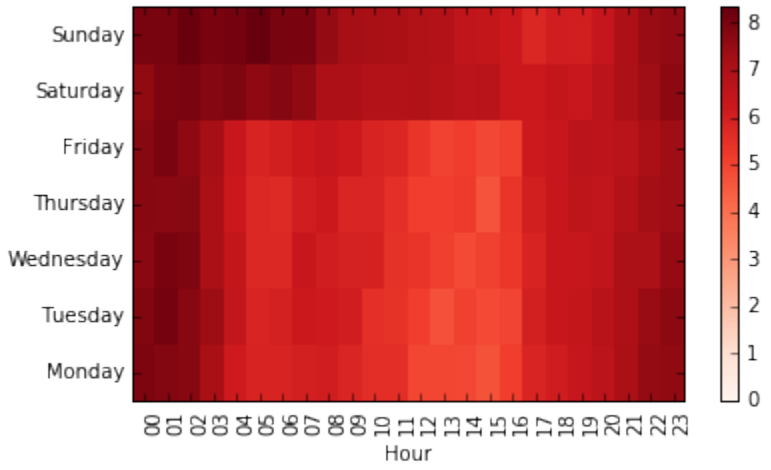


Source: Lawrence Berkeley National Laboratory

The site voltage at Building 90 is drawn down during the working hours of weekdays while the building is at full load, and is relatively high when loads are low on weekends, in the early morning, and during nighttime hours. Foreknowledge of this trend is important, as presented in the case of the extended under-voltage events on October 24, 2017 in the previous section.

### Library of Events

The whole dataset of extracted grid events was appended into a library of events for which each individual event received its own folder denoted by the time stamp. The library is open source to the research community and can be found in Swenson et al. (2019). It currently contains the 27 voltage sag events that occurred at LBNL, but will be continuously updated as new voltage events occur.

## Control Applications

An important aspect of the conducted analysis is the transfer of observations to a control system for mitigation. For this purpose, two clustering methods of clustering were applied: time-series clustering and parameter clustering.

### Time-Series Clustering

Events can be clustered based on the auto-correlated time-series data to identify typical event shapes and parameters. The time-series clustering presented in this report used the Ward method (Ward 1963). Figure 9 displays the clusters produced by feeding all recorded voltage sags for one PMU location into the clustering algorithm, with the stipulation that three clusters should be created. This number was determined as the knee region in the trade-off between number of clusters and loss function, defined as squared distance to the centroids.

**Figure 9: Example of Time-Series Event Clustering**

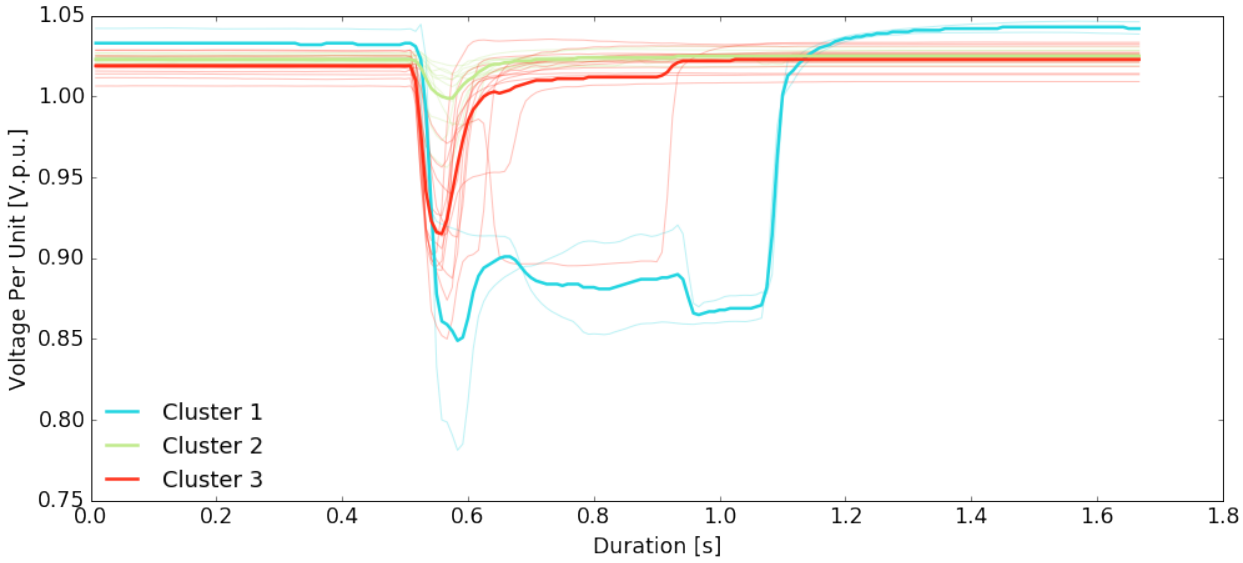


Source: Swenson et al. 2019

The algorithm returned three bold-colored average voltage sags that represent sags that fall into that particular cluster. The individual sags are plotted in a lighter color, in accordance to their cluster. This clustering portrays three archetypal events, where the red cluster corresponds to the most common voltage sag event at LBNL, the green cluster corresponds to voltage sags that occur asymmetrically where this phase is not directly affected, and the blue cluster corresponds to prolonged voltage sags that occur rarely but are distinct in their behavior. The most common event types, represented by the red and green clusters, display similarity in their evolution with time and differ greatly only in sag magnitude. Sags in both clusters take approximately 60 ms to reach their most severe point, and persist for 60 ms past the minimum voltage, making the most typical voltage sags at LBNL about 120 ms in duration, regardless of how deep the sag is. The red cluster was typified by a minimum voltage slope of around -6.67 to -11.67 percent per cycle and tended to sink to about 85 to 90 percent of the nominal value. Meanwhile, for the green cluster, the minimum voltage slope achieved was typically in the range of -1.67 to -3.33 percent per cycle and tended to sink no lower than 95 percent of nominal. The remaining cluster was an abnormally long one, indicated by the blue curve. This cluster sunk lower than the other two clusters, to about 80 to 85 percent, and achieved a more extreme voltage minimum slope of -11.67 percent per cycle on phase one. On phases two and three, the minimum voltage slope achieved for the long cluster was -55 percent per cycle and -21.67 percent per cycle, respectively. Correlations between the various parameters of each cluster can facilitate models which might seek to predict voltage sag severity or duration based upon minimum voltage slope.

## Parameter Clustering

Events may also be clustered based upon their parameters, such as magnitudes, slopes, or durations, calculated by the event parameterization script. The selection of parameter to be clustered is a complex problem of dimension reduction where the many parameters available

must be reduced to a simple subset. This is especially important due to the relatively small set of observations. To exclude phases that were not affected by the event, all observations were filtered by a minimal voltage of less than 95 percent of nominal system voltage. A correlation matrix was generated and four significant parameters were selected to feed the K-Means (MacQueen et al. 1967) clustering process: mean slope and duration in region 2, and minimal voltage and duration in region 3. The regions refer to the definitions established in the section Analysis. By analyzing the loss function of different number of clusters, an optimum of four clusters was chosen. The resulting clusters are shown in Figure 10.

**Figure 10: Parameter Clustering of Voltage Sags**

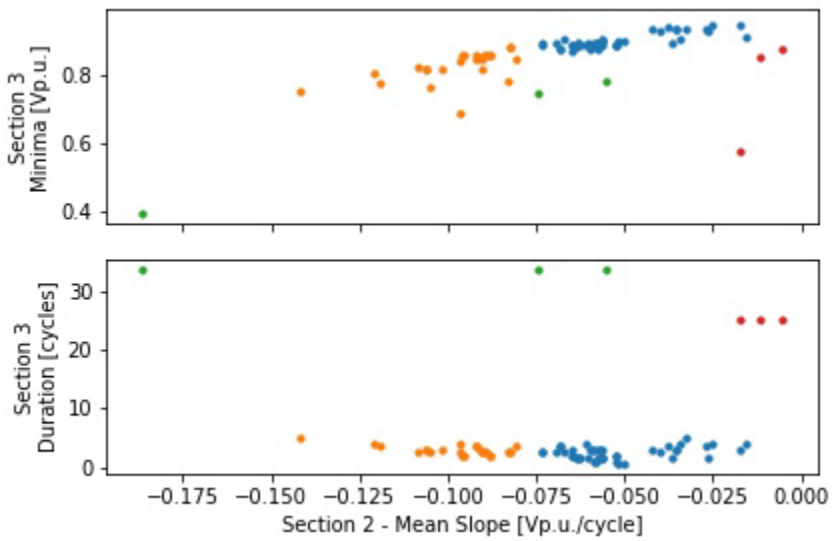


Source: Swenson et al. 2019

The result of the clustering reveals the dependence of the mean slope in the initial region 2 as a good indicator to predict the minimum voltage in region 3. The clustering automatically grouped the events by severity. The two outlier clusters, in green and red, can be further investigated using the duration of region 3, in the lower plot. Both outlier clusters were unusually long events, on the order of 20 to 30 cycles; whereas, all other events clear within 5 cycles. This method verifies the findings of the time-series clustering, which suggests a significant correlation of the initial slope and the severity of the event; that is, in Figure 10 the mean voltage slopes below -7.5 percent of nominal per cycle (in orange) are distinct from those above -7.5 percent (in blue).

## Timing and Communication Requirements

To implement effective smart inverter controls, inverters must be able to communicate with PMUs, detect abnormal grid conditions, and respond as quickly as it takes for an event to fully manifest itself, at a minimum. In the context of voltage sags, a maximum window of about 50 ms exists between event onset and the full extent of the voltage sag, within which the smart inverter must be able to act. From the parameters that might indicate the onset of a voltage sag, the most straightforward option is likely to be the slope of voltage magnitude. Given the

analysis of voltage sag clusters at LBNL, the emergence of voltage slopes around -2.5 to -7.5 percent per cycle seems likely to result in a minor voltage dip, while slopes lower than -7.5 percent per cycle are likely to result in more extreme voltage sags. These slopes present themselves early on in the sag, and so with rapid enough communication times, the smart inverter should be capable of acting to mitigate these events. Early tests using an embedded controller to ping LBNL's PMUs revealed average communication times, through non-deterministic Ethernet, of approximately 20 ms. This is just slightly under half of the time that a typical voltage sag takes to achieve its minimum value. In addition, the measured time constant of an external control setpoint change for the smart inverters at LBNL was about 33 ms. With this knowledge, the value of streaming the live 120 Hz data of potentially thousands of PMUs must be questioned. An alternative solution may be to process PMU data on the device, and communicate based on interrupts, in case of an event.

# CHAPTER 4:
# Modeling and Simulation

This chapter introduces an open-source package of simulation models in the context of smart inverter, battery storage, and distribution grids, and the simulation of variable voltage control setpoints for smart inverters. The Flexgrid facility is used for model development and validation.

## Model Environment

The simulation of distribution grids involves a variety of components, such as smart inverter, PV, battery storage, and distribution feeder models. In addition, control models representing the smart inverter capabilities of Volt-Var and Volt-Watt controls, where the reactive and active power output is regulated in accordance to locally observed voltages, are required. This mode of control is also described in California Rule 21 (CEC 2014). Modelica (Fritzson and Bunus 2002) is an open source modeling language allowing multi-domain simulations, and it is well suited to formulate models of the various components. It allows straightforward decoupling of model and solver due to the equation based formulation. Several tools are available to improve the usability with a graphical user interface and built-in debugger. Examples are the open-source tool OpenModelica[15] and the proprietary Dymola.[16] Other toolchains such as JModelica[17] allow the direct translation of simulation models into optimization problems, that is, to find the optimal size of PV installation, or to minimize the voltage impact of DER. All of the listed tools also support the compilation and export of models in compliance with the functional mockup interface (FMI) co-simulation standard[18] (Modelisar 2014), to use them for third-party applications. Modelica is also backed up by a large community that already developed a variety of model libraries relevant to power systems (Brkic et al. 2018; Einhorn et al. 2011; Vanfretti et al. 2016). This group also includes the Modelica Buildings library (MBL) (Wetter et al. 2014), which is a large ensemble of detailed building models as well as electrical power system models. One example of a simple capacitor model in Modelica is given in Figure 11.

The declaration of a model in Modelica starts with a model statement, followed by the model name. Variables are declared by their type, that is, Real, followed by the name. The declaration also allows some optional arguments such as unit, start value, or lower and upper bounds. Specifying units is a good practice to avoid the connection of incompatible components. In addition to the declaration itself, Modelica provides three basic types – parameter, input, and output – to externally interface with the model. Within the Modelica modeling area, models are represented as blocks with input and output connectors. In the example in Figure 11, the model

[15] OpenModelica. https://openmodelica.org/

[16] Dassault Systemes. DYMOLA Systems Engineering. https://www.3ds.com/products-services/catia/products/dymola/

[17] JModelica.org. https://jmodelica.org/

[18] Functional Mock-up Interface (FMI). https://fmi-standard.org/

would have voltage, *V*, as input connector; current, *I*, as output connector; and the capacity, *C*, as parameter. The model section is followed by the equation section and is completed with an end statement. Equations can be any mathematical formulation, including algebraic operations and derivatives.

**Figure 11: Simple Capacitor Model in Modelica**

```
model Capacitor
  parameter Real C( unit="F");
  input Real V( unit="V");
  output Real I( unit="A");
equation
  I = C * der(V);
end Capacitor;
```

Source: Lawrence Berkeley National Laboratory

# Model Development

The Flexgrid facility involves many basic components of power systems, as well as control loops and grid interaction through PMU sensors. While separate libraries exist (such as detailed battery or PV library), Flexgrid requires the combination of the many models. In addition, simulations should be conducted over longer time frames such as hours, days, or years to thoroughly assess the impact of PV and storage with seasonal effects. To fulfill these requirements, a model package – Smart Control of Distributed Energy Resources (SCooDER) – was developed in the Modelica framework. It relies on other libraries and introduces custom additions to better represent the Flexgrid installation. To illustrate the user interaction in Modelica, the full Flexgrid model is shown in Figure 12.

In Modelica, all models are delivered as blocks with inputs, outputs, and parameters. The blocks can be connected to form larger systems by the input and output connectors. The Flexgrid model is based on the physical infrastructure and components of Flexgrid. Here, a PV system (for example, *pv1*) and a battery (for example, *battery1*) are connected to a single-phase inverter (for example, *inverter1*). The pv system is fed by a weather input (*weaBus*) and a shading input (for example, *shade1*) to simulate shading of the PV string. The inverter provides an inverter control bus (for example, *invCtrlBus1*) which allows to control battery charging and discharging power, PV curtailment, and reactive power, and to read power flow, such as voltage and power data. This setup is duplicated two more times, and then connected to three single-phase transformers which are in turn connected in delta at the grid interconnection, within *mpz_dist*. A meter, *sens_FLEXGRID*, is added before the line of the Flexlab feed, *FL_feed*. Each model allows the setting of a number of parameters, which are described in detail in the following sections. The parameters are preset to reflect the Flexgrid setup, but can be simply overwritten by the user. An example parameter setup of inverter1 is shown in Figure 13. The dialog can be opened with a double-click on the model.

**Figure 12: Example Modelica Model of Flexgrid**

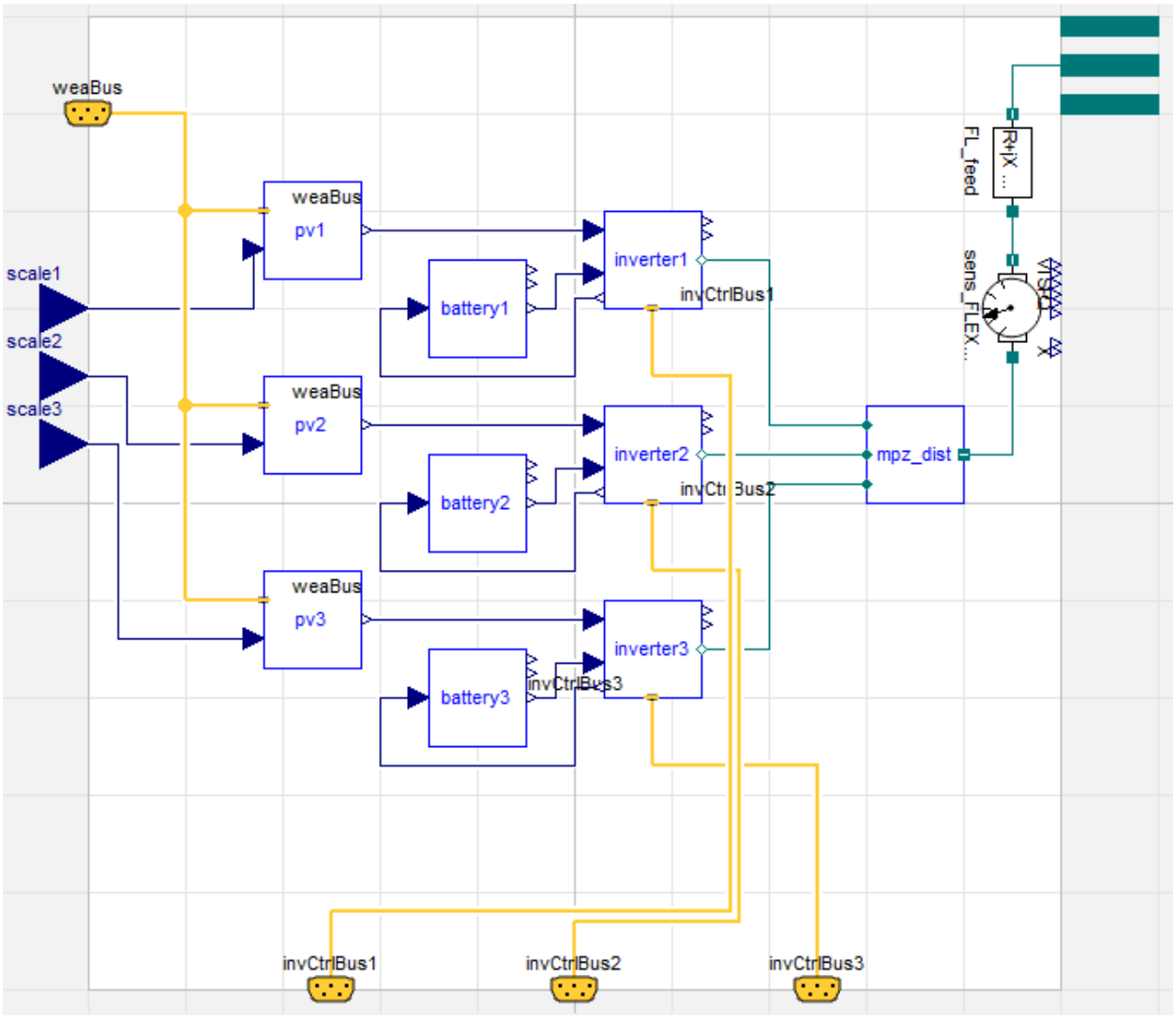


Source: Lawrence Berkeley National Laboratory

All parameters are preset with a value representing Flexgrid, which is indicated by the grayed layout. If a user would like to simulate an inverter with different parameter, the value can be simply overwritten, by typing into the field.

The next section describes a selection of the developed models and provides validation information for single components, partial systems, and finally, the full Flexgrid system.

**Figure 13: Example of Modelica Parameter Window**

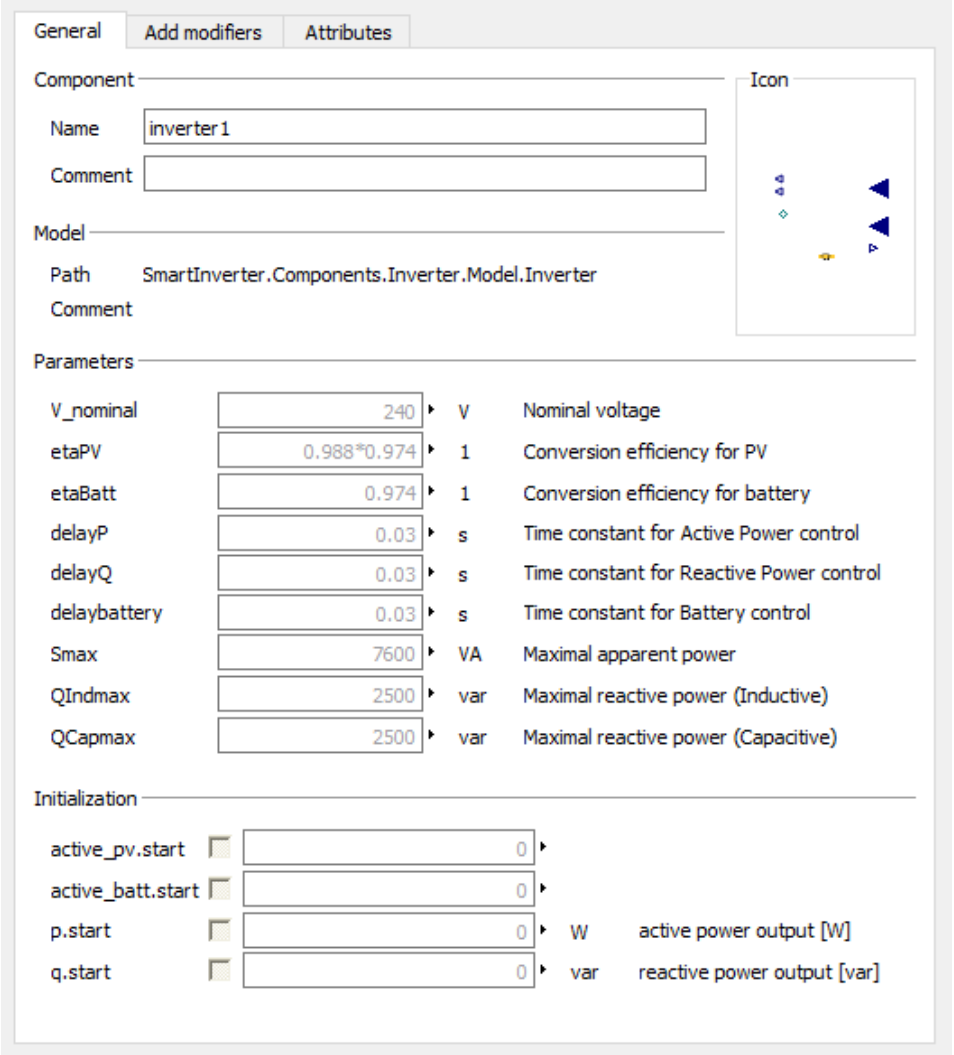


Source: Lawrence Berkeley National Laboratory

## Inverter Model

The inverter is the most detailed model within the SCooDER package, as this is the central point of research in the project. It is therefore required to accurately represent the behavior of SolarEdge's StorEdge[19] inverter installed at Flexgrid. Figure 14 shows the components and layout of the inverter model.

[19] SolarEdge. StorEdge. https://www.solaredge.com/products/storedge#/.

**Figure 14: Inverter Model in SCooDER Modelica Package**

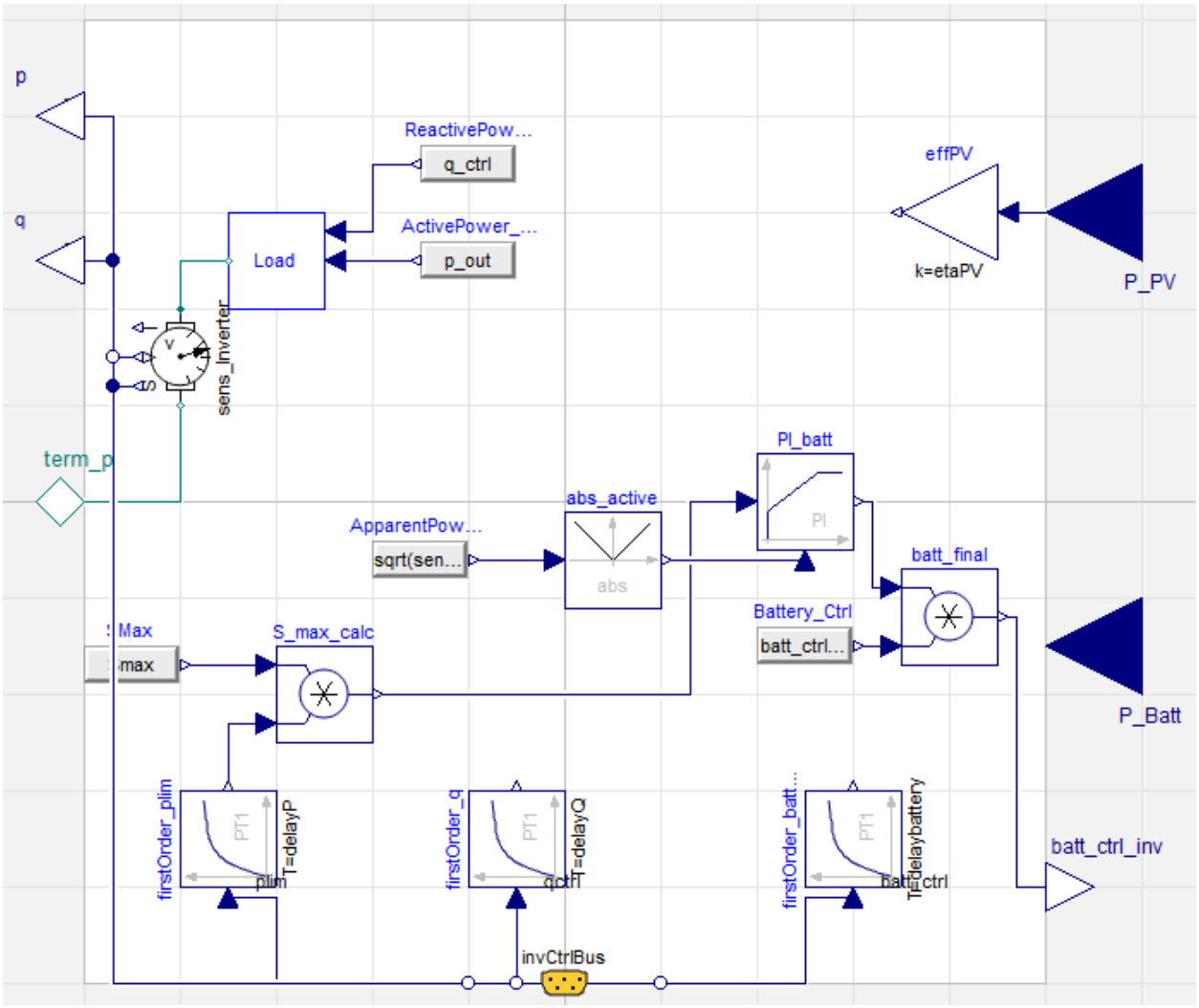


Source: Lawrence Berkeley National Laboratory

The model is defined by:

- Inputs
  - P_PV: Power generation of PV system, in Watts (W). Can only be positive.
  - P_Batt: Battery power demand (negative) or supply (positive), in W.
- Outputs
  - batt_ctrl_inv: Control output to control the battery through the inverter, in W.
  - p: Active power measurement on the AC side, in W.
  - q: Reactive power measurement on the AC side, in var.
- Connectors
  - invCtrlBus: A bus connector can combine any number of inputs and outputs into a single connector. The inverter control bus includes the curtailment of active

power, plim in %, regulate reactive power, qctrl in %, the battery control signal, batt_ctrl in W, and measurements of active power, p in W, reactive power, q in var, and voltage in V.

    - term_p: Connection point to the electrical grid which is defined by the Modelica Buildings library. It includes the voltage, v, and current, i, in complex form, and the reference phase angle, theta.

- Parameters: All parameters are pre-defined to the configuration of Flexgrid, but can be configured for any other inverter type.
    - V_nominal: The nominal system voltage, in V. Default is 240 V.
    - etaPV: Conversion efficiency of PV generation and DC/AC conversion. Default is 0.962.
    - etaBatt: Conversion efficiency of AC/DC or DC/AC battery conversion. Default is 0.974.
    - delayP: Time constant for active power control, in s. Default is 0.03 s.
    - delayQ: Time constant for reactive power control, in s. Default is 0.03 s.
    - delaybattery: Time constant for battery control, in s. Default is 0.03 s.
    - Smax: Total power limit of the inverter, in VA. Default is 7600 VA.
    - QIndmax: Inductive reactive power limit, in var. Default is 2500 var.
    - QCapmax: Capacitive reactive power limit, in var. Default is 2500 var.

The inverter was built to seamlessly connect to any grid model within the framework of the Modelica Buildings library, through the *term_p* connector. To model the StorEdge inverters that are installed at Flexgrid, the model can be simply dragged and dropped into the simulation setup within Modelica. If desired, an external PV generation can be connected to *P_PV* and an external battery can be connected to *P_Batt*. If no external model is connected, the inputs will default to 0 W to keep the structural integrity of the inverter model. If external control is enabled, that is, by a voltage-dependent control loop, then the *invCtrlBus* can be used. The SCooDER package includes a Volt-Var and Volt-Watt control, using the *invCtrlBus*. All inputs communicated to the inverter via the *invCtrlBus* are filtered by a first-order function to simulate the behavior of control execution time. Another input is *plim,* which is used to reduce the power limit in case of PV curtailment. In such case, the *Smax* parameter is linearly scaled down by the *S_max_calc* multiplication, on the lower left in Figure 14. The power limit is then passed along to the battery control Proportional Integral limiting controller, *PI_batt*, which scales the battery control signal, *batt_ctrl_filtered*. The control variable of *PI_batt* is the apparent power output measured at the AC interconnection at *sens_inverter*. The curtailment of PV generation is implemented as a secondary control action, once all battery power is curtailed to 0. This prioritizes the generation of PV over the discharge of battery power.

### Power Balance Control

To test the curtailment features, a test model was built (Figure 15).

**Figure 15: Inverter Power Balance Testing**

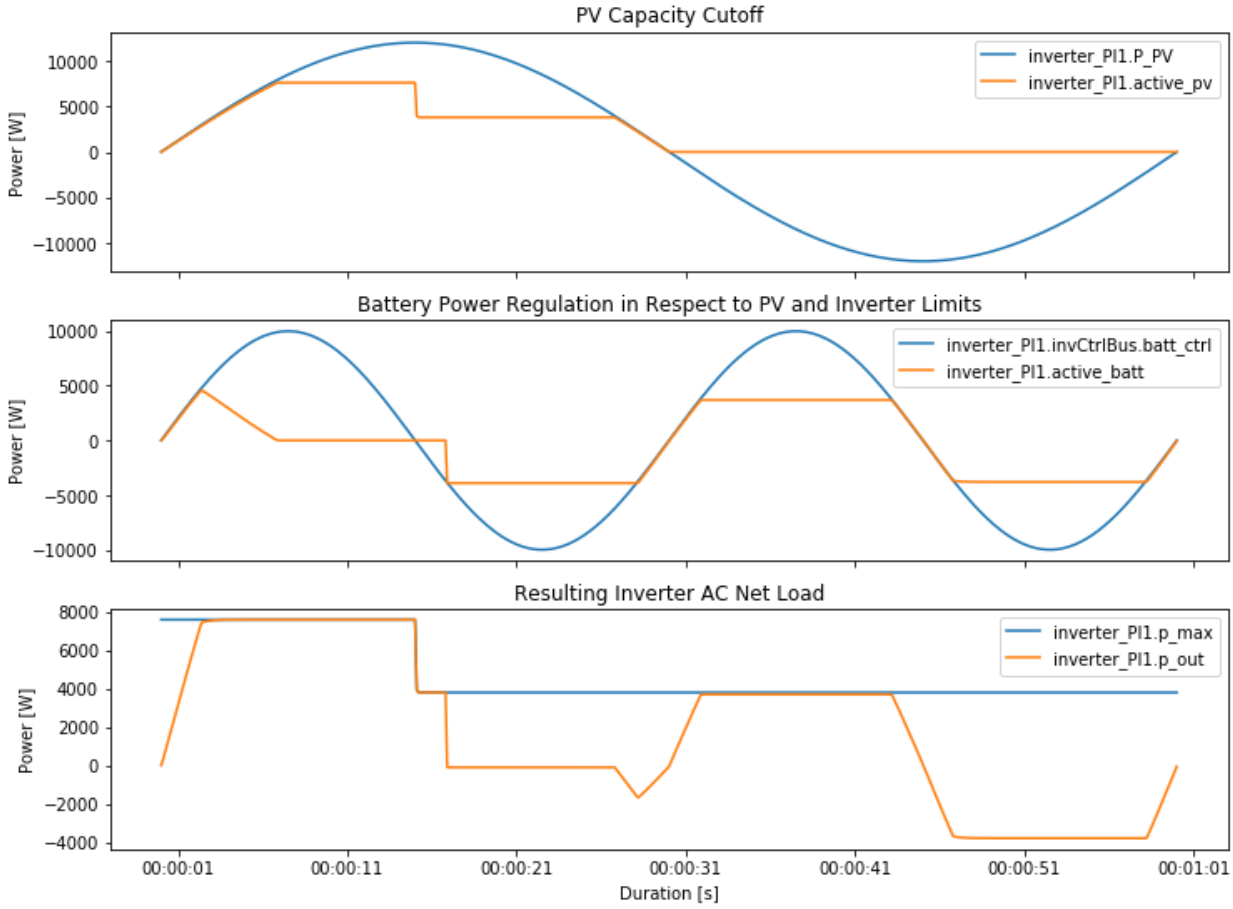


Source: Lawrence Berkeley National Laboratory

In this test, a simple model of sinusoidal PV generation with a magnitude of 12 kW and period of 60 s was used as input. Similarly, a sinusoidal battery control signal with a magnitude of 10 kW and half of the PV period, 30 s, was added. The battery was simplified and assumed to be of infinitive size for this test.

The first plot shows the PV generation in blue and the PV generation actually fed through the inverter in orange. At low generation levels below the inverter limit of 7.6 kVA, the inverter output increased at the same pace as the PV generation. Once the generation reached the inverter limit, the output stayed at its limit, while the PV generation was still rising. At 15 seconds a control action to curtail the inverter output to 50 percent was applied. As shown, the inverter almost instantly executed the control signal and curtailed the PV generation to 3.8 kW. When the PV generation is negative the output of the inverter is fixed to 0 due to the restriction that PV can only generate power, not consume it.

The second plot shows the coherent battery control for the same situation. At the beginning of the test, the battery power (in orange) followed the battery control signal (in blue). However once the PV generation, in the first plot, was high enough to reach the inverter power limit, the battery power started to decrease to meet the power limit of the inverter, until about 6 seconds, where battery power reached 0 W and PV started to get curtailed. The reduction of inverter curtailment at 15 seconds did not affect the battery power as it was already reduced to 0 W. However, when the battery control signal crossed the zero line, it started to charge the battery with a maximum of the negative curtailed power, which was again 3.8 kW. Going forward the PV generation reached 0 W, which allowed the battery to charge and discharge with the set inverter curtailment of 3.8 kW.

The last plot shows the resulting AC load in orange and the inverter power limit in blue. The stepped inverter curtailment can be clearly seen at 15 seconds, as well as the corresponding reduction in power output.

### Response Time Validation

While the control response in the simulation could be modeled as a step function, most physical devices have delays in executing commands and reaching setpoints. This is also the case for the inverters at Flexgrid. Figure 16 shows the measured performance of the inverter and the simulated result, when a step of power curtailment was applied.

**Figure 16: Validation of Transient Inverter Power Control**

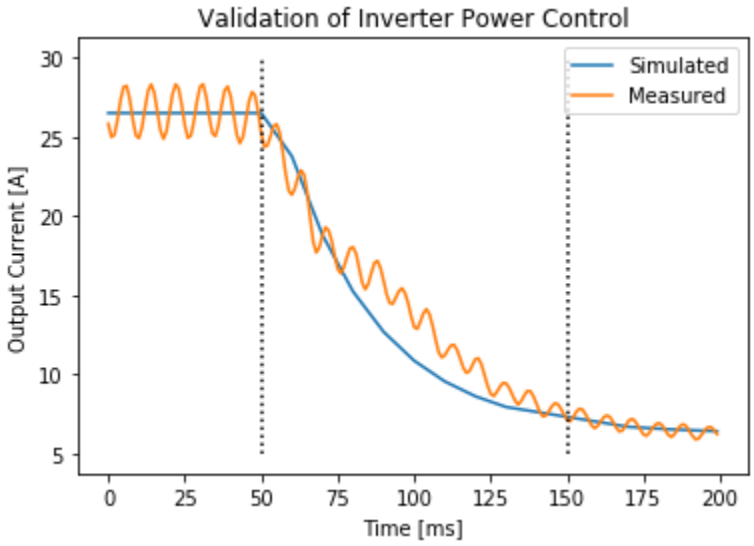


Source: Lawrence Berkeley National Laboratory

The measurements of the inverter show a transition of setpoints when changes were applied. Figure 16 shows the measured current, in A, for a single phase (in orange) and the simulation result of the inverter model in Modelica (in blue). The currents were recorded as sinusoidal measurements and post processed to root mean square values. The remaining oscillative behavior could be measurement error (that is, due to higher order transients) or the Maximum Power Point Tracker of the PV array. The whole transient event took 100 ms in total, starting

from 50 ms and ending at 150 ms. In this time the measurements transitioned from a current magnitude of about 26 A to 7 A in a near exponential function. The time constant for this transition was determined to be 33 ms, and set within the inverter model. The response of the Modelica model showed a very similar behavior by exponentially declining the current output. However, starting from 100 ms the measurements deviated from the simulation model, which could be due to measurement error, non-continuity in inverter control, or coincident change or response in grid conditions.

## Battery Model

The battery model is a more simplified model than the inverter, consisting of a state of charge (SOC) model with over- and under-charge limits. The efficiencies for charging and discharging were separately defined, as well as the total capacity, *E_max,* in watt-hours (Wh), and the minimal and maximal SOC levels. Input to the model was a control signal, *P_ctrl,* in W, and output was the actual battery power, *P_batt,* in W. The *SOC* and state of energy, *SOE,* are in Wh. The base model was taken from the MBL, *Buildings.Electrical.DC.Storage.BaseClasses.Charge*, and is based on Equation (1).

$$\frac{dSOC}{dt} = \frac{P\_batt}{E\_max} \tag{1}$$

### Energy Balance

To test the battery energy performance and compliance with SOC limits, a test example was developed (Figure 17).

**Figure 17: Battery Energy Balance Testing**

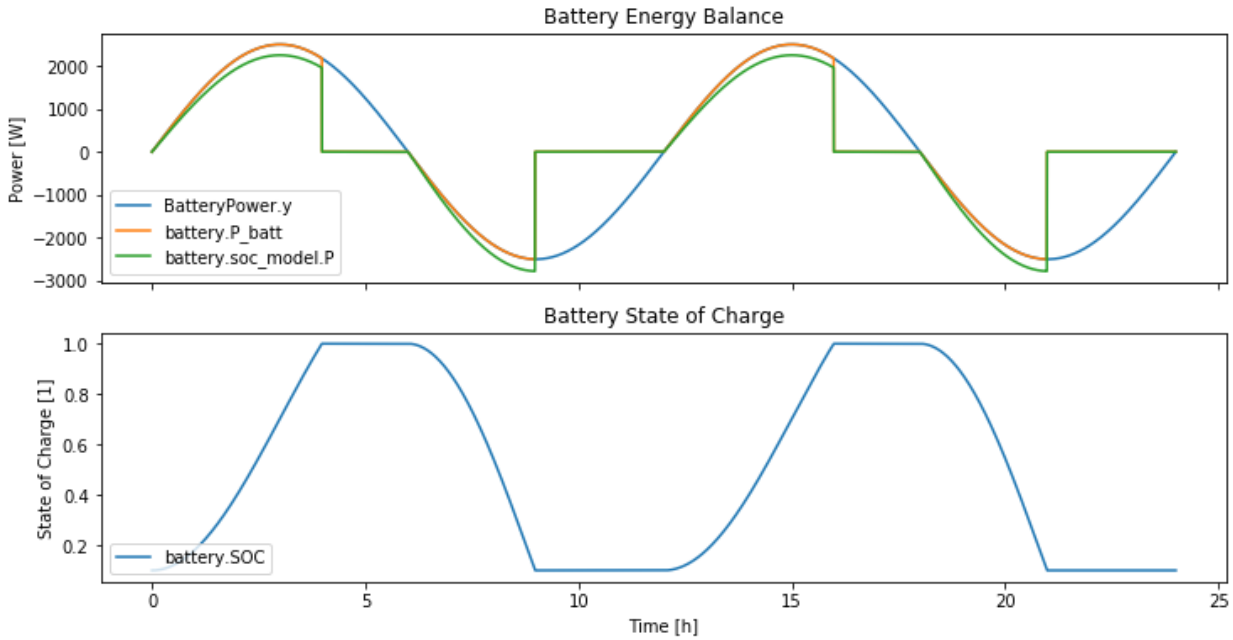


Source: Lawrence Berkeley National Laboratory

Here, a battery control signal, in blue, was modeled as a sinusoidal signal with a magnitude of 2.5 kW and a period of 12 hours. The battery power absorbed from the external sources, that is, the inverter, is shown in orange, and the battery power actually feeding into the SOC model in green. The difference between the absorbed power and the power in the SOC model is the efficiency of the battery, which was set to 0.96 for charging and 0.96 for discharging. The efficiency can be seen in the first plot, where the absorbed power followed the control signal while the SOC power was either below the absorbed power, when charged, or above it, when discharged. After about four hours the battery was fully charged, which caused the battery power to drop to 0 W. The cause can be seen in the lower plot showing the SOC in blue. The battery started with a SOC of 0.1 and SOC limits between 0.1 to 1. Once the battery reached a full state, here 1, the charging power stopped immediately. On the other hand, once the battery control requested to discharge, the battery started to discharge until the lower bound of SOC 0.1 was reached.

#### Model Validation

While the model proved to work on simulated data, a second validation was performed where the model input was defined by measured inputs during a test at Flexgrid, and model outputs were compared to measurements from Flexgrid. The battery was charged with a nearly constant power of 1.12 kW (C-rate of 0.175), with a short reduction in charging power for about 5 minutes. At the end of the charging period the measured SOC was 0.995, and the modeled SOC was 0.999. The marginal difference of 0.5 percent SOC is well below a threshold relevant for this project and also well below the estimated error of SOC measurements, which are on the order of ±2.5 percent.

## Photovoltaic Model

The PV model is a simplified efficiency model where the total solar irradiation is calculated for the tilted and rotated surface, and then multiplied with a static efficiency. The model was based on the MBL, *Buildings.Electrical.AC.OnePhase.Sources.PVSimple*, in conjunction with an anisotropic sky model (Perez et al. 1990).

## Other Models

A variety of supportive and utility models were also added to the library to facilitate usage. Examples are models to incorporate measurement data from PMU sensors, as voltage source within the simulation, and a variety of controls. The most relevant control for this project is a combined Volt-Var-Watt control where the reactive power and active power are regulated in respect to locally observed grid voltages. At its base, this control model consists of two models, one parameterized as Volt-Var and the other as Volt-Watt. It also introduces a higher level of detail, where the inverter output is limited by its apparent power limit and where active power is curtailed in favor of reactive power when reaching the limit. Figure 18 shows an example of its operation.

**Figure 18: Testing of Volt-Var-Watt Control**

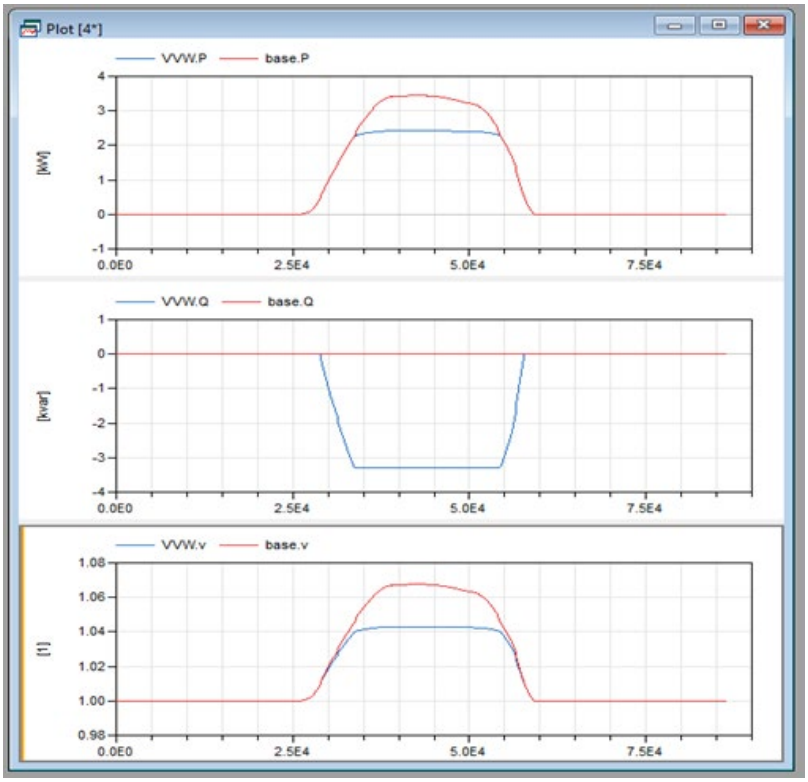


Source: Lawrence Berkeley National Laboratory

The figure shows the active power profile in the upper plot, reactive power in the middle plot, and the resulting local voltage in the lower plot. The response of a base case without control is shown in red, and the case with the Volt-Var-Watt control in blue. The controller provides reactive power support as voltage increases. Once the inverter reactive power limit was reached, the inverter started to curtail the active power in accordance to the voltage. The result was a peak nodal voltage of about 104 percent; whereas, the base case without control resulted in voltages above 106 percent of nominal.

## System Validation

This section describes two steps taken to validate the full Flexgrid model, consisting of a set of three inverters, batteries, PV arrays, and transformers, all parameterized to match Flexgrid.

The first step was the validation of PV generation profiles based on recorded historical weather at LBNL. A toolchain was developed in Python to automatically read the EnergyPlus Weather file (.epw), which is part of the input to Modelica, and to replace the typical meteorological year data with measurements from LBNL. The generated .epw file was then converted to an .mos Modelica readable file. This was done using the existing tool *ConvertWeatherData.jar,* which is part of the MBL. The next step was to determine shading levels from obstructions, which are not included in the model. Figure 19 shows an example screenshot from Google Maps. Note that this image does not show the PV installation, which is located on top of the two lower-bay testbeds on the left and right, marked in red.

**Figure 19: Illustration of Shading of Photovoltaics at Flexgrid**


Source: Google Maps

To model complex shading, time-varying shading profiles can be entered into the model. While these shading profiles could be generated by other simulation tools, a manual tuning for specific days was conducted for this validation. The validation was conducted for one sunny day on September 1, 2018. All parameters within the model were set to represent Flexgrid. The most distinguishing settings were the different sizes of PV. During the construction phase, the decision was made to split the 15 kW PV array into four strings, to feed the three single-phase inverters. The strings adjacent to the high-bay testbed in the middle were both connected to the same PV inverter to match the output to the other, unshaded systems. In reality the SolarEdge Power Optimizers, which are attached to each module to provide maximum power point tracking, are regulating the PV output of shaded and unshaded modules, which results in a power output almost twice as high as the lower-rated PV strings. The result of the model validation, which also shows the PV generation profiles of the individual PV strings, is shown in Figure 20.

The first plot shows the 15-minute solar profile for global horizontal irradiance, in watts per square meter ($W/m^2$). The profile is very smooth and representative of a clear and sunny day. The following three plots show the measured PV generation in orange and the modeled generation in blue for the three individual PV inverters. While the generation profiles match well, slight differences and variations can be observed. These could be attributed to the simulation only using averaged 15-minute data and to unaccounted environmental disturbances. The last plot shows the manually tuned shading parameter for the three inverters. It is clear that the PV array facing east, in green, is showing higher shading in the afternoon hours, when shaded by the high-bay testbed in the middle of Flexlab. On the other hand, the PV array facing west, in blue, shows higher shading in the morning hours. Finally, the PV arrays adjacent to the high-bay testbed show shading during the morning and evening hours.

**Figure 20: Validation of the Flexgrid Model in Modelica**

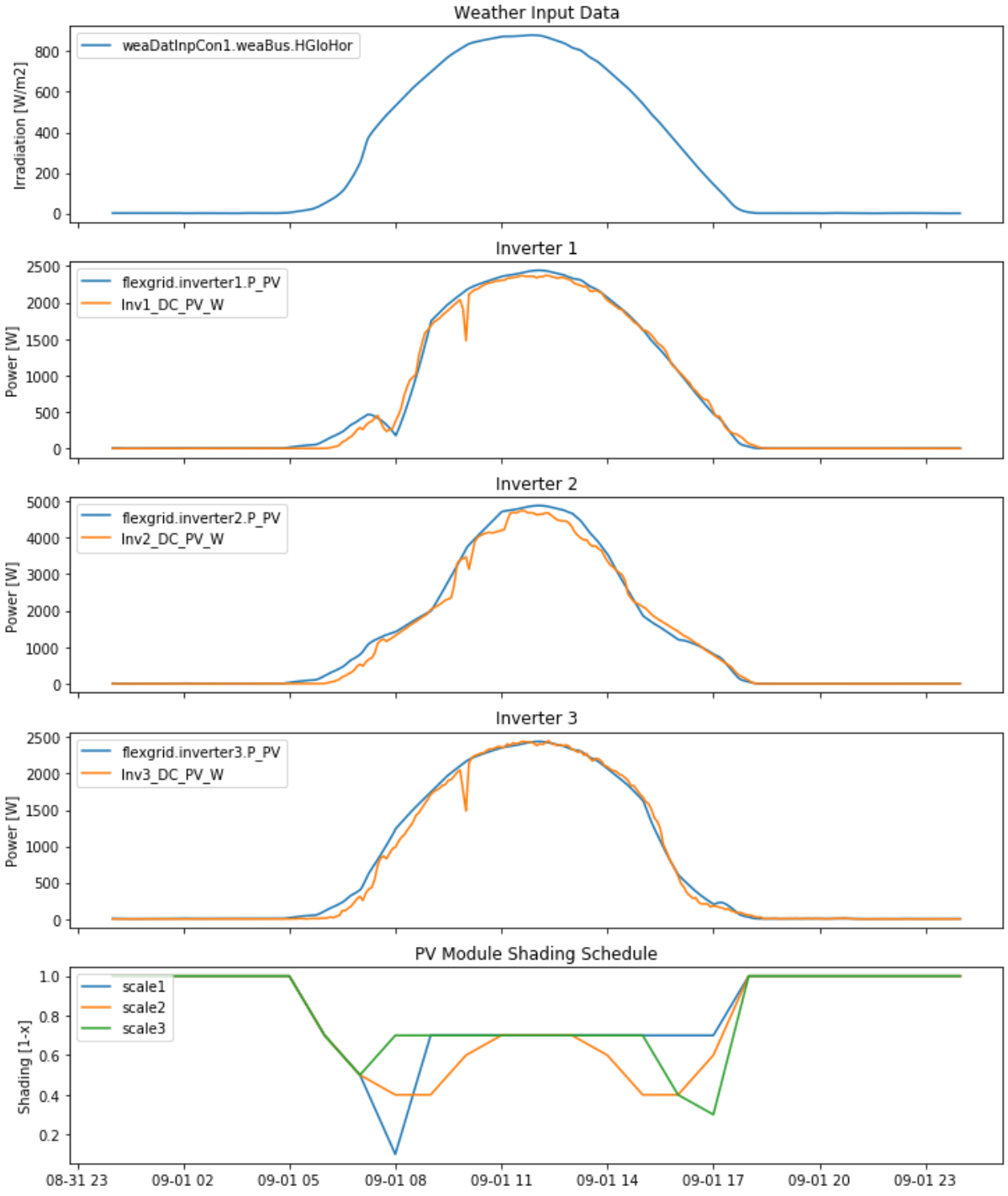


Source: Lawrence Berkeley National Laboratory

# Model Library

Figure 21 shows the basic structure of the developed SCooDER package.

**Figure 21: Structure of SCooDER Package**

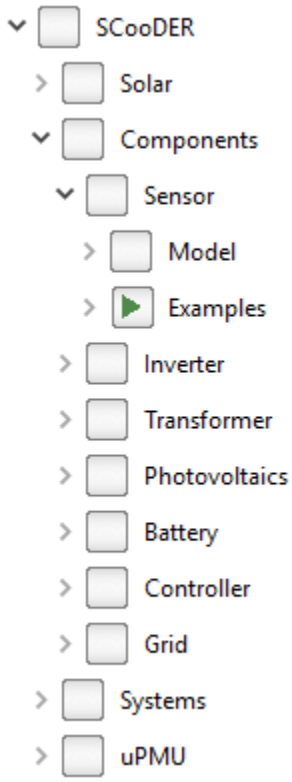


Source: Lawrence Berkeley National Laboratory

This SCooDER package consists of four main libraries, solar data calculation, component models, system models, and PMU data integration. Each library can consist of a number of sub-libraries that further populate until the models are reached. The Components library, for example, contains all the component models needed to form a Flexgrid model. This includes sensors, inverter, transformer, PV, battery, controller, and grid models. Each of these sub-libraries contains a library with the models (that is, Model) and one with examples (that is, Examples) to test the model. The systems library on the other hand includes partial or full system models. This package is open-source and available via download (Gehbauer 2019a).

# Dynamic Simulation

This section focuses on the testing and optimization of smart inverter controls, in accordance with California Rule 21 (CEC 2014). A Volt-Var control scheme is analyzed, which regulates the reactive power output in accordance to the local system voltage, to mitigate high voltages caused by distributed energy resources (DER).

To conduct this study, a feeder model with dynamic PV generation and dynamic loads was required, to accurately capture the dynamics of voltage support during extended periods of time. Compared to a dynamic setup, static or quasi-static time series models would only provide snapshot analytics without the transient behavior of the Volt-Var control. The challenge is that the majority of open-source feeder models and simulators are in the quasi-static time domain. This project developed a dynamic feeder model, based on the IEEE 13 prototypical

feeder model (IEEE 2000), within the framework of Modelica. The IEEE 13 model has a standardized base, is easy to replicate and is widely known in the research community.

Load profiles were gathered from the USDOE prototypical buildings' simulations (Deru et al. 2011) and were assigned to nodes along the feeder using a developed dynamic load generator. PV was evenly distributed along the feeder, and simulated in scenarios of 0, 25, 50, 75, and 100 percent of PV penetration. Initial simulations were conducted for a full year to identify the peak day of the year for each PV penetration scenario. In a second step, the simulations were limited to only this day, and a framework was developed to allow a parameter sweep through Volt-Var configuration. The parameter sweep was conducted using a grid-search methodology, where an evenly sized grid of Volt-Var parameters was tested. Finally, the parameter optimization was conducted in two setups: one where all inverters along the grid used the same setpoints, which is the typical configuration of utilities, and one where inverters were grouped into clusters and individual parameters were assigned.

## Feeder Model

The feeder was modeled in the Modelica environment as a variant of the IEEE 13 prototypical feeder model. The Modelica Buildings library provides a convenient template to rapidly design new feeder models based on existing or new types of lines. A simple connection list was written in Modelica describing the line segments between nodes by their length, type, and nodal connection. Figure 22 shows the developed feeder as a variant of the IEEE 13 prototypical feeder model.

**Figure 22: Modeled IEEE 13 Feeder**

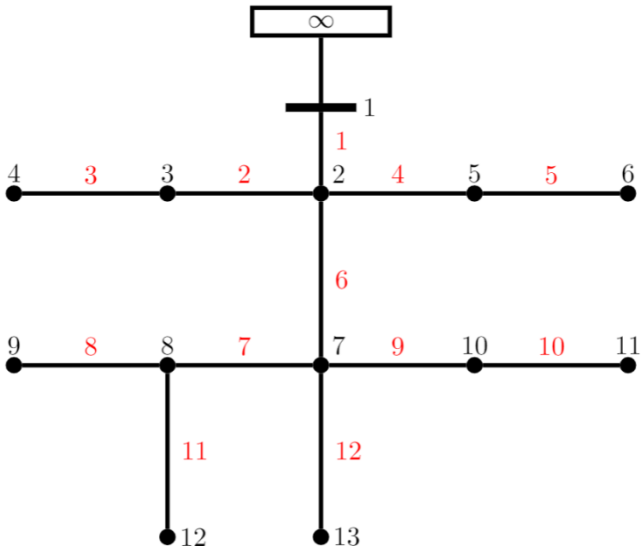


Source: Lawrence Berkeley National Laboratory

The numbering of nodes and lines was replaced by a continuous count from 1 to 13 for nodes and 1 to 12 for lines. The black numbers indicate nodes and the red numbers lines. The transformer between nodes 5 and 6 and the switch between nodes 7 and 10 were replaced by line segments. These modifications were made to simplify the model, because neither a

transformer nor a switch were required to meet this project's objective, and they would have increased the model's complexity and simulation time. Furthermore, all original lines were replaced by Aluminum cables of equivalent length, to simplify the model generation process by leveraging existing models from the MBL. The selected line types, lengths, and reactances can be seen in Table 1.

**Table 1: Feeder Line Parameters**

| line | length [m] | area [mm$^2$] | R/l [Ω/m] | X/l [Ω/m] | R [Ω] | X [Ω] |
|---|---|---|---|---|---|---|
| 1 | 610 | 120 | 2.7e-4 | 7.1e-05 | 0.164 | 0.0433 |
| 2 | 150 | 70 | 5.1e-4 | 7.2e-05 | 0.076 | 0.0108 |
| 3 | 90 | 35 | 9.2e-4 | 7.4e-05 | 0.083 | 0.0067 |
| 4 | 150 | 70 | 5.1e-4 | 7.2e-05 | 0.076 | 0.0108 |
| 5 | 90 | 35 | 9.2e-4 | 7.4e-05 | 0.083 | 0.0067 |
| 6 | 610 | 120 | 2.7e-4 | 7.1e-05 | 0.164 | 0.0433 |
| 7 | 90 | 70 | 5.1e-4 | 7.2e-05 | 0.046 | 0.0065 |
| 8 | 90 | 35 | 9.2e-4 | 7.4e-05 | 0.083 | 0.0067 |
| 9 | 90 | 70 | 5.1e-4 | 7.2e-05 | 0.046 | 0.0065 |
| 10 | 150 | 35 | 9.2e-4 | 7.4e-05 | 0.138 | 0.0111 |
| 11 | 240 | 35 | 9.2e-4 | 7.4e-05 | 0.222 | 0.0178 |
| 12 | 300 | 35 | 9.2e-4 | 7.4e-05 | 0.277 | 0.0222 |

Source: Lawrence Berkeley National Laboratory

The whole feeder model consists of a variety of three different cable types – 120, 70, and 35 square millimeter (mm²) Aluminum cables – and the line length in correspondence with the original IEEE 13 model. The line types were selected based on the original lines and a feeder head voltage of 4.12 kV.

## Dynamic Load Profiles

The IEEE 13 feeder is defined by a single point of operation. However, the objective of this analysis was the optimal setting of voltage-supporting parameter during load-varying conditions throughout days, weeks, or seasons. To fulfill the dynamic load requirement, a random load allocation (RLA) algorithm was developed to use a limited set of load profiles and allocate them to nodes along the feeder.

The first step to create the dynamic feeder model was to gather typical load profiles for California electricity customers. Due to the lack of available open source data for residential users, only data for commercial users was used. The selected load profiles of commercial customers are available in USDOE's open energy information (OpenEI) database (Brodt-Giles 2012). This dataset uses the 16 USDOE commercial reference buildings and simulates their electricity consumption with typical meteorological year weather data of the chosen location. The load data used in this project was based on the San Francisco weather data.

## Random Load Allocation

While the three biggest OpenEI loads – hospital, large office building, and secondary school – are an order of magnitude larger than the IEEE 13 model loads, most other loads are significantly smaller. Thus, it is not possible to directly assign the OpenEI loads to nodes with the original IEEE 13 loads. An approach was developed to allow some loads to be manually assigned to nodes, and scaled down to the peak value, in accordance with IEEE 13, while the remainder of the nodes used randomly assigned load profiles with a peak-power equivalent to the original IEEE 13 loads. The hospital was manually assigned to one of the most stable electrically nodes, node 7, as a balanced three-phase load. Similarly, the secondary school was assigned to another centered node, node 2, as a balanced three-phase load. The large office was not further used in this allocation process due to its similarity with smaller-scale medium and small office buildings, which are more flexible to assign. The remaining 13 loads were assigned using the random load allocation (RLA) algorithm developed for this project. This algorithm adds random loads from the OpenEI loads to each phase at each node, until the annual peak load at this phase and node exceeds the assigned power in the IEEE 13 model, denoted in Table 2. This function is called for every phase at every node until all the nodes have random loads assigned. To make the random results replicable, seeds, which are fixed start points for random load generators, were used for the random generator. With a specific seed, the random function always produces the same random output.

The algorithm is initialized with an assignment of the random seed, which can be any real number, and the peak load to be reached. The RLA then selects a random initial load from the available OpenEI loads and starts the allocation process. An initial step checks if the current peak load is lower than the target peak. If it is below the limit, then another random load is added to the current load profile. To select this new random load, the seed is increased by 1 at each step. This load addition is repeated, until the peak load is higher than the targeted peak. To avoid overlapping seeds during this allocation process, the numbers of node and phase were combined and multiplied by a factor of 1000. For example, the seed for node 12 and phase 2 would be 122000, for node 6 and phase 1 it would be 61000, and for node 6 and phase 2 it would be 62000. During the allocation process this number is increased by one, so assuming it takes three iterations to build up the load profile, the seeds would be 62000, 62001, and 62002 for node 6, phase 2. In case of a balanced three-phase load, the same initial seed can be supplied for all three phases, which would result in the RLA selecting the same loads for each phase. The resulting load profiles were exactly the same, representing a balanced three-phase system. However, the only balanced node in the system was node 7, where the hospital was manually assigned.

While the RLA was assigning active power loads to the nodes, another process was applied to assign reactive power to the nodes. Here the active power profiles generated by the RLA were multiplied with the reactive power peak load, Q, and divided by the active power peak load, P. In other words, the profiles for Q were assigned proportional to P, with a different multiplier for every node, depending on the specified values for maximum active and reactive power.

When applying the RLA algorithm to the feeder model, the resulting loads were to some extent higher than specified within the IEEE13 model. This results in voltage dropps below 95 percent of the nominal voltage for several nodes, for the most critical day of the year. According to the American National Standards Institute, voltages below 95 percent of nominal for an extended period of time are seen as voltage violations (ANSI 2016). To prevent those voltage violations, the original IEEE 13 loads were scaled down until no more voltage violations occurred. The final load table, which was used for the RLA algorithm, can be seen in Table 2.

**Table 2: Original IEEE13 Load Table**

| node | connection | $P_1$ [kW] | $Q_1$ [kVar] | $P_2$ [kW] | $Q_2$ [kVar] | $P_3$ [kW] | $Q_3$ [kVar] |
|---|---|---|---|---|---|---|---|
| 1 | | 0 | 0 | 0 | 0 | 0 | 0 |
| 2 | Y | 10 | 6 | 39 | 22 | 70 | 40 |
| 3 | Y | 0 | 0 | 102 | 75 | 0 | 0 |
| 4 | Y | 0 | 0 | 138 | 79 | 0 | 0 |
| 5 | | 0 | 0 | 0 | 0 | 0 | 0 |
| 6 | Y | 96 | 66 | 72 | 54 | 72 | 54 |
| 7 | Y | 231 | 132 | 231 | 132 | 231 | 132 |
| 8 | | 0 | 0 | 0 | 0 | 0 | 0 |
| 9 | Y | 0 | 0 | 0 | 0 | 102 | 48 |
| 10 | Y | 0 | 0 | 0 | 0 | 102 | 90 |
| 11 | Y | 291 | 114 | 40 | 36 | 174 | 127 |
| 12 | Y | 76 | 51 | 0 | 0 | 0 | 0 |
| 13 | | 40 | 36 | 174 | 127 | 291 | 114 |

Source: Lawrence Berkeley National Laboratory

The loads were significantly decreased, up to 40 percent, to keep voltages above the 95 percent threshold. The reason for this high scaling factor was a compounded error of different feeder topology, line types, connections, and overshooting of the RLA, in comparison to the original IEEE 13 model. However, the feeder model was still representative of a real system with a diversity of load profiles along the different nodes.

In Figure 23, the resulting power and voltage profiles for the generated feeder model are illustrated for two example days. The days represent the peak day of the year, with the lowest measured voltages, and a low-load Sunday in January.

The blue line in Figure 23 shows the active power, and the green line the reactive power, of Phase 3 at the feeder head. Phase 3 was chosen because it has the highest and therefore most critical load. The peak load was approximately 2.5 megawatts (MW) and 1.4 mega volt amps reactive (Mvar). At the low-load Sunday, the peak load was only 1.1 MW and 0.7 Mvar. The shape of active and reactive loads is similar due to the fixed relationship of active and reactive power, by the power factor. To further analyze the load distribution, Figure 24 shows the loads at each node along the grid.

**Figure 23: Power Flow at Feeder Head on Peak- and Low-Load Day**

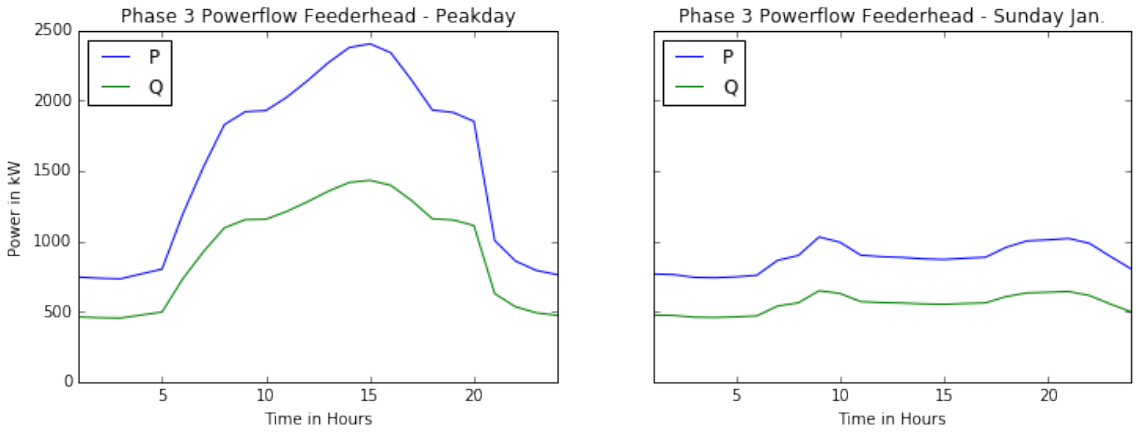


Source: Lawrence Berkeley National Laboratory

**Figure 24: Nodal Power Flow on Peak- and Low-Load Day**

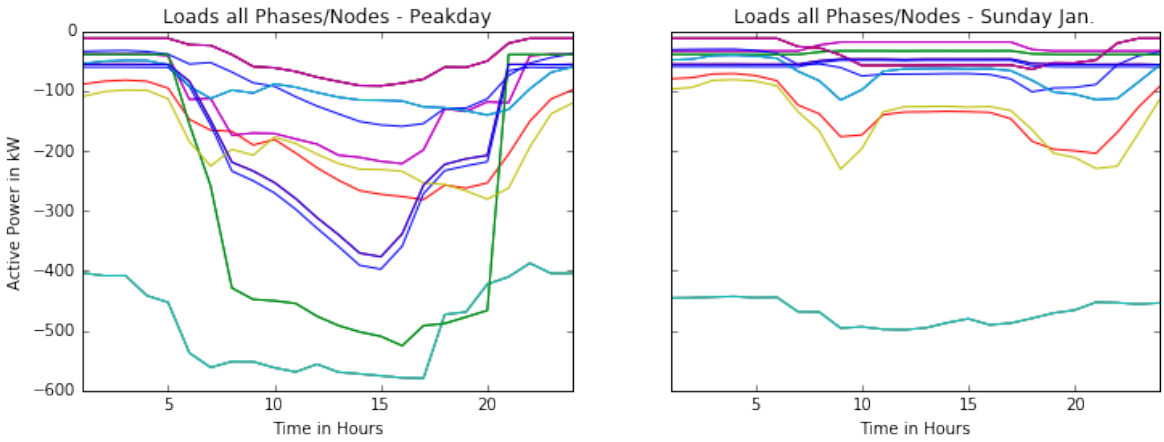


Source: Lawrence Berkeley National Laboratory

The variety of loads was based on the RLA process. Some profiles have a strong similarity to each other, while others are quite different. Some loads overlap, which leads to less visible profiles. Also the balanced loads from the hospital and the secondary school are equivalent for the three phases, and therefore only visible as a single line. Figure 25 shows the voltage distribution of all phases and nodes along the feeder.

A voltage variety between 95 to 98 percent of nominal was present at the most critical point in the afternoon of the peak day. On the Sunday in January, the lowest voltage was approximately 98 percent of nominal. The profiles appear to be uniform due to the stiffness of the feeder model with relatively short line segments, and only two branches each. This process of verification finished the development of the dynamic feeder model as base case. To conduct the specific study of optimal voltage-dependent control settings for smart inverter, this base case was extended to include PV generation at selected nodes.

**Figure 25: Nodal Voltages on Peak- and Low-Load Day**

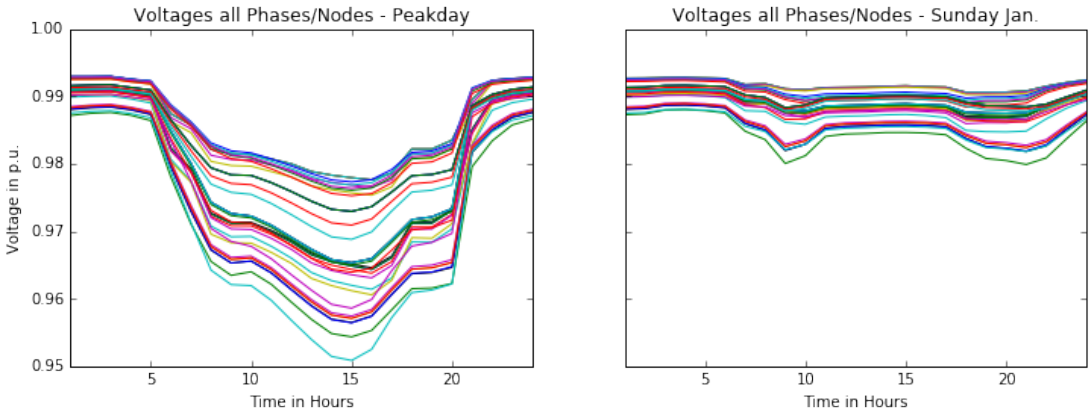


Source: Lawrence Berkeley National Laboratory

## Photovoltaic Allocation

The PV allocation is a simplified assignment algorithm where equally sized PV systems are evenly distributed along the feeder. To reflect situations of varying PV penetration levels, from 0 to 100 percent, it was assumed that every other node was equipped with a PV system. In the feeder model only 10 nodes have a load consumption, which results in 5 nodes of PV generation. To model the distribution of PV throughout the nodes, an even distribution between the electrical impedances of the nodes to the feeder head was applied. Therefore, the electrical resistances, reactances, and impedances for each node to the feeder head were calculated, and the results are presented in Table 3.

**Table 3: Nodes Sorted by Electrical Distance**

| Node | R to feeder [Ω] | X to feeder [Ω] | Z to feeder [Ω] |
|---|---|---|---|
| 13 | 0.605 | 0.109 | 0.615 |
| 12 | 0.595 | 0.111 | 0.606 |
| 11 | 0.512 | 0.104 | 0.523 |
| 9 | 0.457 | 0.100 | 0.468 |
| 10 | 0.374 | 0.093 | 0.385 |
| 8 | 0.374 | 0.093 | 0.385 |
| 7 | 0.328 | 0.087 | 0.339 |
| 6 | 0.323 | 0.061 | 0.329 |
| 4 | 0.323 | 0.061 | 0.329 |
| 5 | 0.240 | 0.054 | 0.246 |
| 3 | 0.240 | 0.054 | 0.246 |
| 2 | 0.164 | 0.043 | 0.170 |
| 1 | 0 | 0 | 0 |

Source: Lawrence Berkeley National Laboratory

The red rows are the nodes without any loads, blue rows show the nodes with assigned PV generation, and the black rows are for nodes with load only. To calculate the impedances from nodes to the feeder head, all the segments of lines to the feeder head were summed. The nodes

were sorted by their impedances to the feeder head and a PV system was assigned to the node with the highest impedances. Moving toward lower impedances, PV was assigned to every second node with load consumption. Note that due to initial problems with the model, the PV system at node 10 was moved to node 9.

The PV generation was split into five scenarios, where the PV penetration was set to 0, 25, 50, 75, and 100 percent of the annual energy demand. A basic PV system was created and scaled up to fit those demands. Each PV panel of the basic PV system has a size of 1.65 m² and an efficiency of 0.158, which results in a power output of 260.7 W per module at standard test conditions (STC). This model was designed using operational data from the Flexgrid facility. Each PV system has an inverter with a maximum apparent power of 7,600 VA and a maximal power factor of 0.9 at peak power. The inverter can accommodate up to 30 PV modules, but only 26 panels were assigned per inverter, to allow a certain capacity range for reactive power control without curtailing the active power generation. This number of panels was determined by a calculation of the maximum apparent power of the inverter multiplied with the power factor and divided by the rated power, shown in Equations (2) and (3).

$$P = S \cdot pf \ = 7600\,VA \cdot 0.9 = 6840\,W \tag{2}$$

$$\frac{6840\,W}{260.7\,W/panel} = 26.24\,panels \tag{3}$$

The applied power factor allows the inverter to still provide or absorb reactive power of up to 3313 var, which results from the following Equation (4):

$$Q = \sqrt{S^2 - P^2} = \sqrt{7600^2 VA^2 - 6840^2 W^2} = 3313\,var \tag{4}$$

The annual PV generation of the feeder for one PV system for each phase at each of the five chosen nodes, here called E_PV, is 206.3 megawatt-hours per year (MWh/a). The energy consumption E_load without PV generation is 27,788.2 MWh/a. Therefore, the amount of PV systems needed to generate 100 percent of the annual electricity consumption can be calculated by dividing the annual consumed energy with the annual generated energy per PV system. This calculation is shown in Equation (5).

$$\frac{E_{load}}{E_{PV}} = \frac{27{,}788.2\,MWh}{206.3\,MWh} = 134.7 \tag{5}$$

The PV generation for the 100 percent scenario was multiplied by 0, 0.25, 0.5, 0.75, and 1, depending on the penetration scenario. This resulted in 0, 34, 67, 101, and 135 PV systems at each of the three phases and each of the five chosen PV nodes. These are 0, 102, 201, 303, and 405 PV systems at each of the nodes or 0, 510, 1005, 1515, and 2025 individual PV systems in the whole feeder.

## Results

The results of the varying PV penetrations for the day with the highest voltage are shown in the following section. Figure 26 shows the active power in blue and the reactive power in green for phase 1 at the feeder head.

**Figure 26: Power Flow at Feeder Head for the Peak Photovoltaic Generation Day with Different Penetrations**

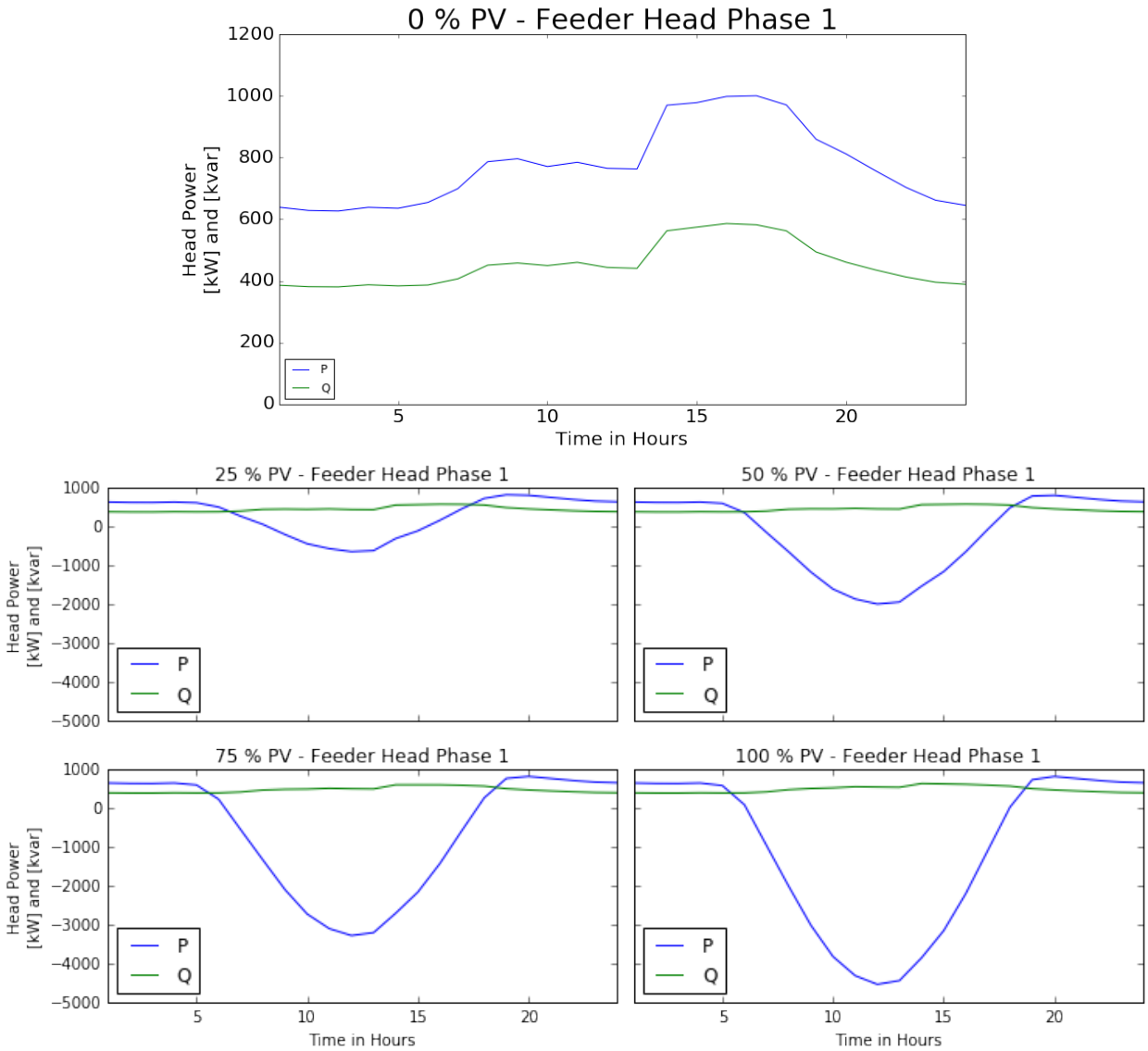


Source: Lawrence Berkeley National Laboratory

Since Volt-Var control was not activated in this scenario, the reactive power was always positive, as a result of load demand and line impedance. It is clearly visible how increasing PV offset the load during the daylight hours. Reverse power flows were apparent in all the PV scenarios. While in the first case the reverse power flow was less than the load demand, all other cases starting from 50 percent penetration showed a reverse power flow as multitudes of

the peak load demand. This could cause overloading of the feeder by exceeding the maximal rated system currents. Figure 27 shows the active power at every phase and node.

**Figure 27: Nodal Power Flow for Peak Photovoltaic Generation Day with Different Penetrations**

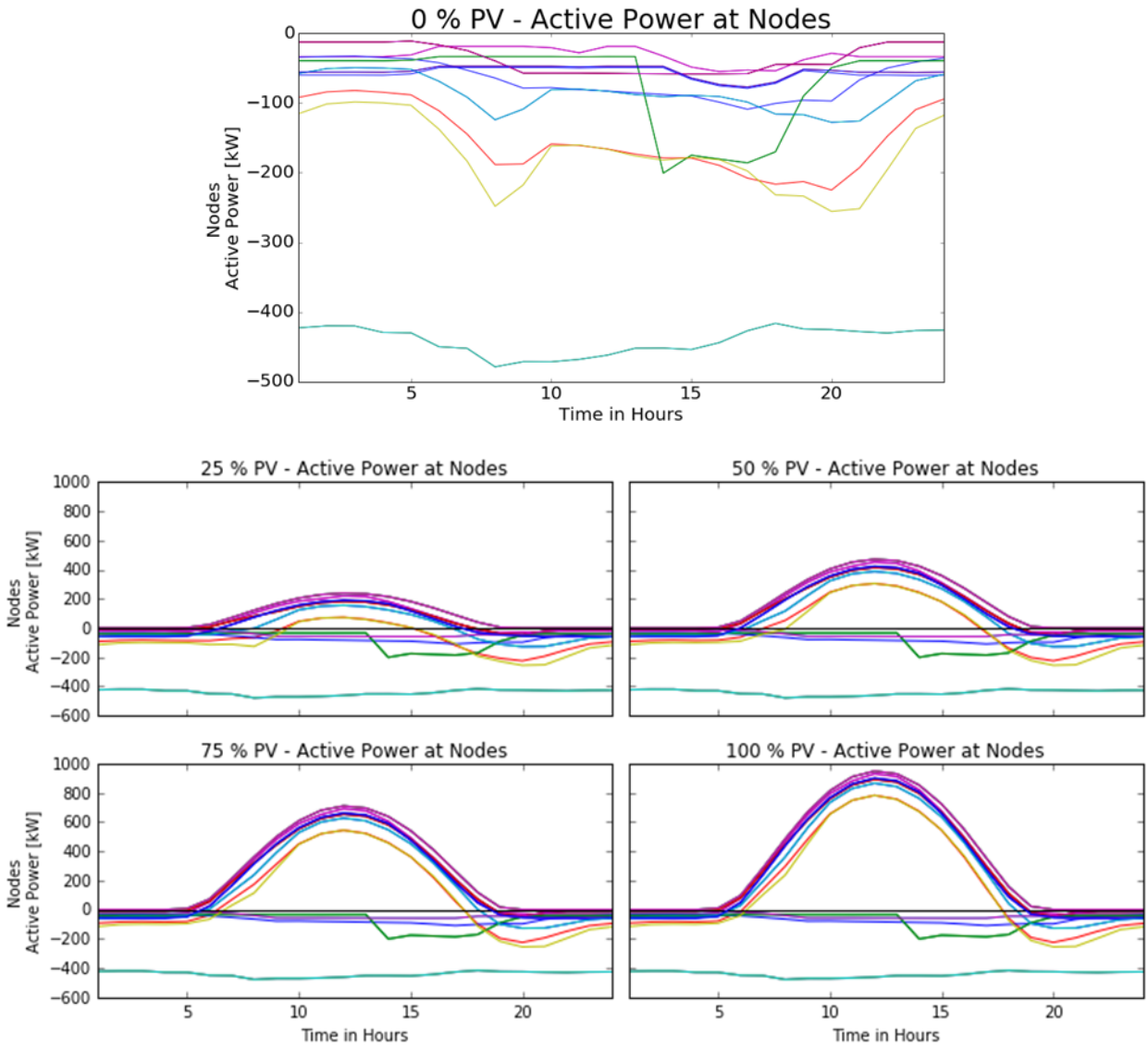


Source: Lawrence Berkeley National Laboratory

The first part, with 0 percent PV, shows the loads of the day only. The turquoise line represents the load of the hospital at node 7, and the dark green line represents the secondary school at node 2. As no PV systems are installed at nodes 2 and 7, the loads at these nodes remain the same in all scenarios, which can be seen in the illustrations with PV generation. It is again clearly visible how PV offset the load. Figure 28 illustrates the resulting nodal voltages for the different PV penetrations.

**Figure 28: Nodal Voltages for Peak Photovoltaic Generation Day with Different Penetrations**

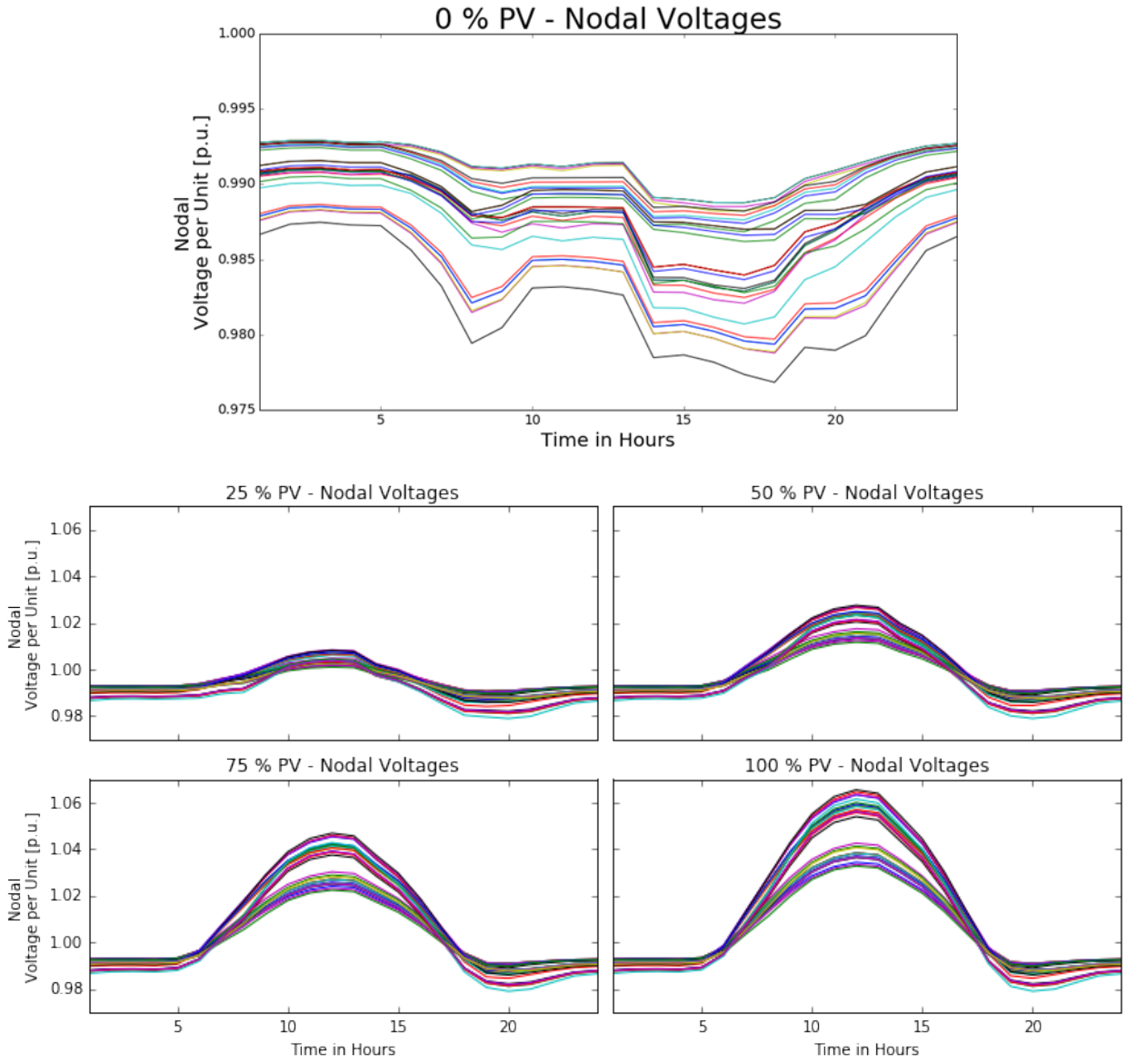


Source: Lawrence Berkeley National Laboratory

While the voltages without PV generation remained below the nominal system voltage, the voltages rose to approximately 101 percent with only 25 percent annual PV generation. With an increasing PV amount, the uncontrolled voltages increased to more than 106 percent of nominal in the 100 percent penetration scenario.

# Control Parameter Optimization

To optimize the Volt-Var setpoints of the inverters, a grid search was used, where many combinations of control setpoints were simulated and evaluated. The user sets the minimum and maximum values, and the step size in between those points, for every optimization variable. With this given grid of parameters, the algorithm then simply tries all possible

combinations of these variables and returns the optimal result. The advantage of the grid search is that it can optimize any kind of problem. Also, all kind of different outputs can be saved to a result table and afterwards analyzed and optimized for different research questions. The biggest disadvantages are the long computation time and that it tries points in a fixed grid.

## Experimental Setup

For the optimization setup, the grid search was applied to the most critical day of high voltage, which is June 17. That day was chosen to optimize for the best Volt-Var control settings. The simulation inputs, which were optimized by the algorithm, are the hysteresis and threshold ranges of each PV system installed in the grid. The *hysteresis*, which also can be referred to as dead band around the nominal voltage, is the parameter where the inverter is not providing any reactive power. When the voltage rises or falls outside the hysteresis, the linear response is activated where reactive power is absorbed or injected as a linear function of voltage. With further increasing or decreasing voltage, the inverter saturates at the maximal reactive power. This setpoint is called *threshold* as a delta from nominal system voltage. Figure 29 shows an example of Volt-Var settings, with a hysteresis of 0.02 per unit and a threshold of 0.05 per unit. The voltages, where the hysteresis range ends, are 98 and 102 percent of nominal. The setpoints, where the threshold range ends, are 0.95 and 105 percent of nominal.

**Figure 29: Volt-Var Parameter Definition**

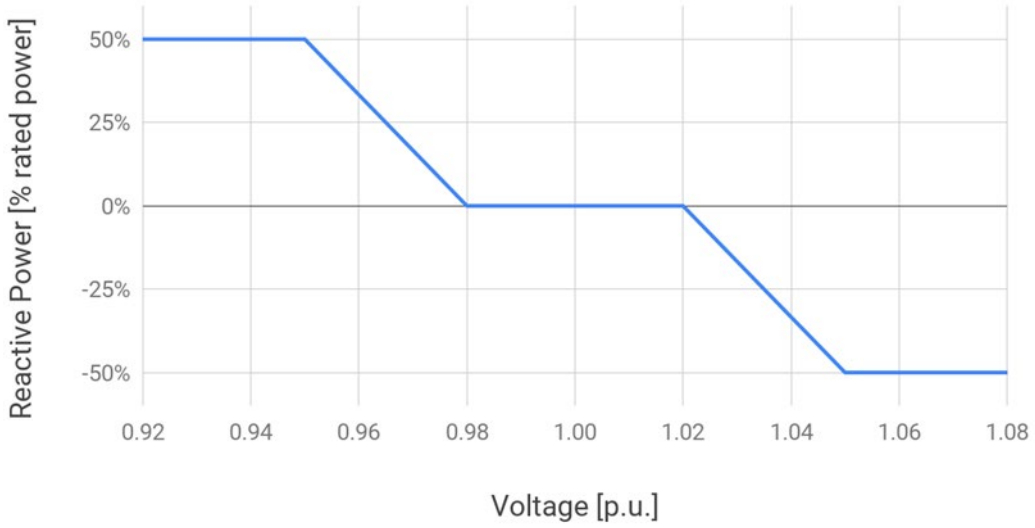


Source: Lawrence Berkeley National Laboratory

For the Volt-Var hysteresis and threshold settings in the grid search, three different setpoints were chosen for each of them. These were 0.01, 0.02, and 0.03 per unit for the hysteresis and 0.04, 0.05, and 0.06 per unit for the threshold. These sum up to 9 possible settings for each node. For all five nodes with PV systems installed, this resulted in 59,049 possible combinations. The results were analyzed for different objectives and are presented in the next section.

## Results

The outputs of the grid search simulation have multiple dimensions, with many combinations to affect each other. It is therefore difficult to show all the results in a single illustration. To give a better understanding of the results, the threshold and hysteresis settings for two out of five PV systems were compared directly. The different settings were compared by the standard deviation of reactive power production of all PV systems in the grid. A low standard deviation represents a more even distribution of reactive power generation between all inverters; whereas, a high standard deviation is the result of an unbalanced generation of reactive power. Figure 30 shows the comparison of the hysteresis settings for inverters at node 3 and 13.

**Figure 30: Comparison of Volt-Var Hysteresis Settings**

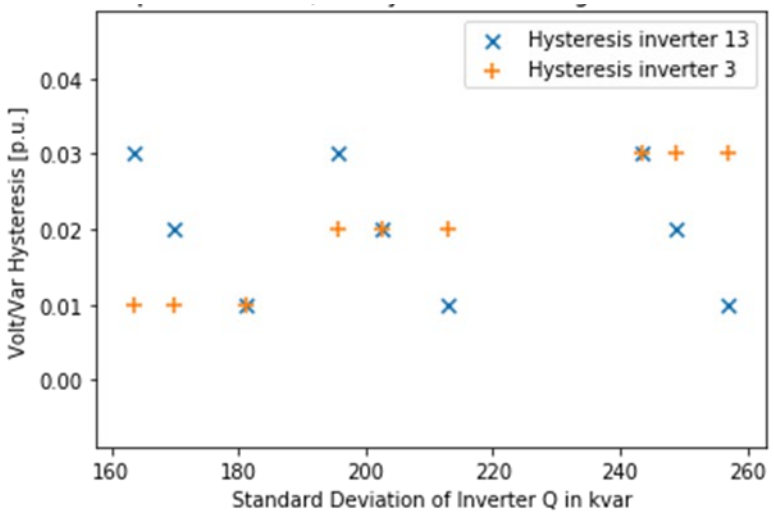


Source: Lawrence Berkeley National Laboratory

The blue x-markers show the different hysteresis settings for node 13, and the orange plus-signs represent the hysteresis settings for node 3. All the inverters at other nodes in the grid used a fixed hysteresis setting of 0.02 per unit and threshold of 0.05 per unit. The standard deviation of reactive power, on the x-axis, represents the distribution of reactive power across all PV systems. It can be seen that a hysteresis setting of 0.01 per unit for inverters at node 3 and 0.03 per unit for inverters at node 13 resulted in the lowest standard deviation, and therefore the most even reactive power generation across all inverters. A hysteresis setting of 0.03 per unit for node 3 and 0.01 per unit for node 13 resulted in the most unbalanced reactive power generation. Figure 31 shows a comparison of the different threshold settings for the same two inverters.

Again, the distribution is more even when the settings for node 3 are lower than for node 13. A setting of 0.04 p.u. for inverters at node 3 and 0.06 p.u. for inverters at node 13 represent the optimal setpoints. Setting the threshold of inverters at node 3 to 0.06 p.u. and for node 13 to 0.04 p.u. shows the most uneven reactive power generation.

**Figure 31: Comparison of Volt-Var Threshold Settings**

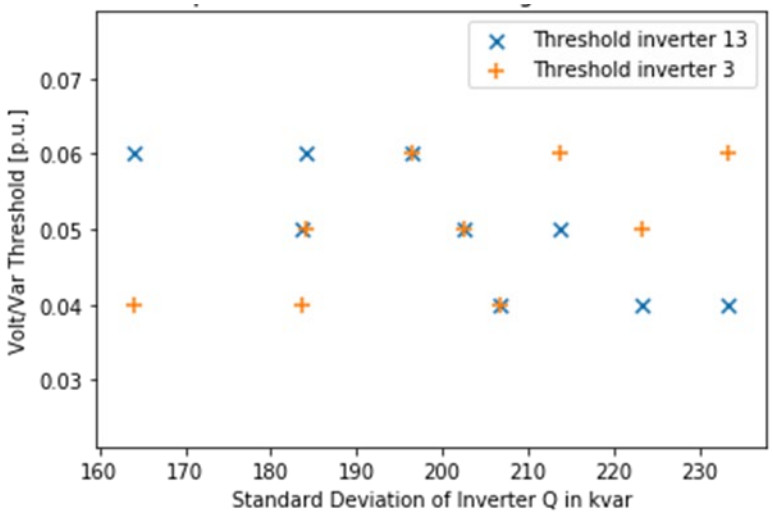


Source: Lawrence Berkeley National Laboratory

To find the settings that result in the most even reactive power generation, the results of all 59,049 simulations were compared, and the one with the lowest standard deviation of reactive power generation was selected. Figure 32 shows the nodal settings for clusters of inverters.

**Figure 32: Optimized Settings for Clustered Inverters to Reduce Reactive Imbalance**

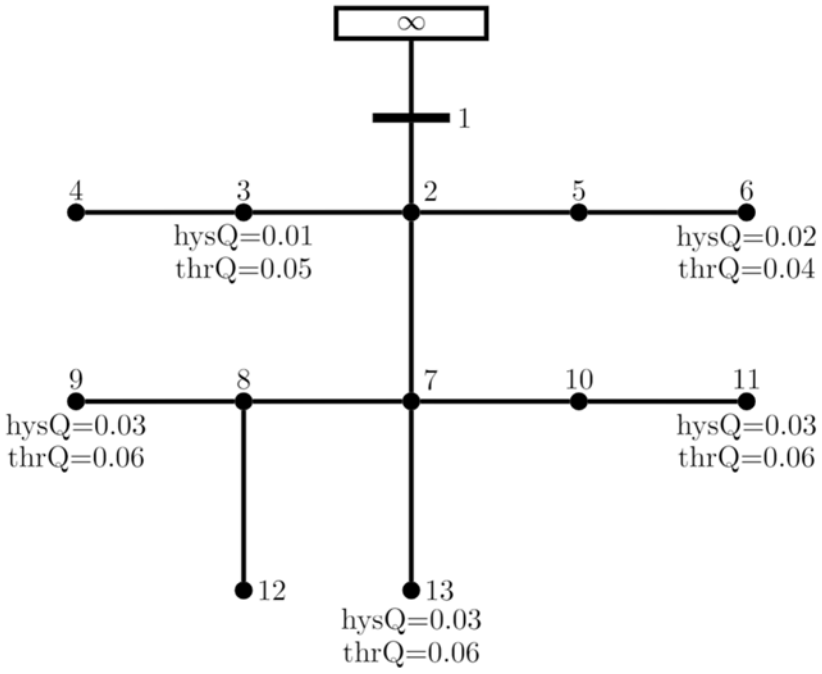


Source: Lawrence Berkeley National Laboratory

Nodes 3 and 6, which have a shorter electrical distance to the feeder head than the nodes 9, 11, and 13, also have tighter Volt-Var settings. This can be explained with the lower voltage deviations these nodes experience. In contrast, when considering uniform setpoints along the

grid, which is the standard for most utilities, the inverters at node 3 and 6 would start to generate reactive power only with a much higher PV penetration than the inverters at nodes 9, 11, and 13. It is therefore necessary to compensate for this effect by having inverters at node 3 and 6 generate reactive power already at lower voltage levels. With these settings applied, the standard deviation between the reactive power generation of all nodes in the grid is 51,350 kVar. The best possible standard deviation, with uniform setpoints, is 142,500 kVar, with a hysteresis setting of 0.01 per unit and a threshold setting of 0.06 per unit.

## Discussion

The created model shows a significant variety of loading and voltages over an entire year. Hence, it can be used to conduct annual simulations to test different control algorithms, but is also applicable for single-day simulations. Due to the distribution of the inverters at several locations along the grid, the impact of individual inverter control settings for different locations can be easily investigated. The models developed in Modelica allow the physics of an electric power grid to be represented realistically and dynamically. The usage of different load profiles, based on local weather conditions, create a realistic variety of customers on the grid.

Another strong advantage of this model and approach is the straightforward implementation of different locations within California and the United States. The load profiles are available for all locations with historical weather data, which is also input to simulate the PV generation. However, one limitation of the current setup is the usage of commercial load data only. This limitation is due to the lack of accessible load data for residential or industrial customers. Another limitation is that the load data are simulated in hourly timesteps, based on the typical meteorological year weather data, which is only partially representative of real loads with more dynamics and noise. Another point of discussion is the computation time of dynamic models compared to static or quasi static time series simulations, and therefore the increased complexity when optimizing them, where each simulation takes longer than a comparable static model would take. Since parameter studies of control setpoints are based on simulations, the computation time of large grid searches can easily become infeasible. One possible workaround to significantly reduce the computation time needed to find the optimal solution is to employ optimization solvers, which use gradients or other heuristics to quickly converge. Future work may focus on such methods to make large, region scale simulations possible.

The results show that different control settings for different clusters of inverters can accomplish a more even reactive power generation across locations. With such optimal settings, inverters at critical nodes, with higher voltages, have to produce less reactive power than they would with non-optimized settings. Conversely, inverters at nodes with lower voltages have to generate more reactive power than they would with uniform settings. With the assumption that inverters typically have similar technical specifications to provide reactive power, inverters would need to be less oversized, or more PV modules could be connected to the same inverter. This can decrease the capital cost when voltage-dependent controls are applied, as is the case with California Rule 21 (CEC 2014). The increased reactive power generation would also result in lower voltages throughout all nodes on the distribution feeder and could therefore decrease possible Volt-Watt curtailments at critical nodes. Such a situation would result in a higher

generation of active power at the nodes, increasing the power output of PV systems. However, a potential downside of this approach is the overall increased reactive power in the system, which can lead to higher distribution losses along the feeder. Future work might focus on the combination of Volt-Var-Watt controls and the economic trade-off when deployed at scale.

# CHAPTER 5:
# Controller Design and Evaluation

This section describes the design, development, and testing of a predictive control algorithm for multi-objective control to coordinate economic and grid supporting objectives. The focus here is on behind-the-meter battery storage in conjunction with PV power generation. The controller framework is designed to be modular, to enable an integration of different controllers with different time constants and objectives.

## Design

Three layers of potential control applications have been explored: (a) a fast-acting control that satisfies real-time control criteria, whose objective is to mitigate reverse power flow at the feeder head by curtailing active power generation based on remote sensing, (b) a slow-acting control to maximize the economy of the system by optimizing the dispatch of the battery, and (c) a day-ahead control, to allow participation in ancillary services markets, such as frequency regulation. The whole controller stack is shown in Figure 33.

**Figure 33: Controller Framework and Communication**

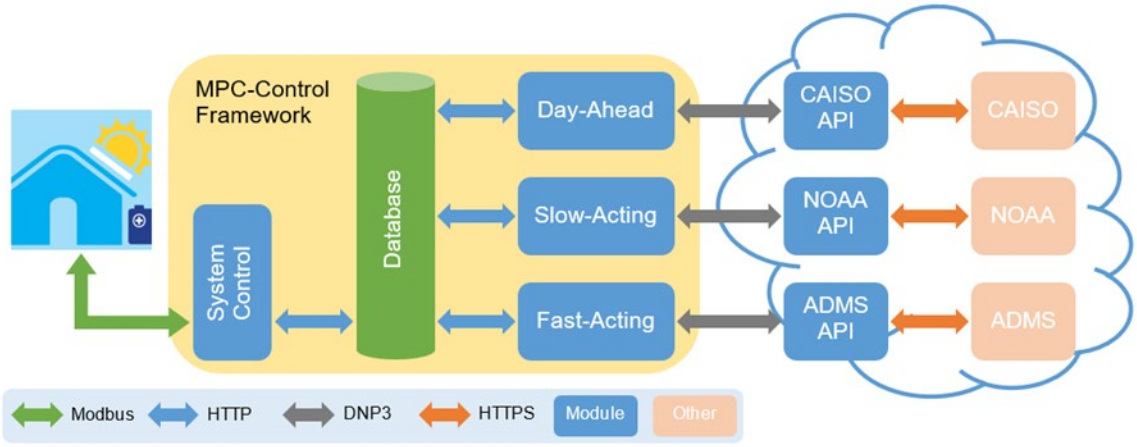


Source: Lawrence Berkeley National Laboratory

The external data sources for each of the controls are illustrated as cloud services on the right side of Figure 33. Communication application programming interfaces allow the secure data transfer from external sources, such as the California Independent System Operator[20] (California ISO) for ancillary services bidding and pricing clearance; the National Oceanic and Atmospheric Administration[21] (NOAA) for weather forecasts; and the advanced distribution management system (ADMS) for external measurement inputs. The controller framework, in the yellow shaded area, is designed to communicate through any secured Ethernet-based protocol,

[20] California ISO. https://www.caiso.com/.

[21] National Oceanic and Atmospheric Administration. https://www.noaa.gov/.

which could be the distributed network protocol or hypertext transfer protocol secure. All control modules, in blue, within the controller stack communicate through a socket communication which allows wide flexibility in integration, such as parallel, asynchronous control. The central resource here is a Python-based database, in green, to store all inputs and outputs of the control modules. The System Control module is then responsible to communicate with the physical devices located on site. The installed inverters at LBNL use Modbus; however, any other protocol could be implemented through Python.

## Framework

One major focus in the development of the controller framework is its modularity, and its ability to host multiple modules with different timesteps, potentially ranging from sub-seconds up to hours to compute a single control action. To satisfy the modularity, the whole framework is built based on Python base classes inspired by the Functional Mockup Interface (FMI) (Modelisar 2014). A functional mockup unit (FMU) is a simulation or control model exported in accordance with the FMI standard. While the framework does not directly support FMUs in its current state, it is built in a similar fashion and relies largely on standard functions found in FMI. To register controller instances in the framework, an emulated FMU, *eFMU*, wrapper class is available to host the control algorithm. Figure 34 shows a simple example of an algorithm wrapped in the eFMU class to be plugged into the controller.

**Figure 34: Example of Emulated Functional Mockup Unit Wrapper**

```
class testcontroller1(eFMU):
    def __init__(self):
        self.input = {'a':None,'b':None}
        self.output = {'c':None}
    def compute(self):
        self.output['c'] = self.input['a'] * self.input['b']
```

Source: Lawrence Berkeley National Laboratory

In this example the *testcontroller1* class is registered as an expansion of the Python base class *eFMU*. Only two functions have to be added to complete the development. First, the *__init__* function must include definitions for inputs (*self.input*) and outputs (*self.output*). Second, the *compute* function, which includes the algorithm to compute the output of the control, must be defined. With these few lines of code a fully functional module is completed and ready to be plugged into the controller framework. For more complex modules, the user can add any number of class functions and local variables. The latest version of the framework includes the ability to store variables and executed classes, which avoids the need to re-instantiate them at each controller evaluation. This feature was implemented with the switch to a parallel architecture using the *multiprocessing* package in Python to spawn the controller modules as sub-processes.

The second part of the framework is the controller stack handler, which links controller modules together and handles the flow control. Controller modules are defined in a Python dictionary containing the controller class, that is, *testcontroller1* in the example above, and the sample time in seconds. Note that the sample time can be in sub-seconds and is only limited by

computational resources. Similarly, the linking relies also on a Python dictionary with the controller name as key and dependent controller as value. A simple example is given in Figure 35.

**Figure 35: Example of Controller Linkage**

```
mapping['mpc1_a'] = 10
mapping['mpc1_b'] = 'forecast1_a'
mapping['control1_a'] = 'mpc1_a'
mapping['control1_b'] = 'mpc1_c'
```

Source: Lawrence Berkeley National Laboratory

Here the controller modules – *forecast1*, *mpc1*, and *control1* – are linked. In the first line the input variable *a* of *mpc1* is assigned a fixed value of 10. In the next line the output variable *a* of *forecast1* is linked to the input *b* of *mpc1*. Similarly, the outputs *a* and *c* of *mpc1* are linked to inputs *a* and *b* of *control1*, accordingly.

While for typical applications controllers are stacked, the framework also allows the definition of constants by replacing the dependent controller name with any real number. This is particularly useful to set parameters of the controller such as time zone or external data addresses.

The third and last part of the framework is a triggering class that allows the flow control of the control modules. Here, timesteps for the main loop (typically 100 ms), data logging (typically 5 minutes), and printing (typically 5 minutes) are defined.

The controller stack is initiated by passing the three described inputs. During operation each control module is monitored using Python-implemented failsafe functions, such as *try* and *except*, to improve the resilience and reliability of the control. At each control evaluation of the main loop (typically 100 ms), all controller modules are queried to check if they are due to trigger. If triggered, the inputs to the control module are written to the central database, and the controller module function is evaluated in a parallel thread.

## Forecasting

Predictive controllers require a forecast of PV generation and load demand. Therefore, a forecast module was developed in Python. This novel hybrid power forecasting method with parallel architecture combines a seasonal auto-regressive integrated moving average (SARIMA) model with an artificial neural network (ANN) model using weighting factors. These factors are computed periodically using a least-squares custom optimization method. Optionally, persistence or a regression model can be used within a post-processing unit to improve very short-term predictions, a few time steps ahead. The overall structure of the hybrid forecasting model is shown in Figure 36. This whole section is based on a conference paper submitted to the Power Tech conference, in 2019 (Vrettos and Gehbauer 2019).

**Figure 36: Schematic of the Hybrid Photovoltaic Forecasting Algorithm**

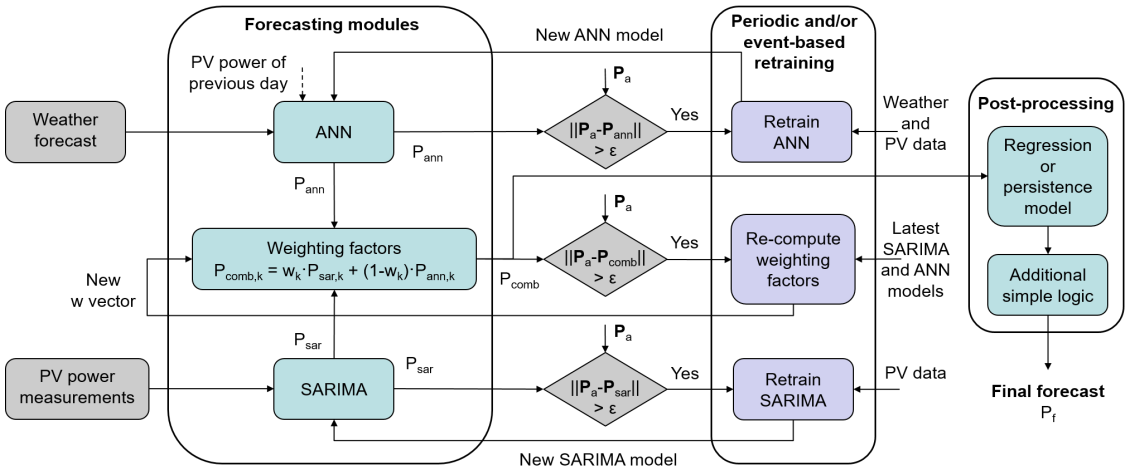


Source: Vrettos and Gehbauer 2019.

The inputs to the algorithm are the weather forecast, that is, sky cover and temperature forecast, and the observed PV generation, shown on the left. The inputs are fed to the ANN and SARIMA model accordingly, and combined by the weighting factors shown in the center. In the next step hierarchical operations are applied to determine if the model needs to be re-trained, if the projected error is above a defined threshold. The last step is the post-processing block, where persistence, or other logics can be applied. The output is a vector of PV generation forecasts.

Extensive simulations showed that the forecasting method has high accuracy. The root mean square error for a 24-hour ahead prediction was in the range of 5 to 10 percent, depending on the PV power volatility level. In addition, it is worthwhile to mention that the hybrid method outperformed the best of SARIMA and ANN models by up to 10 percent on days with high PV volatility. Even though the model had been deployed to forecast PV power production, it is in principle also applicable for load forecasting.

### Example of Operation

The prediction models were trained with data from one of the three single-phase PV systems of Flexgrid, and then used to forecast the PV power production. Figure 37 shows an example evaluation for three days.

The day-ahead forecasts, which were obtained at midnight of each day, are shown for SARIMA in blue, ANN in magenta, the hybrid model in green, and actual values in black. In addition, the one-step ahead forecasts with the hybrid model are shown as the dashed red line. The upper plot shows a dataset from September 30 to October 7, and the bottom plot shows October 26 to November 2. The day-ahead hybrid forecast is always between the SARIMA and ANN forecasts and closer to the actual PV power.

**Figure 37: Evaluation of Hybrid Photovoltaic Forecasting Algorithm**

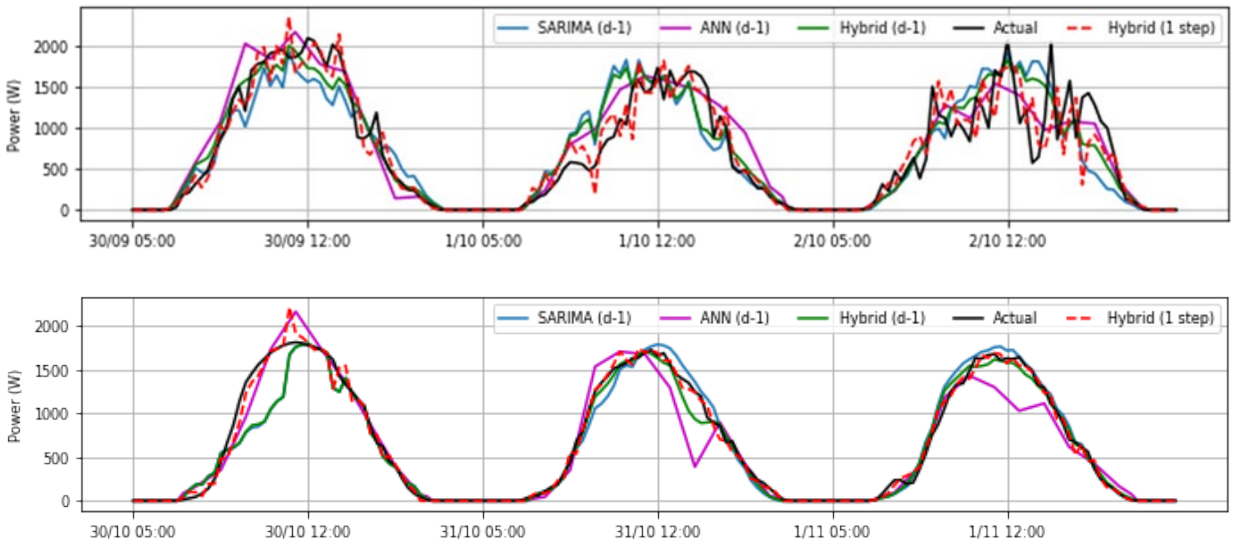


Source: Vrettos and Gehbauer 2019.

Figure 38 shows the dependence of the forecast root mean square error on the prediction horizon.

**Figure 38: Time-Varying Error of Hybrid Photovoltaic Forecasting Algorithm**

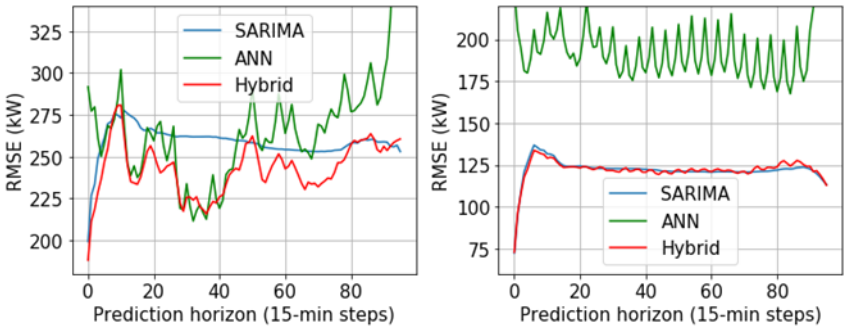


Source: Vrettos and Gehbauer 2019.

In the first dataset from September 30 to October 7, shown in the left plot, there is a potential for improvement because the PV power is volatile and, as a result, the hybrid model achieves lower errors than both SARIMA and ANN models. In contrast, the SARIMA model already performs very well in the second dataset from October 26 to November 2, on the right, due to less volatility, and thus the potential for improvement is limited.

## Controller

Another core component of the controller stack is the battery dispatch controller which is based on model predictive control (MPC). The typical layout of an MPC controller consists of a mathematical model which represents the physical system, that is, battery and PV generation in

this case, and a model for the policy, that is, time-of-use tariff[22] (TOU) structure and regulation bidding[23]. These models are linked to each other by the objective function which defines the objective of the controller, such as energy cost minimization or PV utilization maximization. The second part of MPC is the optimization solver, which finds the optimal parameter and setpoints to minimize the objective function. In addition, constraints can be added to the model, for example, the battery has the physical constraint of a SOC between 10 and 100 percent. The setup of timesteps and horizon of the MPC controller are usually dependent on the timescale of the system to be controlled. For battery applications, a typical optimization horizon[24] is defined as a full day-cycle or 24 hours; a typical optimization timestep[25] is between 5 to 15 minutes. The controller is reevaluated at every timestep with updated weather and forecast data, and the control solution for the next 5 to 15 minutes is applied to the system. The method of reevaluation is illustrated in Figure 39.

**Figure 39: Reevaluation Process of the Model Predictive Control Controller**

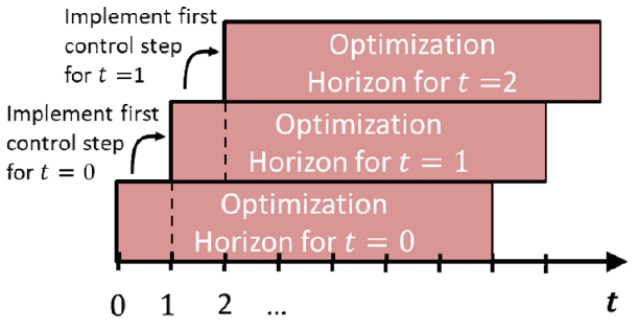


Source: Blum and Wetter 2018.

The MPC controller developed for this project was built as outlined above, with the objective of total energy cost minimization. It was implemented within the open-source Python framework Pyomo (Hart et al. 2017), a development of Sandia National Laboratory. The battery model contains an SOC model with a numerical battery balance model to represent the SOC at the discretized time, *t*, which allows the problem formulation as a mixed-integer linear problem. This has the advantage of fast solving times, typically well below one second, and the utilization of an open source solver such as COIN-OR Branch and Cut (Forrest et al. 2018).

The parameters of the model were separated into four categories: (1) tariff structure containing the TOU tariff; (2) battery containing the various parameters of the battery such as efficiencies, capacity, and power constraints; (3) site-specific information such as type of customer and power limits; and (4) a controller containing settings for the controller such as internal timestep. The required parameters were selected to keep the specific inputs at a minimum to

[22] An electricity tariff which has different rates depending on the time of day.

[23] The frequency regulation is a type of service to the electrical power grid, where power is either dissipated or generated based on fast-changing control signals.

[24] The period the controller looks ahead.

[25] The timestep within the optimization model.

allow a rapid deployment. While parameters are typically set only once during initialization and remain constant during the time of operation, this module allows them to change dynamically during run time.

### Example of Operation

The controller was built to incorporate any tariff structure. A simple modification could positively benefit the California power grid to mitigate emerging ramping in the late afternoon hours, when PV generation decreases and residential load ramps up, known as the California duck curve (CAISO 2016). The scenario below was modified to reflect an extreme grid situation, manifested by largely increased electricity cost, in Figure 40.

**Figure 40: Example of Model Predictive Control Control During Extreme Grid Event**

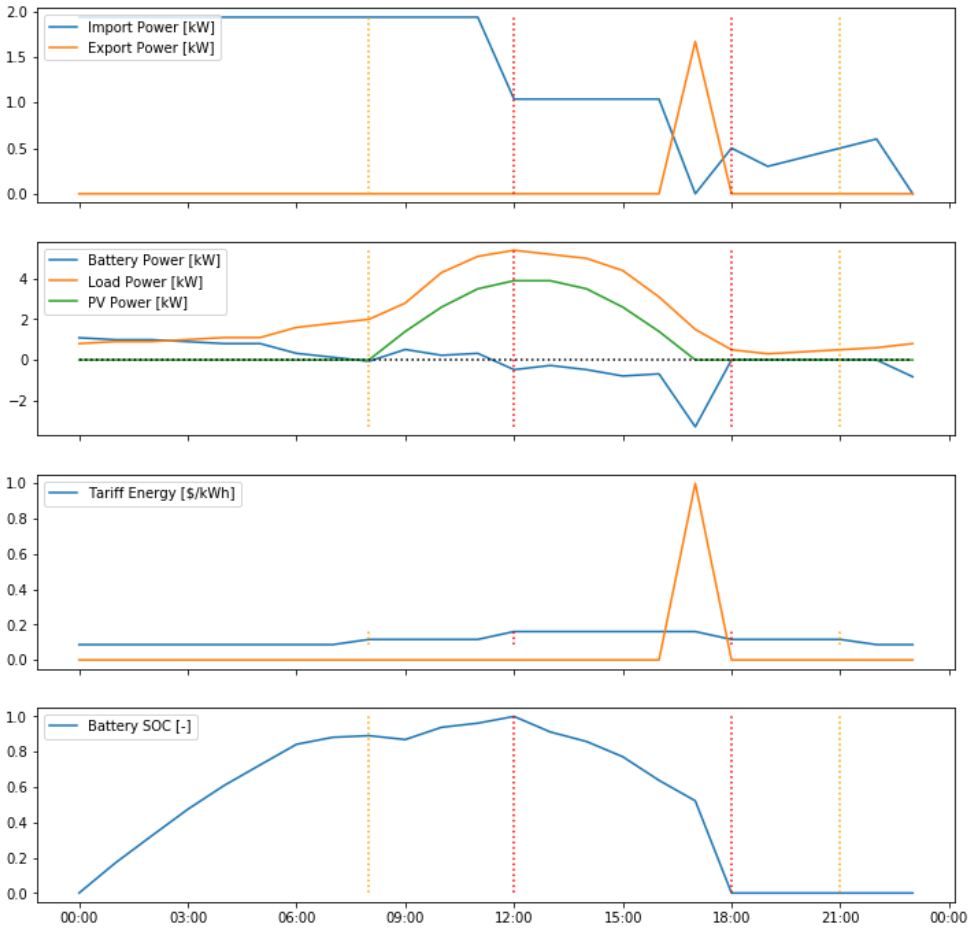


Source: Lawrence Berkeley National Laboratory

The inputs to the controller are shown in the second plot as the forecast of building load in orange and the PV forecast in green. The resulting battery operation defined by MPC is shown in blue. The overall operation can be explained by the third plot, which shows the TOU price profile with the spike in cost at 5 PM. During night it is less expensive to charge the battery, which enables it to discharge over the more expensive periods during the day. However, as PV generation arises and load varies the solution is more complex, and as seen in the SOC in the

fourth plot, charging also takes place during the mid-peak period starting from 8 AM to 12 PM. In addition, the battery is discharged in a non-continuous pattern, shown in blue in the second plot. The result of this control action can be seen in the first plot where the net load at the utility meter is shown in blue. The optimization seeks to generate a flat load profile, which is the most economic strategy for the TOU tariff structure. However, during the price spike, the electricity demand is largely reduced, which practically mitigates the duck curve. Further, a price for energy export is defined within the controller to feed in power to the grid and actively mitigate any grid event. This capability of providing energy to the electrical grid is especially interesting when largely deployed. While this example is simplistic, the controller is capable of reacting to real-time pricing signals, as well as a price event trigger. All of the functionality is built into the controller and tested in simulation mode. One possible extension would be to further develop and field test the controller.

### Utility Modules

The MPC controller and PV forecast are the main modules of the controller stack, but a number of utility modules are required to enable the interface with real equipment. Among others, the controller stack at LBNL uses a time synchronization module to get accurate time measurements, a module to read the inverter telemetry, and a module to control the inverter.

While other modules are generic to fit different applications, the inverter telemetry and inverter control module are somewhat specific to the inverters installed at LBNL. They use a hypertext transfer protocol wrapper for Modbus to communicate with the actual inverter at Flexgrid. For different types of inverters, these modules would have to be adopted to fit the specific communication protocol.

## Simulation Evaluation

This section highlights the findings of the MPC controller for behind-the-meter battery storage in conjunction with PV, in an annual simulation study, which represent the technical potential of the developed MPC algorithm.

### Setup

The MPC controller requires a variety of inputs, such as weather and load forecasts, and real-time measurements, such as PV generation and battery SOC. To conduct annual simulations of the MPC controller, all external links to data must be emulated. For this study the PV generation was emulated using the PV model introduced in the Model Development section in Chapter 4, and parameterized to represent Flexgrid in a simplified way. Here, all three PV systems are oriented toward the south, with a 10-degree tilt and no module shading. The PV generation profile was then simulated with historical weather data from San Francisco. Figure 41 shows the annual PV profile.

**Figure 41: Annual Photovoltaic Generation Profile for Simulation**

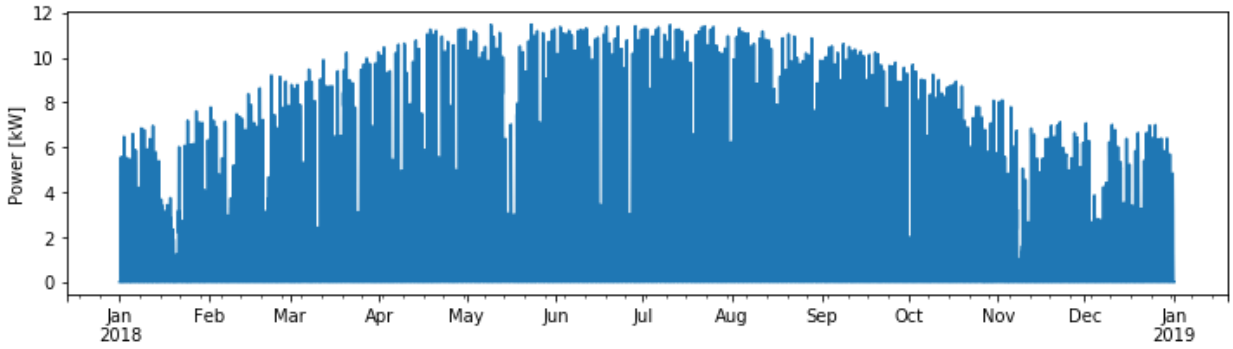


Source: Lawrence Berkeley National Laboratory

The load profile is another input required by the MPC controller which was collected from measurements at LBNL's Flexgrid facility for this study. The base load for the MPC controller is the medium-sized office building, introduced in the "Installation of Advanced Measurement Devices" section in Chapter 2. An annual plot is shown in Figure 42.

**Figure 42: Annual Load Profile for Simulation**

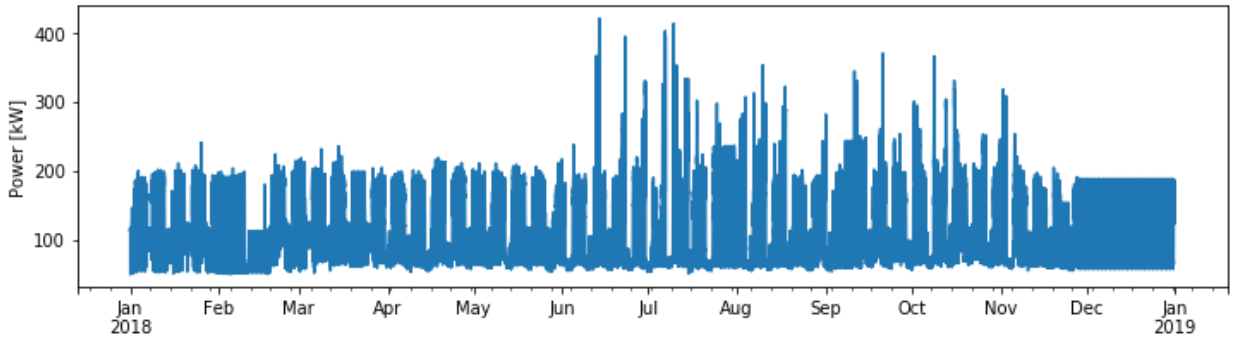


Source: Lawrence Berkeley National Laboratory

With the PV generation and load profile in place, the only remaining component to be emulated was the battery storage. The MPC controller already included a battery model, within the internal optimization model, to determine the optimal utilization of storage, which is used for the purpose of simulation. The controller was configured to control the battery over a 24-hour horizon, with a five-minute control timestep, which allowed one optimization to be conducted per day. The assumptions here were an initial SOC of 0 percent at midnight and a final SOC of 0 percent at the optimization horizon of 24 hours, which is again at midnight. Fixing the SOC in such a way avoids the artificial addition of energy in the system (that is, by starting with a SOC greater than zero) and allows it to seamlessly add days one to another without affecting the operation, as PV generation is only present during daylight hours. The Pacific Gas and Electric time-of-use E-19 tariff (PG&E 2018) was used, where three pricing periods are apparent in summer, and two in winter. One simplification made was that all days were treated as weekdays, whereas the E-19 tariff distinguishes between weekdays and weekends. The tariff and MPC configuration are provided in Appendix B.

The simulation was conducted with three different cases and two scenarios:

- Building load only without PV and battery, as base case
- Building load and PV, but without battery, to quantify the benefit of PV only
- Building load, PV, and battery, controlled by the MPC controller

The first scenario used the 15 kW PV array installation at Flexgrid, and three of the most recent Tesla PowerWall 2 units with a total of 40.5 kWh storage. In the second scenario, the installation was scaled by a factor of 10, due to its relatively small size in comparison to the approximately 400 kW peak building load. The resulting system was 150 kW of PV with 405 kWh of battery storage.

## Results

The simulation was conducted for one full year to capture the full seasonal effects of PV and loads. The results were aggregated for the summer and winter seasons, which are May to October and November to April, respectively.

The first study conducted was the Flexgrid installation and medium-office building load, shown in Table 4.

**Table 4: Simulation Results of the Model Predictive Control at Lawrence Berkeley National Laboratory**

| | | Load only | Load + PV | Load + PV + Battery |
|---|---|---|---|---|
| **Summer** | **Total cost [$]** | 150,210.00 | 146,449.80 | 143,775.60 |
| | **Savings [$]** | | 3,760.20 | 6,434.40 |
| **Winter** | **Total cost [$]** | 77,746.80 | 76,373.50 | 75,149.10 |
| | **Savings [$]** | | 1,373.30 | 2,597.70 |

Source: Lawrence Berkeley National Laboratory

Both cases, Load+PV and Load+PV+Battery resulted in savings in both the summer and winter seasons. The total annual savings were $5,133.50 (2.3 percent) and $9,032.10 (4.0 percent) for the two cases. The total incremental savings of battery utilization was $3,898.60 (1.7 percent). The savings in winter were significantly lower, which can be attributed to the decreased solar generation and lower electricity demand cost. The overall battery utilization, defined as the time when battery is either charged or discharged divided by the 8,760 hours of a full year, came to 37.8 percent. As described in the previous section, the savings are overall very small in comparison to the load of the office building. A second simulation was conducted where the installation was scaled by a factor of 10. Results are presented in Table 5.

**Table 5: Simulation Results of Model Predictive Control at Lawrence Berkeley National Laboratory (Scaled by 10)**

| | | Load only | Load + PV | Load + PV + Battery |
|---|---|---|---|---|
| **Summer** | **Total cost [$]** | 150,210.0 | 115,092.20 | 86,457.90 |
| | **Savings [$]** | | 35,117.80 | 63,752.1 |
| **Winter** | **Total cost [$]** | 77,746.80 | 66,586.70 | 59,949.70 |
| | **Savings [$]** | | 11,160.10 | 17,797.1 |

Source: Lawrence Berkeley National Laboratory

The total annual savings were $46,277.90 (20.3 percent) for Load+PV and $81,549.20 (35.8 percent) for Load+PV+Battery, which is a significant increase from the previous scenario but less than the scaling factor of 10. The reason could be the nature of the demand cost, which is based on the single peak demand of each month. The higher the peak reduction, the more energy is necessary, resulting in less-effective cost reduction. The battery utilization increased to 75.3 percent. The incremental annual savings, this includes the summer and winter season, of battery utilization were $35,271.30 (19.4 percent).

# Pilot Test

To confirm the results from the simulation study, the MPC controller was integrated and tested at the Flexgrid facility. The setup included the control of one inverter at Flexgrid with a system size of 3.75 kW of PV and 6.4 kWh of battery storage. The MPC controller was configured to a control timestep of five minutes, and an optimization horizon of 22 hours. A significant amount of the field testing time was used to establish and test communication, validate models, test continuous operation over multiple days, and further advance the controller based on the tests conducted. The results presented in this section are the most representative for the controller to (a) demonstrate the functionality of the controller and (b) confirm the results from the simulation study. The field tests are typically conducted in five-day periods, where the first day can be seen as a warmup period and should not be considered in the analysis.

## Results

The Figure 43 shows the forecast results for PV and load, which are conducted by the internal control modules and then fed to the MPC controller.

**Figure 43: Field Test Results for Photovoltaic and Load Forecast**

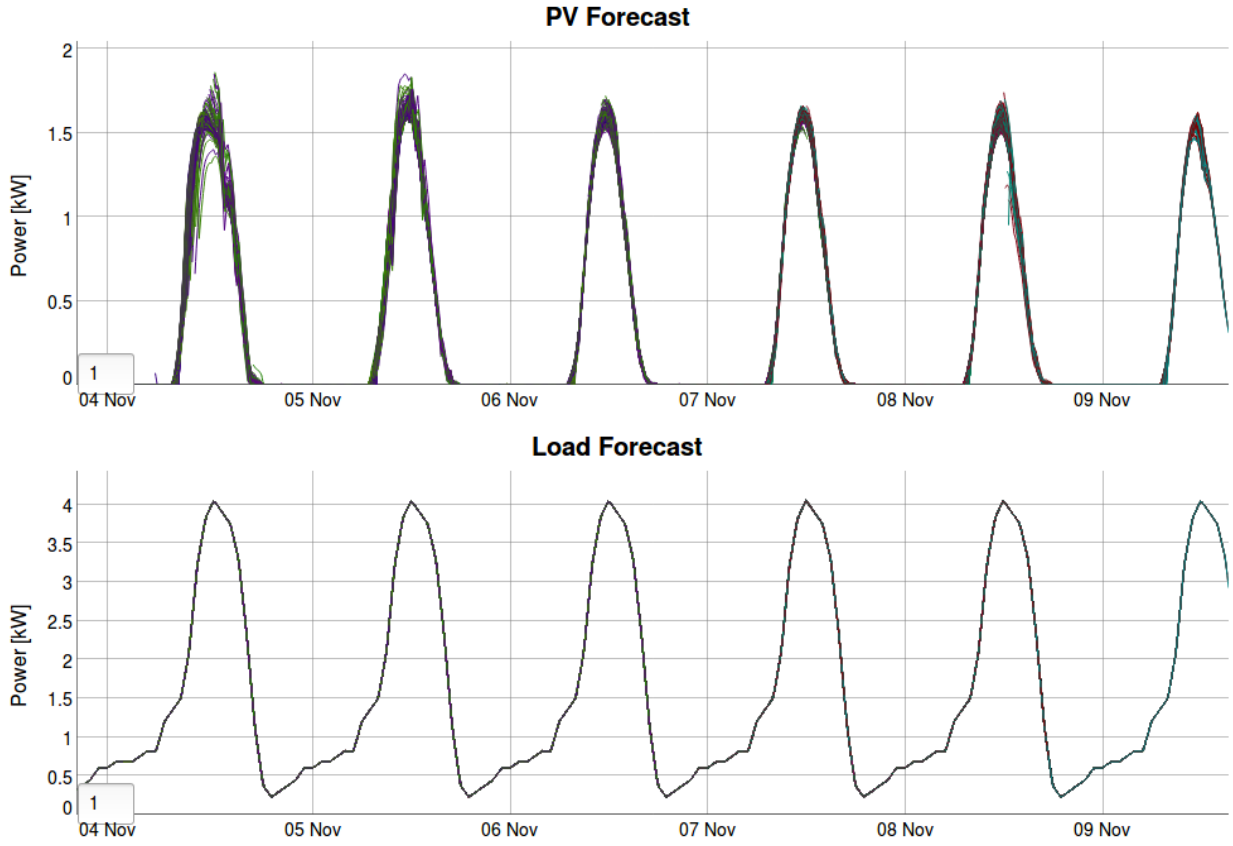


Source: Lawrence Berkeley National Laboratory

Each plot consists of many lines plotted on top of each other, where each line represents one of the five-minute control steps and a projection of 22 hours ahead. The PV generation was consistently smooth, indicating a clear and sunny sky. Similarly, the load forecast appeared very smooth, but the reason for the smooth load forecast is the lack of load forecasting capability and replacement with a static load profile of a test cell at Flexlab. This test started on November 3 at 9 PM and lasted for about six days, until November 8 at 7 PM. However, the projected results are 22 hours ahead, resulting in an apparent end date of November 9 at 3 PM.

Figure 44 shows the resulting battery control and net load of the MPC controller. These quantities are resampled measurements, and do not have multiple projected lines in them. The resampling to 15 minutes was applied to match the utility accounting period, which was also 15 minutes.

**Figure 44: Field Test Results for the Battery Control and Net Load using Model Predictive Control**

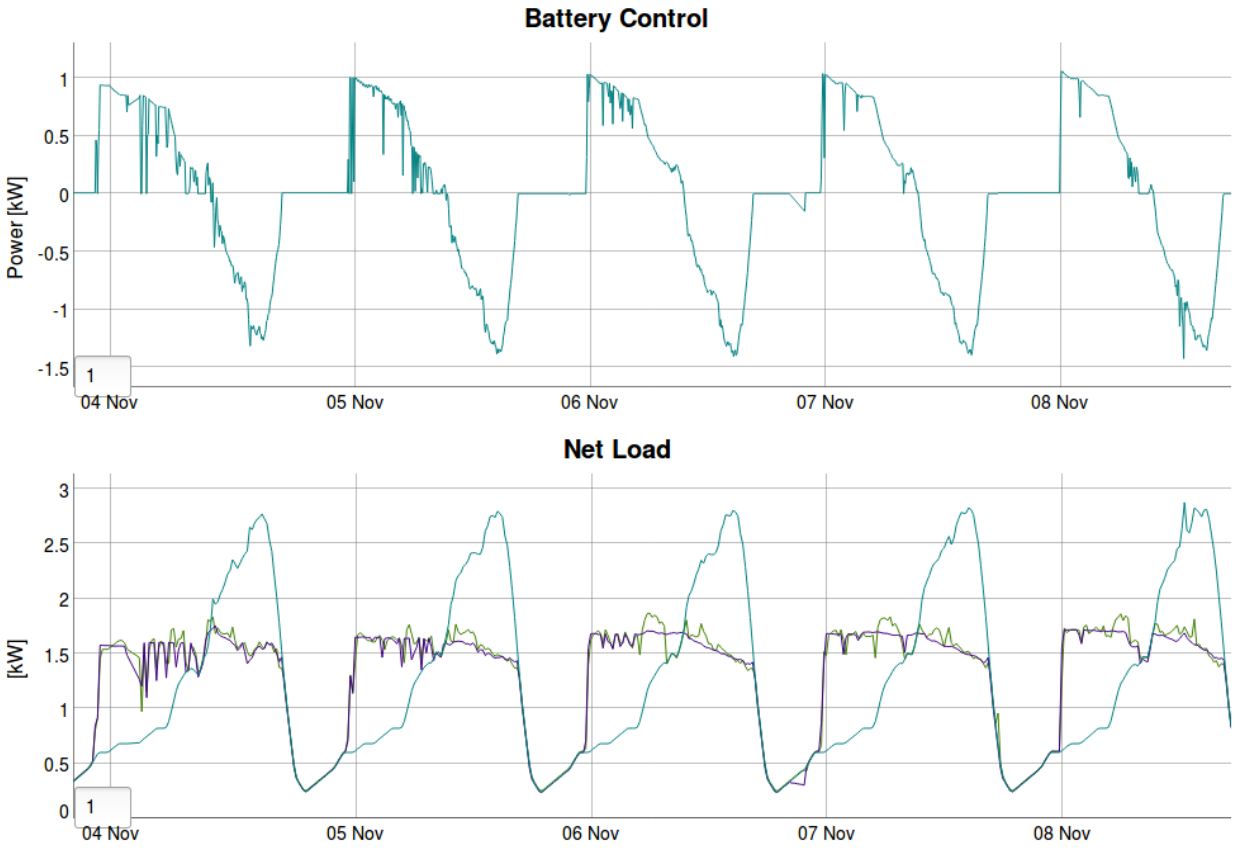


Source: Lawrence Berkeley National Laboratory

The resulting battery control is shown in the upper plot. This is the control actually applied to the battery. During the field test multiple iterations were necessary to closely match the control signal from the MPC controller to the control signal actually sent to the battery. As all communication is handled by the inverter, setpoints are not directly passed to the battery, which results in small but constant offsets in power, and occasional signal timeouts. One example for a timeout can be seen on November 5 at about 3 AM, as the negative drop in battery power from about 0.85 kW down to 0.3 kW and then back up to 0.85 kW. Zooming into the five-minute data, a drop to 0 kW was found, caused by an inverter timeout. However, it appears that the timeout problems only happen during the night, and therefore have little effect on the MPC controller performance. The lower plot shows the resulting net-load profile where the base case of Load+PV is shown in turquoise, the MPC projected result for the five-minute ahead is in purple, and the measured MPC performance is in yellow. The difference between the MPC projected and measured performance is the compounded error of forecast error, control error, and MPC model error. The effect of this compounded error on the energy cost can be seen in Figure 45.

**Figure 45: Measured Total Energy Cost at Field Test**

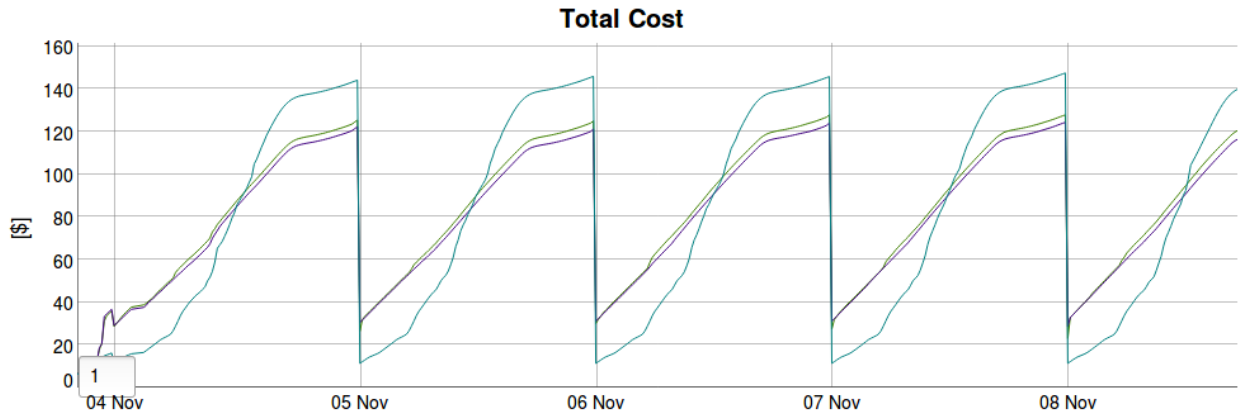


Source: Lawrence Berkeley National Laboratory

The total energy cost is the cost of energy and demand, but reset to zero every day at midnight. Note that the results include the full demand charge and the daily energy cost multiplied by 30 days, to represent a whole month of similar operation but without the consideration of weekend days. This allowed the MPC controller to be evaluated on a day-by-day basis and to avoid the compounding of errors. For example, if the MPC controller had a problem on day two, leading to a high demand charge, all consecutive test days would be affected by this result, and the MPC controller evaluation would be distorted. However, the controller worked as intended during the presented testing period. For most of the day the measured MPC performance, in yellow, tracked the projected MPC performance, in purple. Both profiles matched an optimal dispatch, where flat net-load profiles are desired to maximally use the demand charge. However, a small mismatch of PV projection in the morning hours caused the MPC controller to slightly overestimate the PV generation, which led to a decreased battery output, and then in turn increased the net load and set a new demand charge. The monthly results for the second test day were $146, $125, and $121 for the Load+PV base case, measured MPC performance, and projected MPC performance, respectively. The total energy cost savings were $20 (13.6 percent). While these savings are already significant, it is important to note that this field test was conducted in November, where the low-priced winter period of the PG&E E-19 tariff was applied.

# Discussion

The simulation study revealed significant savings for both the summer and winter seasons. Annual savings of $3,898.60 (1.7 percent) could be achieved by adding behind-the-meter battery storage with the MPC control algorithm. However, the PV generation data was based on a simulation with historical weather data, while the load data was measured at LBNL, in 2018. The inputs were not compatible due to the different weather conditions, and therefore the results of the simulation study are only preliminary. Comparing the annual savings of $3,898.60 with the listed price of three Tesla Powerwall 2 units, a total of $25,700 (Tesla 2016) – which includes three batteries at $6,700 per unit, installation cost of approximately $1,500 per unit and mounting equipment for a total of $1,100 – the payback time would be about 6.6 years.

Considering that Tesla offers a warranty of 10 years, the 6.6 years of payback would be very cost effective. However, it is important to note that the savings are subject to a perfect knowledge of forecasted PV and load, which is not practical and one of the challenges with MPC.

Another consideration is the size of the PV and battery system. While the first scenario of the simulation study included the Flexgrid system as built as a pilot facility for research applications, a second scenario scaled both the PV and battery to more closely match the load. This increased the savings, but at a lower rate than the scale of the system. An important decision for a customer would be to size the system right to gain maximum revenue. Sizing tools such as the Distributed Energy Resources Customer Adoption Model (Stadler et al. 2014) from Berkeley Lab are available as a public resource to assist with DER investment decisions.

The MPC controller requires a load forecast for the next 24 hours ahead at each control timestep of five minutes. However, the load profile of the field test was fixed to a single profile for a sunny day of a test cell at Flexlab. The reason behind this modification was the lack of simplified load forecasts that can be implemented on an embedded controller. The developed PV forecasting module could, in principle, provide load forecasts to feed the MPC controller. However, at the time of the field test the forecasting module was not validated, and would likely have led to bad control. The conducted field test is relevant because PV generation was fully forecasted, and the loop between measurements and actuation was closed through the MPC controller. The basic application of MPC was demonstrated in this field test, and potential energy cost savings and benefits for the power grid were outlined. MPC can significantly facilitate large PV penetrations while cost-effectively relieving the accompanying contingency on the power grid. In particular, the colocation of battery storage can be beneficial for both customers and grid operation.

The measured savings of the field test, which were 13.6 percent, are significantly higher than those from the simulation study, which were about 1.5 percent for the winter period. In addition, the simulation study showed that the savings for the winter period were lower than those achieved in the summer, so higher savings from the field test could be expected when the test is conducted in summer. While the savings are significant, the results were distorted by the fact that the test setup was different. The simulation study used the full Flexgrid system in conjunction with the medium-sized office building load, with a peak load of about 400 kW, but the field test only used one of the PV and battery systems in conjunction with an emulated load of a single test cell at Flexlab, with a peak load of approximately 4 kW. So, while the PV and battery system was reduced by a factor of 3, the load was reduced by a factor of 100. The tests were set up this way because of Flexgrid's physical size and the option to use the remaining inverters to conduct other tests of the controller, and to continue on data collection.

# CHAPTER 6:
# Summary and Benefits Assessment

This project designed and built the Flexgrid facility with its PV, storage, and distribution PMU installation; developed and validated a broad range of simulation models to conduct annual simulations of DER; used these models to determine optimal setpoints for a smart inverter, in accordance with California Rule 21; and developed and field tested an MPC controller to maximize battery use for the customer, while supporting the power grid during critical periods.

The Flexgrid facility serves as a central testbed and utility for hardware-in-the-loop and DER technology integration testing in California. It allows the evaluation of novel control systems in a controlled, emulated environment and enables real-time comparisons between demand, renewables, inverters, and storage. Flexgrid was used throughout this four-year project, supporting data collection; simulation model development of PV, smart inverter, and battery storage; development of a grid event detection algorithm; and evaluation of a novel MPC controller and the associated forecasting methods. Investments from other USDOE-funded projects further expanded the capabilities by adding power systems testing hardware.

Throughout this project, high-fidelity grid measurements in a 120 Hz rate (120 samples per second) were recorded at three strategic positions within the LBNL distribution grid. An event detection algorithm was developed and applied, which resulted in the detection of 27 voltage-sag events in the last two years of the project. The events were stored in a digital library of grid events and two methods to perform short-term forecasting of grid event parameters were applied. Both methods revealed the initial slope of a voltage-sag as a good parameter to predict its severity and duration. This information can be important for determining inverter ride-through settings, in accordance with California Rule 21, with the overall objective of improving electrical grid reliability.

To further explore the potential of smart inverters, a framework to optimally select Volt-Var control setpoints for different nodes along the feeder was developed. The result of this algorithm showed that it could be advantageous to distribute the burden of reactive power generation, by having variable Volt-Var setpoints for clusters of inverters. Variable Volt-Var settings could decrease the curtailment of active power generation in the feeder when less critical nodes provide reactive power at lower voltages than critical ones. This results in a reduced oversizing of inverters and decreased curtailment of active power generation, which both can reduce the levelized cost of electricity for distributed PV applications. However, one downside of this approach is the increased distribution loss due to higher reactive currents. A further investigation of the associated grid distribution losses and inverter investment cost is needed to thoroughly evaluate the control approach for different types of customers in California. Ratepayers would see improved reliability compared to a case where high PV penetration exists but is not coordinated and managed as proposed in this project.

The data collected at Flexgrid was also used to develop an advanced control system for PV and battery storage, using the state-of-the-art MPC technology. In this process, a new hybrid forecasting method was developed for short-term PV power forecasting, which was shown to outperform existing common approaches. Through coordinated control using this predictive algorithm, high penetrations of renewable resources at the feeder scale can be achieved. One key attribute here is the capability to shape the load using battery storage. In the case of the California duck curve, the MPC controller optimally controls the battery dispatch by charging the battery during periods with excess PV generation and discharging it during the critical afternoon hours. This active participation in grid management helps to maximize the deployment of distributed generation overall.

The controller was evaluated in annual simulations and revealed the potential cost-effectiveness of behind-the-meter battery storage. In the simulation conducted, 35 percent of the annual electricity bill could be saved, with a payback time of the investment in the battery storage of about 6 years. This duration is significantly shorter than the manufacturer's warranty of 10 years. Therefore, the installation of a behind-the-meter battery storage system can financially benefit both residential and commercial ratepayers, as well as the grid operation and reliability overall. The controller was also tested in a field test at Flexgrid, where it showed significant savings, but with different sizes of PV, storage, and load.

Both control approaches, the variable Volt-Var settings and the MPC control, can increase the allowable PV penetration, which (a) offsets retail energy purchases, (b) increases the ability to earn PV-based revenue due to an increase in the type of energy services PV and battery storage can provide, such as reactive power support or mitigation of the duck curve, and (c) supports California with its aggressive climate goals to decarbonize the grid.

All developed simulation models, the grid event library, and the MPC controller are open-source and available in Gehbauer (2019a), Gehbauer (2018), and Gehbauer (2019b), accordingly.

# GLOSSARY

| Term | Definition |
|---|---|
| ANN | Artificial neural network; A machine-learning model based on neural connections in multiple dimensions. |
| ANSI | American National Standards Institute |
| ARPA-E | Advanced Research Projects Agency for Energy |
| BTrDB | Berkeley Tree Database; A time-series database designed to handle large amounts of data. |
| California ISO | California Independent System Operator; the electrical power grid operator for California |
| DER | Distributed energy resources; examples are photovoltaics, electric vehicles, batteries, or buildings equipped with remote controllable loads. |
| EPIC | Electric Program Investment Charge |
| Flexgrid | Facility for power systems testing located at Lawrence Berkeley National Laboratory |
| Flexlab | Facility for Low Energy Experiments for Buildings; A testing facility at Lawrence Berkeley National Laboratory. |
| FMI | Functional mockup interface; A variant of application programming interface relevant for simulation applications. |
| FMU | Functional mockup unit; A simulation model exported in accordance to FMI. |
| IEEE | Institute of Electrical and Electronics Engineers |
| LBNL | Lawrence Berkeley National Laboratory |
| MBL | Modelica Buildings Library; A Modelica library for buildings simulation. |
| MPC | Model predictive control; A type of controller which is based on a model of the system to be controlled, and an optimization engine to determine optimal operation to minimize or maximize an objective function. |
| NOAA | National Oceanic and Atmospheric Administration; the United States weather service. |
| OpenEI | Open Energy Information; A database with simulation results from USDOE reference buildings using typical meteorological weather data. |

| Term | Definition |
|---|---|
| PMU | Phasor measurement unit; A precise measurement device to monitor the electric power grid. |
| PV | Photovoltaics; A technology which converts solar irradiation to electrical energy. |
| RLA | Random load allocation; An algorithm to generate dynamic load profiles in power systems simulation. |
| SARIMA | Seasonal Auto-Regressive Integrated Moving Average; A machine-learning model based on the correlation of data-points in time. |
| SCooDER | Smart Control of Distributed Energy Resources; A Modelica library for power systems simulation. |
| SOC | State of charge; The energy level currently available in a storage device. Must be grater or equal than zero, and smaller or equal then the capacity. |
| STC | Standard test conditions; An industry-wide standard to evaluate the performance of PV modules. It specifies a cell temperature of 25 degree Celsius (°C) and an irradiance of 1,000 watt per square-meter ($W/m^2$) with an air mass of 1.5. |
| TMY | Typical meteorological year; A detailed weather file of historic and representative weather. |
| TOU | Time-of-use; This represents a type of electricity rate which varies based on time of the day and day of the year. |
| µPMU | Microsynchrophasor measurement unit; a low-cost PMU specifically designed for the electrical distribution grid |
| USDOE | United States Department of Energy |

# REFERENCES


Alves, M. F. & Ribiero T. N. 1999. Voltage Sag: An Overview of IEC and IEEE Standards and Application Criteria. IEEE Transmission and Distribution Conference.

Andersen, M. P. & Culler, D. E. 2016. BTrDB: Optimizing Storage System Design for Timeseries Processing. 14th USENIX Conference on File and Storage Technologies.

ANSI - American National Standard for Electric Power Systems and Equipment. 2016. Voltage Ratings (60 Hertz).

Blum, D. and M. Wetter. 2018. Next-Generation Building Control with Model Predictive Control.

Brkic, J., Ceran, M., Elmoghazy, M., Kavlak, R. & Kral, C. 2018. PhotoVoltaics Modelica library. Github.

Brodt-Giles, D. 2012. Wref 2012: OpenEI – An Open Energy Data and Information Exchange for International Audiences. National Renewable Energy Laboratory (NREL).

California Energy Commission (CEC). 2014. Rule 21. Smart Inverter Working Group Technical Reference Materials.

California Independent System Operator. 2016. What the duck curve tells us about managing a green grid.

Dargatz, M. 2010. Utility Interactive: What it Means, What Protection it Ensures. Enphase Energy.

Deru, M., Field, K., Studer, D., Benne, K., Griffith, B., Torcellini, P., Liu, B., Halverson, M., Rosenberg, D. & Yazdanian, M. 2011. Commercial Reference Building Models of the National Building Stock. United States Department of Energy.

Einhorn, M. Conte, F. V., Kral, C., Niklas, C., Popp, H. & Fleig, J. 2011. A Modelica Library for Simulation of Electric Energy Storages.

Forrest, J., Ralphs T., Vigerske, S., Hafer, L., Kristjansson, B., Straver, E., Lubin, M., Santos, H. G. & Saltzman, M. 2018. COIN-OR Branch and Cut.

Fritzson, P. & Bunus P. 2002. Modelica – A General Object-Oriented Language for Continuous and Discrete-Event System Modeling. IEEE Proceedings 35th Annual Simulation Symposium.

Gehbauer, C. 2018. PMU Event Library. https://github.com/LBNL-ETA/pmu_event_library.git.

Gehbauer, C. 2019a. Smart Inverter Modelica Library. https://github.com/LBNL-ETA/SCooDER.git.

Gehbauer, C. 2019b. An Optimal Control for Behind-the-Meter Storage. https://github.com/LBNL-ETA/DOPER.git.

Hart, W. E., Laird, C. D., Watson, J. P., Woodruff, D. L., Hackebeil, G. A., Nicholson, B. L. & Siirola, j. D. 2017. Pyomo – Optimization Modeling in Python. Springer Vol. 67.

Institute of Electrical and Electronics Engineers (IEEE). 2000. Radial Distribution Test Feeders. IEEE Distribution Planning Working Group Report. http://sites.ieee.org/pes-testfeeders/files/2017/08/testfeeders.pdf.

MacQueen, J. 1967. Some Methods for Classification and Analysis of Multivariate Observations. Proceedings of the Fifth Berkeley Symposium on Mathematical Statistics and Probability, Vol. 1, No. 14, 281–297.

Modelisar 2014. Functional Mock-up Interface 2.0.

Pacific Gas and Electric (PG&E). 1999. Voltage tolerance boundary.

Pacific Gas and Electric (PG&E). 2018. Electric Schedule E-19.

Perez, R., Ineichen, P., Seals, R., Michalsky, J. & Stewart, R. 1990. "Modeling Daylight Availability and Irradiance Components from Direct and Global Irradiance." *Solar Energy* 44(5): 271–289.

Stadler, M., Groissböck, M., Cardoso, G. & Marnay, C. 2014. "Optimizing Distributed Energy Resources and Building Retrofits with the Strategic DER- CAModel." *Applied Energy* 132, 0306–2619.

Swenson, T. J., Vrettos, E., Muller, J. & Gehbauer, C. 2019. Open PMU Event Dataset: Detection and Characterization at LBNL Campus. IEEE PES General Meeting.

Tesla. 2016. PowerWall 2, https://www.tesla.com/powerwall.

Vanfretti, L., Rabuzin, T., Baudette M. & Murad, M. 2016. iTesla Power Systems Library (iPSL): A Modelica library for phasor time-domain simulations. SoftwareX, ISSN 2352-7110, DOI: 10.1016/j.softx.2016.05.001.

Vrettos, E. & Gehbauer, C. 2019. A Hybrid Approach for Short-Term PV Power Forecasting in Predictive Control Applications. Power Tech conference in Milano.

von Meier, A., Stewart, E., McEachern, A., Andersen, A., & Mehrmanesh, L. 2017. "Precision Micro-Synchrophasors for Distribution Systems: A Summary of Applications." IEEE Transactions on Smart Grid Vol. 8, No. 6.

Ward, J. H. Jr. 1963. "Hierarchical grouping to optimize an objective function." *Journal of the American statistical Association* 58 (301): 236–244.

Wetter, M., Zuo, W., Nouidui, T.S. & Pang, X. 2014. "Modelica Buildings Library." *Journal of Building Performance Simulation* 7 (4): 253–270.

# APPENDIX A:
# Documentation of Flexgrid

A brief documentation of Flexgrid.

## Pictures

# Overview

## PV Array

REC 260PEZ

260 W-peak

15.8 % efficiency

4 strings a 14 modules

Total: 14,560 W-peak

## Inverter


SolarEdge StorEdge

7,600 VA; 240 V single-phase

98 % efficiency

3 inverter; 3 battery inputs

Total: 22,800 VA (incl. battery)

## Battery


Tesla Powerwall

3,300 W / 6,400 kWh (350-450 V)

92 % efficiency (roundtrip)

1 battery per inverter (3 total)

Total: 9,900 W / 19,200 kWh

## Measurement

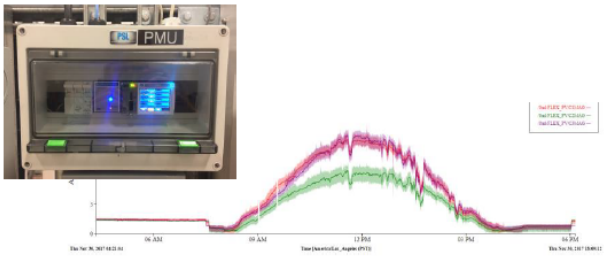


Power Standards Lab

Micro-Synchrophasor (µPMU)

~30 kHz sampling

120 Hz data acquisition

feeds BtrDB database

## Real-time Simulator

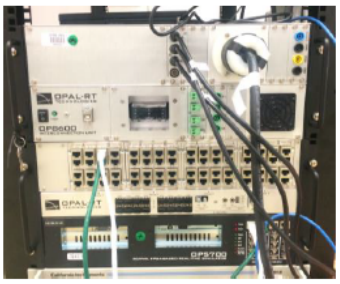

Opal-RT OP5600

4 x 3.46 GHz

Virtex 6 FPGA Platform

16x AI/AO; 32x DI/DO

## Grid Emulator

Ametek MX-30

30,000 VA (300 $V_{RMS}$-peak)

AC, DC, AC+DC output

3 phase output

LCLC output filter

# APPENDIX B:
# Simulation Settings

A brief overview of the MPC settings for the simulation study and the electricity tariff implemented.

## Simulation Settings

### MPC Settings

```
parameter['battery'] = {}
parameter['battery']['capacity'] = 6.4 # kWh
parameter['battery']['power'] = 3.3 # kW
parameter['battery']['soc_initial'] = 0 # State of Charge initially in 1
parameter['battery']['soc_final'] = 0 # State of Charge finally in 1
parameter['battery']['soc_min'] = 0 # State of Charge initially in 1
parameter['battery']['soc_max'] = 1 # State of Charge initially in 1
parameter['battery']['efficiency_charging'] = 0.96 # Charging efficiency [0-1]; Tesla: 0.96
parameter['battery']['efficiency_discharging'] = 0.96 # Discharging efficiency [0-1]; Tesla: 0.96
parameter['battery']['self_discharging'] = 0.3 # % of SoC per 24 hours
parameter['site'] = {}
parameter['site']['customer'] = 'Commercial' # Type of customer [commercial or none]; decides if demand charge
parameter['site']['regulation'] = True # Enables or disables the regulation bidding
parameter['site']['regulation_reserved'] = False # Flag to reserve capacity in battery (disables site regulation!)
parameter['site']['import_max'] = 1000 # kW
parameter['site']['export_max'] = 20 # kW
parameter['site']['demand_periods_prev'] = {0:0,1:0,2:0} # kW peak previously set for periods 0-offpeak, 1-midpeak,
parameter['site']['demand_coincident_prev'] = 0 # kW peak previously set for coincident
parameter['controller'] = {}
parameter['controller']['timestep'] = 60*60 # Controller timestep in seconds
```

### Pacific Gas & Electric E-19 Tariff

| | Energy [$/kWh] | | | Demand [$/kW] | | | |
|---|---|---|---|---|---|---|---|
| | **Off-peak** | **Mid-peak** | **On-peak** | **Base** | **Off-peak** | **Mid-peak** | **On-peak** |
| **Summer** | 0.08671 | 0.11613 | 0.16055 | 17.74 | 0 | 5.4 | 19.65 |
| **Winter** | 0.09401 | 0.11004 | - | 17.74 | 0 | 0.12 | - |

Periods:

- Summer (May – October):
  - Off-peak: 12 AM – 7 AM & 10 PM – 12 AM
  - Mid-peak: 8 AM – 11 AM & 6 PM – 9 PM
  - On-peak: 12 AM – 5 PM
- Winter (January – April & November – December):
  - Off-peak: 12 AM – 7 AM & 10 PM – 12 AM
  - Mid-peak: 8 AM – 9 PM